CHAPTER

6 Constitutive relations and formulation of classical linear theories of solids and fluids

Chapters 6–9 will explore numerous types of constitutive equations for a broad class of materials commonly found in engineering and scientific applications. Constitutive relations characterize a continuum material's macroscopic response to applied mechanical, thermal, or other types of loadings. Such relations are often based on the material's internal constitution and commonly result in idealized material models such as *elastic solids* or *viscous fluids*. These models do not come directly from general principles, but rather are normally developed from observed behaviors found in collected experimental data. As shown in Fig. 1.5, we also wish to combine various constitutive laws with our previous kinematical, stress, and general principle relations in order to create a closed system of field equations that contains sufficient numbers of relations to solve for all model unknowns (see discussion in Section 5.8 and Table 5.1).

For each theoretical model, the complete formulation will require various manipulations of the governing equations and the creation of proper boundary and/or initial conditions appropriate to the model. Following these steps, we will then explore some particular basic solutions to problems of interest. We will generally limit the number of solutions presented for each model, in order to spend more time on expanding the number of material theories developed. This will provide a much broader background on how continuum mechanics is applied to a very large group of materials with quite different behaviors. Many of the classical continuum theories (elasticity, plasticity, fluid mechanics, rheology, etc.) have separate courses and textbooks entirely devoted to each of them. We will thus try to avoid duplication of some of this material and keep our presentations brief.

Because of our interest in the wide application of continuum mechanics, we will divide this study into four separate chapters. This chapter will focus on the classical linear theories of solids and fluids, neglecting thermal effects. This material will provide the foundation for further, more advanced study. Subsequent chapters will then explore more complex problems dealing with multiple constitutive fields, thermomechanical effects, nonlinear theories, materials with microstructure, and damage mechanics.

Continuum Mechanics Modeling of Material Behavior. http://dx.doi.org/10.1016/B978-0-12-811474-2.00006-X

6.1 INTRODUCTION TO CONSTITUTIVE EQUATIONS

As previously mentioned, constitutive equations describe the macroscopic behavior resulting from the material's *internal constitution*. Such internal composition is primarily related to the material makeup at several orders of length scale below that being used in the continuum study, thus commonly focusing on *microstructure or nanostructure*. Because of the wide variety of materials we wish to study, internal microstructure can vary significantly. For example, such microstructure in solids normally includes crystalline, polycrystalline, and amorphous (molecular) types as illustrated in Fig. 6.1. Many solids also have a composite microstructure with fiber or particulate reinforcement embedded in a somewhat uniform matrix material as shown in Fig. 6.2. Additionally, some solids have porous and/or cellular microstructure as illustrated in Fig. 6.3. Fluids can also have complex internal structure such as: liquid mixtures, flows of polymerics, slurries, biological fluids, etc. The classical linear theories to be discussed in this chapter commonly neglect much (but not all) of these microstructures. More sophisticated continuum theories that incorporate some of these details will be discussed in Chapter 9.

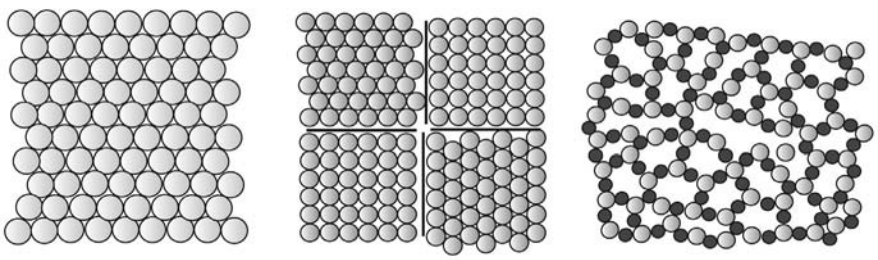

FIGURE 6.1

Typical microstructures in solids.

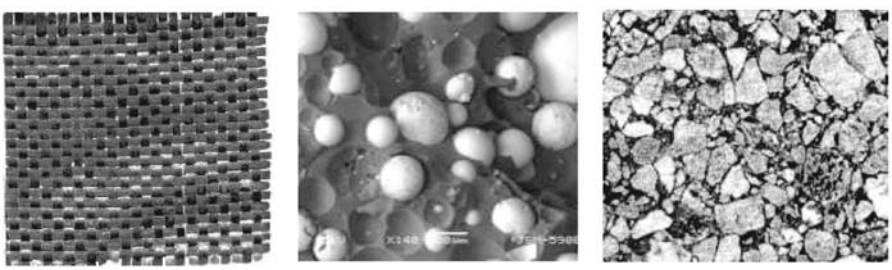

FIGURE 6.2

Typical microstructures in composite materials.

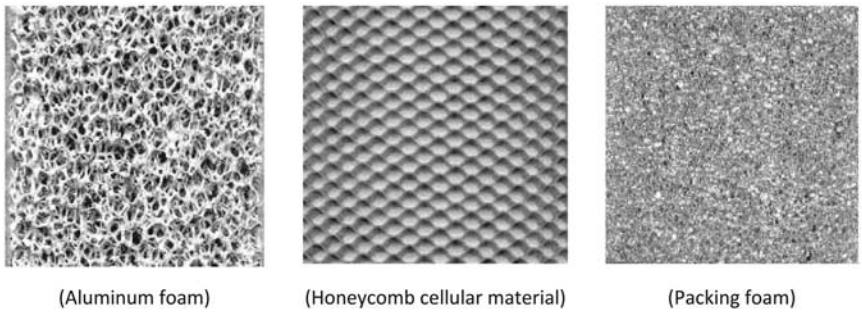

FIGURE 6.3

Microstructures in porous and cellular materials.

For solids, internal material microstructure is also related to two important constitutive issues commonly referred to as *homogeneity* and *isotropy*. If the material is *homogeneous*, the constitutive behavior will not depend on *spatial position* within the body. For many materials, this is a reasonable assumption and will simplify the resulting constitutive equations and subsequent overall formulation. However, there are some important applications (geomechanics and functionally graded materials) where nonhomogeneous behavior must be included in the model. The second issue, the concept of *isotropy*, has to do with *directional dependence* on the constitutive properties. A material with no directional dependence is referred to as *isotropic*, whereas *anisotropic* materials have some form of constitutive dependency on direction. Again assuming an isotropic model will suffice for many applications and will reduce the complexity of the resulting model equations. However, for many materials with significant internal directional microstructure like fiber composites and wood, an anisotropic constitutive model is necessary. Note that fluid media will normally have sufficient internal mixing behavior to eliminate inhomogeneity and anisotropy.

In addition to microstructure, many materials also exhibit complicated rate- and temperature-dependent behavior. With this vast amount of variation, it is generally difficult to establish one constitutive law that can accurately model a real material over a wide range of behavior that includes mechanical, thermal, rate-dependent and microstructural effects. Thus, we commonly formulate specific equations describing the *macroscopic behavior of ideal material types* (e.g. elastic solids, viscoelastic materials, plastic materials, viscous fluids, etc.), each of which will yield a mathematical formulation designed to *approximate real material behavior* over a *restricted range* of deformations, loading rates, and temperatures. In this chapter, we will consider only linear mechanical theories and not explore thermal effects. Subsequent chapters will cover many other continuum material theories that include much broader modeling.

Our study of solid behaviors in this chapter will comprise both elastic and inelastic responses, whereas our fluid modeling will encompass inviscid and Newtonian viscous flows. More precise definitions of these terms will be provided in later sections. Since it is well known that some materials exhibit both solid- and fluid-like be-

haviors together, we also wish to develop linear viscoelastic continuum theories for such materials. For the nonthermal case, we will be developing six constitutive equations characterizing the particular material's response to applied mechanical loadings. Such material response relations provide the link between applied forces and the material deformation and typically establish a functional relationship between stress and strain or strain rate. For each material model, we will develop the constitutive law, present the general model formulations of the governing field equations, and then present analytical solutions to a few basic problems of interest. We begin each case, with particular experimental evidence to help motivate the constitutive formulation and understand the nature of the modeling. Much more sophisticated and general procedures for constitutive equation development will be given in later chapters.

6.2 LINEAR ELASTIC SOLIDS

Linear elasticity is perhaps one of the most studied fields in continuum mechanics. For over a century, numerous books have been written on the subject and a very large body of research papers has been published on formulation and solution strategies in this field. We will now explore the basics of this formulation and present a few common solutions to boundary value problems within the static theory. Our emphasis will be on the application of continuum mechanics principles to the elasticity formulation. More complete coverage of this topic can be found in Sadd (2014), Barber (2010), Timoshenko and Goodier (1970), and Kachanov et al. (2003) provides an extensive compendium of elasticity solutions.

6.2.1 CONSTITUTIVE LAW

For many centuries, experimental testing has been employed to characterize the behavior of real materials. One such technique to determine the mechanical response is the *simple tension test* in which a specially prepared cylindrical or flat stock sample is axially loaded in a testing machine. This creates a simple and uniform one-dimensional deformation field. Strain is determined by the change in length between prescribed reference marks on the sample and is usually measured by a clip gage. Load data collected from a load cell is divided by the cross-sectional area in the test section to calculate the stress. Axial stress and strain data are recorded and plotted using standard experimental techniques. Typical qualitative data for three types of common structural metals (mild steel, aluminum, cast iron) are shown in Fig. 6.4. It is observed that each material exhibits an initial linear stress–strain response for small deformation. This is followed by a change to nonlinear behavior that can lead to large deformation, finally ending with sample failure.

For each material, the initial linear response ends at a point normally referred to as the *proportional limit*. Another observation in this initial region is that if the loading is removed, the sample will return to its original shape, and the strain will

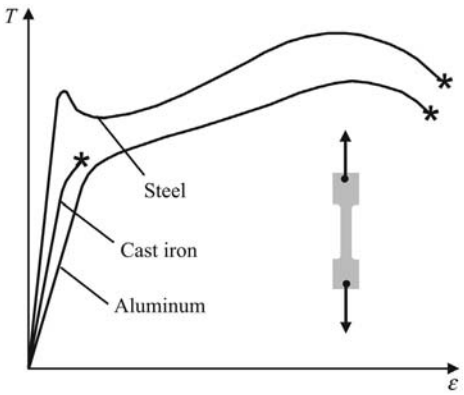

FIGURE 6.4

Typical uniaxial stress–strain curves for three structural metals.

disappear. This characteristic is the primary descriptor of elastic behavior. However, at some further point on the stress–strain curve, unloading will not bring the sample back to zero strain, and some permanent inelastic or plastic deformation will result. The point at which this nonelastic behavior begins is called the *elastic limit*. Although some materials exhibit somewhat different elastic and proportional limits, many times these values are taken to be approximately the same. Another demarcation on the stress–strain curve is referred to as the *yield point*, defined by the location where large inelastic deformation begins. Such inelastic behavior will be discussed in Section 6.6.

Since mild steel and aluminum are ductile materials, their stress–strain response indicates extensive plastic deformation, and during this period the sample dimensions will be changing. In particular, the sample's cross-sectional area will undergo significant reduction and the stress calculation using division by the original area will now be in error. This accounts for the reduction in the stress at large strain. If we were to calculate the load divided by the true area, the *true stress* would continue to increase until failure. On the other hand, cast iron is a brittle material, and thus its stress–strain response does not show large plastic deformation. For this material, very little nonelastic or nonlinear behavior is observed.

We may thus summarize that for many solids under small deformations, the relation between the applied load and deformation is linear; upon removal of the loads, the deformations disappear; and the rate of loading did not affect these observations. These characteristics lead to the formulation of the ideal material model referred to as *linear infinitesimal elasticity theory*. For the one-dimensional axial loading case, we can then write the constitutive response between the stress T and strain ε by the simple relation $T = E\varepsilon$, Twhere E is the slope of the uniaxial stress–strain curve. We will now use this simple concept to develop the general three-dimensional forms of the linear elastic constitutive model.

First, we can generalize things a little and say that for elastic materials, the stress is only a function of the current strain and thus the general constitutive equation would read

$$\begin{aligned} \boldsymbol{T} &= \boldsymbol{f}(\boldsymbol{E}) \\ T_{ij} &= f_{ij}(E_{kl}) \end{aligned} \tag{6.2.1}$$

where $\boldsymbol{T}$ is the Cauchy stress defined in Section 4.3, $\boldsymbol{E}$ is Lagrangian strain defined in Section 3.6, and $\boldsymbol{f}$ is a general tensor-valued material response function. We choose the condition $\boldsymbol{f}(\boldsymbol{0}) = \boldsymbol{0}$, so that when the strain vanishes the stress also becomes zero. Now we wish to limit this model to small deformations and would then drop the distinction between Lagrangian and Euler descriptions and only make use of the small strain tensor ε_{ij} defined by Eq. (3.8.1). Furthermore, the general response function in (6.2.1) must reduce to a general linear form, and thus the response relation is given by

$$T_{ij} = C_{ijkl}\varepsilon_{kl} \tag{6.2.2}$$

where C_{ijkl} is a *fourth-order elasticity tensor* whose components include all the material parameters necessary to characterize the material. This relation is called the *generalized Hooke's law*.

EXAMPLE 6.2.1 PROVE THAT C_{ijkl} IS A FOURTH-ORDER TENSOR

Given that the Cauchy stress T_{ij} and the small strain tensor ε_{ij} are the components of a second-order tensor, explicitly show that the elasticity tensor is a fourth-order tensor.

Solution: From relation (6.2.2) $\Rightarrow T'_{ij} = C'_{ijkl}\varepsilon'_{kl}$.

Since the stress and strain are second-order tensors, $T'_{ij} = Q_{im}Q_{jn}T_{mn}$ and $\varepsilon'_{kl} = Q_{kr}Q_{ls}\varepsilon_{rs}$.

Thus, we get $Q_{im}Q_{jn}T_{mn} = C'_{ijkl}Q_{kr}Q_{ls}\varepsilon_{rs} \Rightarrow Q_{im}Q_{jn}C_{mnrs}\varepsilon_{rs} = C'_{ijkl}Q_{kr}Q_{ls}\varepsilon_{rs}$ $\Rightarrow Q_{im}Q_{jn}C_{mnrs} = C'_{ijkl}Q_{kr}Q_{ls}$. Multiply both sides by $Q_{pr}Q_{qs} \Rightarrow$ $Q_{im}Q_{jn}C_{mnrs}Q_{pr}Q_{qs} = C'_{ijkl}Q_{kr}Q_{ls}Q_{pr}Q_{qs} = C'_{ijkl}\delta_{kp}\delta_{lq} = C'_{ijpq}$ $C'_{ijpq} = Q_{im}Q_{jn}Q_{pr}Q_{qs}C_{mnrs}$ and thus the elasticity tensor $\boldsymbol{C}$ is a fourth-order tensor.

Based on the symmetry of the stress and strain tensors, the elasticity tensor must have the properties (see Exercise 6.1)

$$\begin{aligned} C_{ijkl} &= C_{jikl} \\ C_{ijkl} &= C_{ijlk} \end{aligned} \tag{6.2.3}$$

In general, the fourth-order tensor C_{ijkl} has 81 components. However, relations (6.2.3) reduce the number of independent components to 36, and this provides an alternative way to express Hooke's law in the contracted *Voigt matrix notational form*

$$\begin{bmatrix} T_{11} \\ T_{22} \\ T_{33} \\ T_{23} \\ T_{31} \\ T_{12} \end{bmatrix} = \begin{bmatrix} C_{11} & C_{12} & \cdot & \cdot & \cdot & C_{16} \\ C_{21} & \cdot & \cdot & \cdot & \cdot & \cdot \\ \cdot & \cdot & \cdot & \cdot & \cdot & \cdot \\ \cdot & \cdot & \cdot & \cdot & \cdot & \cdot \\ \cdot & \cdot & \cdot & \cdot & \cdot & \cdot \\ C_{61} & \cdot & \cdot & \cdot & \cdot & C_{66} \end{bmatrix} \begin{bmatrix} \varepsilon_{11} \\ \varepsilon_{22} \\ \varepsilon_{33} \\ 2\varepsilon_{23} \\ 2\varepsilon_{31} \\ 2\varepsilon_{12} \end{bmatrix} \tag{6.2.4}$$

The components of C_{ijkl} or equivalently C_{ij} are called *elastic moduli* and have the same units as stress (force/area).

Next, let us go back to the differential form of energy equation (5.6.12). Neglecting all thermal terms and considering only small deformations, this equation reduces to

$$\rho\dot{\varepsilon} = T_{ij}\dot{\varepsilon}_{ij} \tag{6.2.5}$$

where ε is the internal energy per unit mass. Using our conservation of mass relation (5.2.8) for small deformations (with $J = 1$) gives $\rho = \rho_o$, and thus the mass density remains a constant. For our purely mechanical theory, we define a strain energy density function (per unit volume) as $U = \rho\varepsilon$ and assume that it depends only on the strain, $U = U(\varepsilon_{ij})$. Thus, $\rho\dot{\varepsilon} = \dot{U} = \dfrac{\partial U}{\partial \varepsilon_{ij}}\dot{\varepsilon}_{ij}$, and combining this result with relation (6.2.5) gives

$$T_{ij} = \frac{\partial U}{\partial \varepsilon_{ij}} \tag{6.2.6}$$

Relation (6.2.6) can be thought of as a constitutive form for the stress written in terms of a strain energy function, and this form is commonly referred to as a *hyperelastic* or *Green elastic* material.

Differentiating form (6.2.6), we can write

$$\frac{\partial T_{ij}}{\partial \varepsilon_{kl}} = \frac{\partial^2 U}{\partial \varepsilon_{kl}\,\partial \varepsilon_{ij}} \quad \text{and} \quad \frac{\partial T_{kl}}{\partial \varepsilon_{ij}} = \frac{\partial^2 U}{\partial \varepsilon_{ij}\,\partial \varepsilon_{kl}} \Rightarrow \frac{\partial T_{ij}}{\partial \varepsilon_{kl}} = \frac{\partial T_{kl}}{\partial \varepsilon_{ij}} \tag{6.2.7}$$

Combining Eqs. (6.2.7) with (6.2.2) produces another symmetry relation for the elasticity tensor

$$C_{ijkl} = C_{klij} \quad \text{or equivalently} \quad C_{ij} = C_{ji} \tag{6.2.8}$$

and this result implies that for a general linear elastic solid there are only 21 independent elastic moduli. On occasion we may wish to invert (6.2.2) and write strain in terms of stress

$$\varepsilon_{ij} = S_{ijkl}T_{kl} \tag{6.2.9}$$

where S_{ijkl} is the *elastic compliance tensor* which has identical symmetry properties as those of the elasticity tensor C_{ijkl}.

To go further with the constitutive equation development, we need to decide on the isotropy and homogeneity of the material to be investigated. These issues will reduce the 21 independent elastic moduli to more manageable numbers. For our limited study, we will only consider homogeneous materials and thus all elastic moduli C_{ijkl} will be constants. Further details on nonhomogeneous linear elasticity can be found in Sadd (2014). In regard to the directional dependence, it has been commonly observed that many materials exhibit particular *microstructural symmetries*. Examples of this include the hexagonal crystalline solid shown in Fig. 6.1 and the carbon fiber composite illustrated in Fig. 6.2. Many other crystalline materials and fiber composites exist with various symmetries producing identical constitutive response for *particular* directions within the solid. Some symmetries even follow a curvilinear reference system such as that found in natural wood. These symmetries will generally lead to a reduction in the complexity of the stress–strain constitutive relations, and examples of this will now be shown.

Orientations for which a material has the same stress–strain response can be determined by coordinate transformation (rotation) theory previously developed in Sections 2.7 and 2.8. Such particular transformations are sometimes called the *material symmetry group*. Further details on this topic have been presented by Zheng and Spencer (1993) and Cowin and Mehrabadi (1995). We will have more to say on this topic when we explore more general issues related to nonlinear material behavior in Chapter 8. In order to determine various material symmetries, we review the results from Example 6.2.1 in which we established the fourth-order transformation law for the elasticity tensor

$$C'_{ijkl} = Q_{im}Q_{jn}Q_{kp}Q_{lq}C_{mnpq} \tag{6.2.10}$$

If under a specific transformation $\boldsymbol{Q}$, the material response is to be the same, relation (6.2.10) reduces to

$$C_{ijkl} = Q_{im}Q_{jn}Q_{kp}Q_{lq}C_{mnpq} \tag{6.2.11}$$

This material symmetry relation will provide a system of equations that will allow reduction in the number of independent elastic moduli. We now consider some specific cases of practical interest.

Plane of Symmetry (Monoclinic Material)

We first consider the case of a material with a *plane of symmetry*. Such a medium is commonly referred to as a *monoclinic material*. We consider the case of symmetry with respect to the x_1,x_2-plane as shown in Fig. 6.5.

For this particular symmetry, the required transformation is simply a mirror reflection about the x_1,x_2-plane and is given by

$$Q_{ij} = \begin{bmatrix} 1 & 0 & 0 \\ 0 & 1 & 0 \\ 0 & 0 & -1 \end{bmatrix} \tag{6.2.12}$$

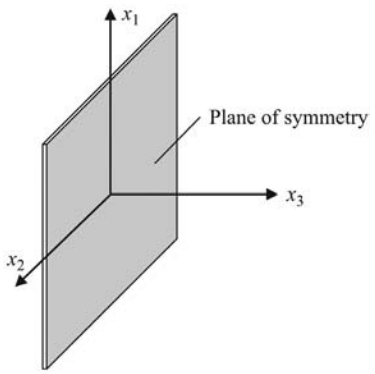

FIGURE 6.5

Plane of symmetry for a monoclinic material.

Note that this transformation is not a simple rotation that preserves the right-handedness of the coordinate system, that is, it is not a proper orthogonal transformation. Nevertheless, it can be used for our symmetry investigations. Using this specific transformation in relation (6.2.11) gives $C_{ijkl} = -C_{ijkl}$ if the index 3 appears an *odd* number of times and thus these particular moduli would have to vanish. In terms of the contracted notation, this gives

$$C_{i4} = C_{i5} = C_{46} = C_{56} = 0, \quad (i = 1, 2, 3) \tag{6.2.13}$$

Thus, the elasticity matrix takes the form

$$C_{ij} = \begin{bmatrix} C_{11} & C_{12} & C_{13} & 0 & 0 & C_{16} \\ \cdot & C_{22} & C_{23} & 0 & 0 & C_{26} \\ \cdot & \cdot & C_{33} & 0 & 0 & C_{36} \\ \cdot & \cdot & \cdot & C_{44} & C_{45} & 0 \\ \cdot & \cdot & \cdot & \cdot & C_{55} & 0 \\ \cdot & \cdot & \cdot & \cdot & \cdot & C_{66} \end{bmatrix} \tag{6.2.14}$$

It is, therefore, observed that *13 independent elastic moduli* are needed to characterize monoclinic materials.

Three Perpendicular Planes of Symmetry (Orthotropic Material)

A material with three mutually perpendicular planes of symmetry is called *orthotropic*. Common examples of such materials include wood and fiber-reinforced composites. In order to investigate the material symmetries for this case, it is convenient to let the symmetry planes correspond to coordinate planes as shown in Fig. 6.6.

The symmetry relations can be determined by using 180° rotations about each of the coordinate axes. Another convenient scheme is to start with the reduced form from the previous monoclinic case and re-apply the same transformation with respect

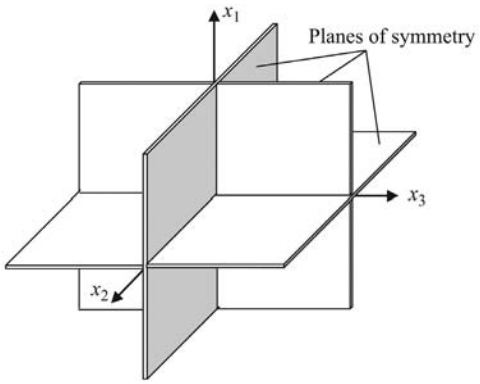

FIGURE 6.6

Three planes of symmetry for an orthotropic material.

to say the x_2,x_3-plane. This results in the additional elastic moduli being reduced to zero

$$C_{16} = C_{26} = C_{36} = C_{45} = 0 \tag{6.2.15}$$

Thus, the elasticity matrix for the orthotropic case reduces to having only *nine independent* elastic moduli given by

$$C_{ij} = \begin{bmatrix} C_{11} & C_{12} & C_{13} & 0 & 0 & 0 \\ \cdot & C_{22} & C_{23} & 0 & 0 & 0 \\ \cdot & \cdot & C_{33} & 0 & 0 & 0 \\ \cdot & \cdot & \cdot & C_{44} & 0 & 0 \\ \cdot & \cdot & \cdot & \cdot & C_{55} & 0 \\ \cdot & \cdot & \cdot & \cdot & \cdot & C_{66} \end{bmatrix} \tag{6.2.16}$$

It should be noted that only two transformations were needed to develop the final reduced constitutive form (6.2.16). The material also must satisfy a third required transformation that the properties would be the same under a reflection of the x_1,x_3-plane; however, this transformation is already identically satisfied. Thus, for some materials, the reduced constitutive form may be developed by only using a portion of the total material symmetries (see Ting, 1996 for more on this topic). On another issue for orthotropic materials, vanishing shear strains imply vanishing shear stresses, and thus the principal axes of stress coincide with the principal axes of strain. This result is of course not true for general anisotropic materials; see for example, the monoclinic constitutive form (6.2.14).

Complete Symmetry (Isotropic Material)

For the case of complete symmetry where all directions have the same constitutive response, the material is referred to as *isotropic*. For this case, the fourth-order elasticity tensor must reduce to an isotropic tensor and this form has been previously given in Table 2.15.1 as

$$C_{ijkl} = \alpha\delta_{ij}\delta_{kl} + \beta\delta_{ik}\delta_{jl} + \gamma\delta_{il}\delta_{jk}, \quad \text{for any constants} \quad \alpha, \beta, \gamma \tag{6.2.17}$$

Invoking the symmetry relations (6.2.3), allows Eq. (6.2.17) to be written as

$$C_{ijkl} = \lambda\delta_{ij}\delta_{kl} + \mu(\delta_{ik}\delta_{jl} + \delta_{il}\delta_{jk}) \tag{6.2.18}$$

where we have redefined some of the general constants associated with (6.2.17). In contracted matrix form, this result would be expressed as

$$C_{ij} = \begin{bmatrix} \lambda+2\mu & \lambda & \lambda & 0 & 0 & 0 \\ \cdot & \lambda+2\mu & \lambda & 0 & 0 & 0 \\ \cdot & \cdot & \lambda+2\mu & 0 & 0 & 0 \\ \cdot & \cdot & \cdot & \mu & 0 & 0 \\ \cdot & \cdot & \cdot & \cdot & \mu & 0 \\ \cdot & \cdot & \cdot & \cdot & \cdot & \mu \end{bmatrix} \tag{6.2.19}$$

Thus, only *two* independent elastic constants exist for isotropic materials. For each of the presented cases, a similar compliance elasticity matrix could be developed.

Focusing now on the isotropic case, using (6.2.18) in Hooke's law (6.2.2) yields

$$T_{ij} = \lambda\varepsilon_{kk}\delta_{ij} + 2\mu\varepsilon_{ij} \tag{6.2.20}$$

where the elastic constant λ is called *Lamé's constant* and μ is referred to as the *shear modulus* or *modulus of rigidity*. Some studies use the notation G for the shear modulus. Eq. (6.2.20) can be written out as six individual scalar equations as

$$\begin{aligned} T_{11} &= \lambda(\varepsilon_{11}+\varepsilon_{22}+\varepsilon_{33})+2\mu\varepsilon_{11} \\ T_{22} &= \lambda(\varepsilon_{11}+\varepsilon_{22}+\varepsilon_{33})+2\mu\varepsilon_{22} \\ T_{33} &= \lambda(\varepsilon_{11}+\varepsilon_{22}+\varepsilon_{33})+2\mu\varepsilon_{33} \\ T_{12} &= 2\mu\varepsilon_{12} \\ T_{23} &= 2\mu\varepsilon_{23} \\ T_{31} &= 2\mu\varepsilon_{31} \end{aligned} \tag{6.2.21}$$

Stress–strain relations (6.2.20) may be inverted to express the strain in terms of the stress. This can easily be done in index notation by first setting the two free indices the same (contraction process) to get

$$T_{kk} = (3\lambda+2\mu)\varepsilon_{kk} \tag{6.2.22}$$

This relation can be solved for ε_{kk} and substituted back into (6.2.20) to get

$$\varepsilon_{ij} = \frac{1}{2\mu}\left(T_{ij} - \frac{\lambda}{3\lambda+2\mu}T_{kk}\delta_{ij}\right)$$

which is more commonly written as

$$\varepsilon_{ij} = \frac{1+\nu}{E}T_{ij} - \frac{\nu}{E}T_{kk}\delta_{ij} \tag{6.2.23}$$

where $E = \dfrac{\mu(3\lambda+2\mu)}{\lambda+\mu}$ and is called *the modulus of elasticity* or *Young's modulus*, and $\nu = \dfrac{\lambda}{2(\lambda+\mu)}$ is referred to as *Poisson's ratio*. It is easy to show that the principal

axes of stress and stain are the same for isotropic elastic materials. For cylindrical and spherical coordinates (shown in Figs. 2.6 and 2.7), the basic forms of Hooke's law will remain the same with simple interchange of (x_1,x_2,x_3) to (r,θ,z) or to (R,ϕ,θ).

The previously defined isotropic elastic moduli have simple physical meaning. These can be determined through investigation of particular states of stress commonly used in laboratory materials testing as shown in Fig. 6.7.

Simple Tension

The simple tension test as discussed previously includes a sample subjected to uniaxial tension σ with an approximate state of stress shown in the figure. The strain field is determined from relations (6.2.23). These results give the following information: $E = \sigma / \varepsilon_x$ and is simply the slope of the stress–strain curve, whereas $\nu = -\varepsilon_y / \varepsilon_x = -\varepsilon_z / \varepsilon_x$ is minus the ratio of the transverse strain to the axial strain. Standard measurement systems can easily collect axial stress and transverse and axial strain data, and thus through this one type of test both elastic constants can be determined for materials of interest.

Pure Shear

This test involves a thin-walled circular tube subjected to torsional loading. The approximate state of stress on the surface of the cylindrical sample is shown in the figure. Again using Hooke's law, the corresponding strain field can easily be determined. These results indicate that the shear modulus is given by $\mu = \tau / 2\varepsilon_{xy}$, and this moduli is therefore related to the slope of the shear stress–shear strain curve.

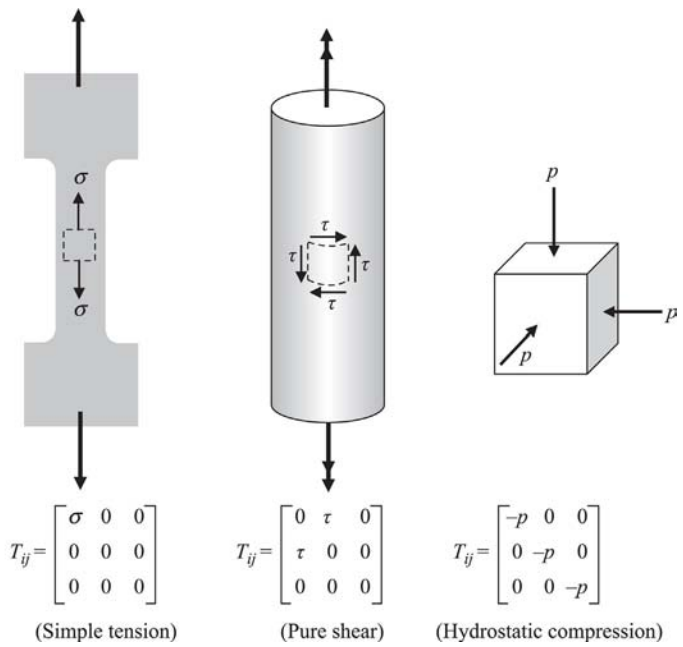

FIGURE 6.7

Special characterization states of stress.

Hydrostatic Compression (or Tension)

The final example is associated with the uniform compression (or tension) loading of a cubical specimen. This type of test could be realizable if the sample was placed in a high-pressure compression chamber. The approximate state of stress is shown in the figure, and the corresponding strains follow from Hooke's law. The dilatation which represents the change in material volume (see Exercise 3.18) is thus given by $\vartheta = \varepsilon_{kk} = -\dfrac{3(1-2\nu)}{E}p$, which can be written as

$$p = -k\vartheta \tag{6.2.24}$$

where $k = \dfrac{E}{3(1-2\nu)}$ is called the *bulk modulus of elasticity*. This additional elastic constant represents the ratio of pressure to the dilatation, which could be referred to as the volumetric stiffness of the material. It can be argued that the elastic constants E, k, and μ must be positive and this will imply that $-1 < \nu < \dfrac{1}{2}$ (see Exercise 6.3). Notice that as Poisson's ratio approaches 0.5, the bulk modulus will become unbounded and the material will not undergo any volumetric deformation and hence will be incompressible.

Our discussion of elastic moduli for isotropic materials has led to the definition of five constants λ, μ, E, ν, and k. However, it should be kept in mind that only two of these are needed to characterize the material. While we have developed a few relationships between various moduli, many other such relations can also be found. In fact, it can be shown that all five elastic constants are interrelated, and if any two are given, the remaining three can be determined using simple formulae (see Sadd, 2014 for details).

EXAMPLE 6.2.2 HYDROSTATIC COMPRESSION OF AN ELASTIC MONOCLINIC AND ISOTROPIC CUBE

In order to demonstrate the difference in linear elastic behavior between isotropic and anisotropic materials, consider a simple example of a cube of both monoclinic and isotropic material under hydrostatic compression p. For this case, the state of stress is given by $T_{ij} = -p\delta_{ij}$, and we wish to determine the corresponding deformations in each type of material.

Solution: for the monoclinic case, hooke's law in compliance form would read

$$\begin{bmatrix} \varepsilon_{11} \\ \varepsilon_{22} \\ \varepsilon_{33} \\ 2\varepsilon_{23} \\ 2\varepsilon_{31} \\ 2\varepsilon_{12} \end{bmatrix} = \begin{bmatrix} S_{11} & S_{12} & S_{13} & 0 & 0 & S_{16} \\ \cdot & S_{22} & S_{23} & 0 & 0 & S_{26} \\ \cdot & \cdot & S_{33} & 0 & 0 & S_{36} \\ \cdot & \cdot & \cdot & S_{44} & S_{45} & 0 \\ \cdot & \cdot & \cdot & \cdot & S_{55} & 0 \\ \cdot & \cdot & \cdot & \cdot & \cdot & S_{66} \end{bmatrix} \begin{bmatrix} -p \\ -p \\ -p \\ 0 \\ 0 \\ 0 \end{bmatrix} \tag{6.2.25}$$

Expanding this matrix relation gives the following deformation field components:

$$\begin{aligned}
\varepsilon_{11} &= -(S_{11}+S_{12}+S_{13})p \\
\varepsilon_{22} &= -(S_{12}+S_{22}+S_{23})p \\
\varepsilon_{33} &= -(S_{13}+S_{23}+S_{33})p \\
\varepsilon_{12} &= -\frac{1}{2}(S_{16}+S_{26}+S_{36})p \\
\varepsilon_{23} &= \varepsilon_{31} = 0
\end{aligned} \tag{6.2.26}$$

The corresponding strains for the isotropic case follow from (6.2.23) And are given by

$$\varepsilon_{11} = \varepsilon_{22} = \varepsilon_{33} = -\left(\frac{1-2\nu}{E}\right)p, \quad \varepsilon_{12} = \varepsilon_{23} = \varepsilon_{31} = 0 \tag{6.2.27}$$

Thus, the response of the monoclinic material is considerably different from isotropic behavior and yields a nonzero shear strain even under uniform hydrostatic stress. Additional examples using simple shear and/or bending deformations can also be used to demonstrate the complexity of anisotropic stress–strain behavior (see Sendeckyj, 1975). It should be apparent that laboratory testing methods attempting to characterize anisotropic materials would have to be more complicated than those used for isotropic solids.

6.2.2 GENERAL FORMULATION

We now wish to establish the general formulation of the linear elasticity model. This process combines the constitutive law with the other governing equations and looks for solution strategies to solve these equations. We will limit our study to only static problems and will thus drop the acceleration term in the equations of motion. Since we are essentially setting up a mathematical boundary value problem, we must also establish appropriate boundary conditions suitable for the theory.

We first start listing all of the governing equations that we have previously developed:

$$\text{Strain-Displacement Relations} \quad \varepsilon_{ij} = \frac{1}{2}(u_{i,j}+u_{j,i}) \tag{6.2.28}$$

$$\text{Compatibility Relations} \quad \varepsilon_{ij,kl}+\varepsilon_{kl,ij}-\varepsilon_{ik,jl}-\varepsilon_{jl,ik} = 0 \tag{6.2.29}$$

$$\text{Equilibrium Equations} \quad T_{ij,j}+F_i = 0, (F_i = \rho b_i) \tag{6.2.30}$$

$$\text{Constitutive Law} \qquad \begin{aligned} T_{ij} &= (\lambda+\mu)\varepsilon_{kk}\delta_{ij} + 2\mu\varepsilon_{ij} \\ \varepsilon_{ij} &= \frac{1+\nu}{E}T_{ij} - \frac{\nu}{E}T_{kk}\delta_{ij} \end{aligned} \tag{6.2.31}$$

As mentioned in Section 3.11, the compatibility relations ensure that the displacements are continuous and single-valued and are necessary only when the strains are arbitrarily specified. If, however, the displacements are included in the problem formulation, the solution will normally generate single-valued displacements, and strain compatibility will automatically be satisfied. Thus, in discussing the general system of equations of elasticity, the compatibility relations (6.2.29) are normally set aside, to be used only with the stress formulation that we will discuss shortly. Therefore, the general system of elasticity field equations will refer to the 15 relations (6.2.28), (6.2.30), and (6.2.31). This system involves 15 unknowns including three displacements u_i, six strains ε_{ij}, and six stresses T_{ij}. The equation system also includes two elastic material constants (for isotropic materials) and the body force density and these are to be given *a priori* with the problem formulation. It is re-assuring that the number of equations matches the number of unknowns to be determined. However, this general system of equations is of such complexity that solutions via analytical methods are extremely difficult and further simplification is required to solve problems of interest. Before proceeding with the development of such simplifications, it will be useful to first discuss typical boundary conditions connected with elasticity problems and this will lead us to the classification of the fundamental problems.

The common types of boundary conditions for linear elasticity normally include specification of how the body is being *supported* or *loaded*. This concept is mathematically formulated by specifying either the *displacements* or *tractions* at boundary points. Fig. 6.8 illustrates this general idea for three typical cases including tractions, displacements, and a *mixed case* where tractions are specified on boundary S_t and displacements are given on the remaining portion S_u such that the total boundary is given by $S = S_t + S_u$.

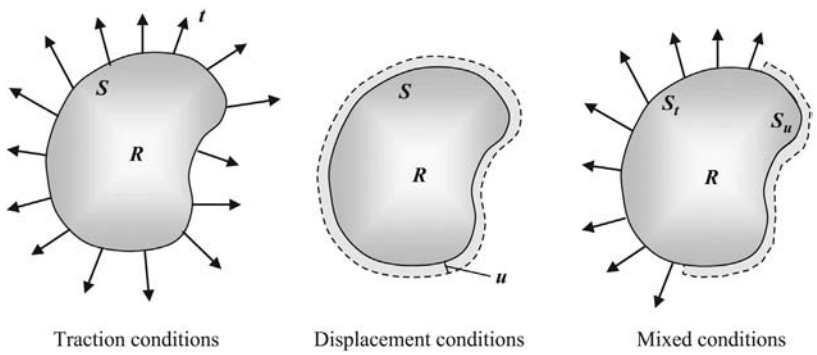

FIGURE 6.8

Typical elasticity boundary conditions.

Traction boundary conditions simplify for the case where the boundary coincides with a coordinate surface. Fig. 6.9 illustrates particular two-dimensional cases where the boundaries coincide with Cartesian or polar coordinate surfaces. Using results from Section 4.3, the traction specification can be reduced to a Cauchy stress specification. For the Cartesian example where x_2 = constant, the normal traction becomes simply the stress component T_{22}, whereas the tangential traction would reduce to T_{12}. For this case, T_{11} exists only *inside* the region, and thus this component of stress cannot be specified on the boundary surface x_2 = constant. A similar situation exists on the vertical boundary x_1 = constant, where the normal traction is now T_{11}, the tangential traction is T_{12}, and the stress component T_{22} exists inside the domain. Similar arguments can be made for polar coordinate boundary surfaces as shown. Drawing the appropriate element along the boundary as illustrated allows for a clear visualization of the particular stress components that act *on* the surface in question. Such a sketch also allows for the determination of the positive directions of these boundary stresses, and this is useful to properly match with boundary loadings that might be prescribed.

We now formulate and classify the *three fundamental boundary-value problems in the theory of linear elasticity* that are related to solving the general system of field equations.

Problem 1 (Traction Problem). Determine the distribution of displacements, strains, and stresses in the interior of an elastic body in equilibrium when body forces are given and the distribution of the tractions are prescribed over the surface of the body:

$$t_i^{(n)}(x_i^{(s)}) = f_i(x_i^{(s)}) \tag{6.2.32}$$

where $x_i^{(s)}$ denotes boundary points and $f_i(x_i^{(s)})$ are the prescribed traction values.

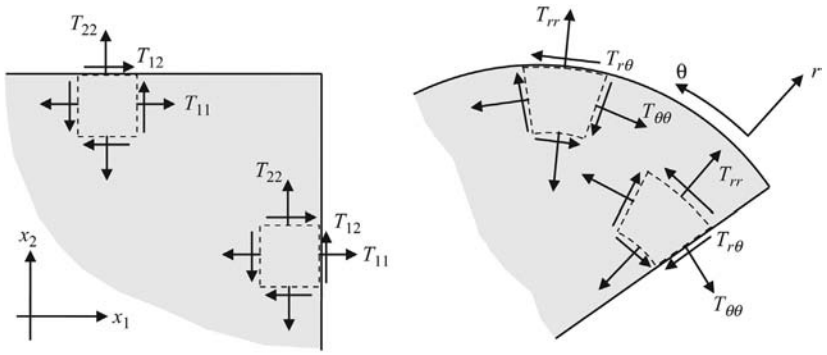

(Cartesian coordinate boundaries) (Polar coordinate boundaries)

FIGURE 6.9

Boundary stress components on coordinate surfaces.

Problem 2 (Displacement Problem). Determine the distribution of displacements, strains, and stresses in the interior of an elastic body in equilibrium when body forces are given and the distribution of the displacements are prescribed over the surface of the body:

$$u_i(x_i^{(s)}) = g_i(x_i^{(s)}) \tag{6.2.33}$$

where $x_i^{(s)}$ denotes boundary points and $g_i(x_i^{(s)})$ are the prescribed displacement values.

Problem 3 (Mixed Problem). Determine the distribution of displacements, strains, and stresses in the interior of an elastic body in equilibrium when body forces are given and the distribution of the tractions are prescribed as per (6.2.32) over the surface S_t and the distribution of the displacements are prescribed as per (6.2.33) over the surface S_u of the body (see Fig. 6.8).

As mentioned previously, the solution to any of these types of problems is formidable, and further reduction and simplification of the general field equation system is normally required to develop analytical solutions. Based on the description of Problem 1 with only traction boundary conditions, it would appear to be desirable to express the fundamental system solely in terms of stress, thereby reducing the number of unknowns in the system. Likewise, for Problem 2, a displacement-only formulation would appear to simplify the problem. We will now pursue these two specialized formulations and explicitly determine these reduced field equation systems.

6.2.2.1 Stress formulation

For the first fundamental problem in elasticity, the boundary conditions are to be given only in terms of the tractions or stress components. In order to develop solution methods for this case, it will be very helpful to reformulate the general system (6.2.28)–(6.2.31) by eliminating the displacements and strains, thereby casting a new system solely in terms of the stresses. By eliminating the displacements, we must now include the compatibility equations in the fundamental system of field equations. Starting with Hooke's law $(6.2.31)_2$ and eliminate the strains in the compatibility relations (6.2.29) to get

$$\begin{aligned} &T_{ij,kk} + T_{kk,ij} - T_{ik,jk} - T_{jk,ik} = \\ &\frac{\nu}{1+\nu}(T_{mm,kk}\delta_{ij} + T_{mm,ij}\delta_{kk} - T_{mm,jk}\delta_{ik} - T_{mm,ik}\delta_{jk}) \end{aligned} \tag{6.2.34}$$

where we have used the arguments of Section 3.11, that the six independent compatibility relations are found by setting $k = l$ in (6.2.29). Although Eqs. (6.2.34) represent the compatibility in terms of stress, a more useful result is found by incorporating the equilibrium equations into the system. Skipping the details (see Sadd, 2014), the final relation becomes

$$T_{ij,kk} + \frac{1}{1+\nu}T_{kk,ij} = -\frac{\nu}{1-\nu}\delta_{ij}F_{k,k} - F_{i,j} - F_{j,i} \tag{6.2.35}$$

This result is the compatibility relations in terms of the stress and is commonly called the *Beltrami–Michell compatibility equations*. Recall that the six developed relations (6.2.35) actually represent three independent results as per our discussion in Section 3.11. Thus, combining these results with the three equilibrium equations (6.2.30) provides the necessary six relations to solve for the six unknown stress components for the general three-dimensional case. This system constitutes the stress formulation for linear elasticity theory and would be appropriate for use with traction boundary condition problems. Once the stresses have been determined, the strains may be found from Hooke's law $(6.2.31)_2$, and the displacements can be then computed through integration of (6.2.28).

The system of equations for this stress formulation is still rather complex, and analytical solutions are commonly determined by making use of *stress functions.* This concept establishes a representation for the stresses that will automatically satisfy the equilibrium equations. For the two-dimensional case, this concept represents the in-plane stresses in terms of a single function. The representation satisfies equilibrium, and the remaining compatibility equations yield a single partial differential equation (biharmonic equation) in terms of the stress function. Having reduced the system to a single equation then allows many analytical methods to be employed to find solutions of interest. We will explore such solutions in the Problems Solution section.

6.2.2.2 Displacement formulation

We now wish to develop the reduced set of field equations solely in terms of the displacements. This system will be referred to as the *displacement formulation* and would be most useful when combined with displacement-only boundary conditions found in the Problem 2 statement. For this case, we wish to eliminate the strains and stresses from the fundamental system (6.2.28)–(6.2.31). This is easily accomplished by using the strain displacement relations in Hooke's law to give

$$T_{ij} = (\lambda + \mu) u_{k,k} \delta_{ij} + \mu (u_{i,j} + u_{j,i}) \tag{6.2.36}$$

Using these relations in the equilibrium equations gives the result

$$\mu u_{i,kk} + (\lambda + \mu) u_{k,ki} + F_i = 0 \tag{6.2.37}$$

which are the equilibrium equations in terms of the displacements and are referred to as *Navier's or Lamé's equations*. This system can be expressed in vector form as

$$\mu \nabla^2 u + (\lambda + \mu) \nabla (\nabla \cdot u) + F = 0 \tag{6.2.38}$$

Navier's equations are the desired formulation for the displacement problem, and the system represents three equations for the three unknown displacement components. Although this formulation represents a considerable reduction in the number of equations, each relation is difficult to solve since all three displacement components appear in each equation. Similar to the stress formulation, additional mathematical techniques have been developed to further simplify these equations for problem solution. Common methods normally employ the use of *displacement potential*

functions. These schemes generally simplify the problem by yielding uncoupled governing equations, and this then allows several analytical methods to be employed to solve problems of interest.

Before moving to the problem solutions, consider a few more details on the strain energy function U that was previously introduced. Boundary tractions and body forces will do work on an elastic solid and this work will be stored inside the material in the form of strain energy. For the elastic case, removal of these loadings will result in the complete recovery of the stored energy. It can be easily shown (Sadd, 2014) that the strain energy function (strain energy per unit volume) can be expressed by

$$U = \frac{1}{2} T_{ij} \varepsilon_{ij} \tag{6.2.39}$$

For the isotropic case, using Hooke's law, the stresses can be eliminated from relation (6.2.39) and the strain energy can be expressed solely in terms of strain

$$\begin{aligned} U(\boldsymbol{\varepsilon}) &= \frac{1}{2}\lambda \varepsilon_{jj}\varepsilon_{kk} + \mu \varepsilon_{ij}\varepsilon_{ij} \\ &= \frac{1}{2}\lambda\left(\varepsilon_{11}+\varepsilon_{22}+\varepsilon_{33}\right)^2 + \mu(\varepsilon_{11}^2+\varepsilon_{22}^2+\varepsilon_{33}^2+2\varepsilon_{12}^2+2\varepsilon_{23}^2+2\varepsilon_{31}^2) \end{aligned} \tag{6.2.40}$$

Likewise, the strains can be eliminated and the strain energy can be written in terms of stress

$$\begin{aligned} U(\boldsymbol{T}) &= \frac{1+\nu}{2E} T_{ij}T_{ij} - \frac{\nu}{2E} T_{ii}T_{jj} \\ &= \frac{1+\nu}{2E}(T_{11}^2+T_{22}^2+T_{33}^2+2T_{12}^2+2T_{23}^2+2T_{31}^2) - \frac{\nu}{2E}\left(T_{11}+T_{22}+T_{33}\right)^2 \end{aligned} \tag{6.2.41}$$

These forms for the strain energy will be useful in other parts of the text.

6.2.3 PROBLEM SOLUTIONS

In this section, we shall explore the solution to a few selected two-dimensional problems in isotropic linear elasticity. This will provide some additional insights and details as to how the material model solutions are found and how the stress, strain, and displacement distributions are determined. As is normally the case, analytical solutions are more likely to be found for one- and two-dimensional problems of limited geometric complexity.

For linear elasticity, there exist several two-dimensional formulations including *plane strain, plane stress*, and *antiplane strain*. For now, we will limit our study to only plane stress and focus on problems in the x_1,x_2-plane. Since we will be dealing primarily with a scalar analysis, variables (x_1,x_2,x_3) will be replaced by the usual (x,y,z) notation. Plane stress (in x,y-plane) is a two-dimensional approximation to a three-dimensional world, such that the state of stress is of the form

$$T_{xx} = T_{xx}(x,y), \quad T_{yy} = T_{yy}(x,y), \quad T_{xy} = T_{xy}(x,y), \quad T_{zz} = T_{xz} = T_{yz} = 0 \tag{6.2.42}$$

Thus, only in-plane stresses exist and they are functions only of the in-plane coordinates. This particular assumption is most applicable to bodies that are thin in the out-of-plane direction and are loaded only with in-plane forces. Examples of this type of geometry are plate-like structures with stress free surfaces on $z = \pm h$ as shown in Fig. 6.10.

Neglecting body forces, under plane stress conditions, the equilibrium equations reduce to

$$\begin{aligned} \frac{\partial T_{xx}}{\partial x} + \frac{\partial T_{xy}}{\partial y} &= 0 \\ \frac{\partial T_{xy}}{\partial x} + \frac{\partial T_{yy}}{\partial y} &= 0 \end{aligned} \tag{6.2.43}$$

The equilibrium equations in terms of the in-plane displacements u, v become

$$\begin{aligned} \mu \nabla^2 u + \frac{E}{2(1-\nu)} \frac{\partial}{\partial x}\left(\frac{\partial u}{\partial x} + \frac{\partial v}{\partial y} \right) &= 0 \\ \mu \nabla^2 v + \frac{E}{2(1-\nu)} \frac{\partial}{\partial y}\left(\frac{\partial u}{\partial x} + \frac{\partial v}{\partial y} \right) &= 0 \end{aligned} \tag{6.2.44}$$

The compatibility equations reduce to the single relation

$$\frac{\partial^2 \varepsilon_{xx}}{\partial y^2} + \frac{\partial^2 \varepsilon_{yy}}{\partial x^2} = 2 \frac{\partial^2 \varepsilon_{xy}}{\partial x \partial y} \tag{6.2.45}$$

and expressing this relation in terms of stress gives the corresponding Beltrami–Michell equation

$$\nabla^2 (T_{xx} + T_{yy}) = 0 \tag{6.2.46}$$

The plane stress problem is then formulated in a two-dimensional region R in the x,y-plane. The displacement formulation is specified by the two governing

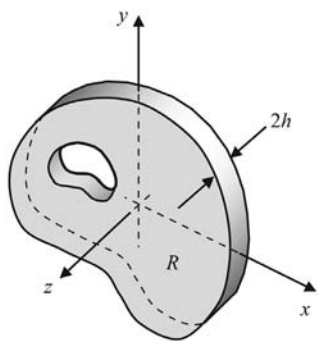

FIGURE 6.10

Thin elastic plate representing plane stress conditions.

Navier relations (6.2.44) with displacement boundary conditions on u and v. The stress formulation includes the three governing equations (6.2.43) and (6.2.46) with appropriate stress or traction boundary conditions. The solution to the plane stress problem then involves determination of the in-plane displacements, strains, and stresses $\{u, v, \varepsilon_{xx}, \varepsilon_{yy}, \varepsilon_{xy}, T_{xx}, T_{yy}, T_{xy}\}$ in R. The out-of-plane strain ε_z can be determined from the in-plane strains via an additional Hooke's law relation.

Even with this two-dimensional reduction in the field equations, the resulting system is still challenging, and additional mathematical help is needed to find solutions. The significant breakthrough for the stress formulation is found by introducing the *Airy stress function* $\phi(x,y)$, such that the stresses can be expressed by the form

$$T_{xx} = \frac{\partial^2 \phi}{\partial y^2}, \quad T_{yy} = \frac{\partial^2 \phi}{\partial x^2}, \quad T_{xy} = -\frac{\partial^2 \phi}{\partial x \partial y} \tag{6.2.47}$$

Using this form, it is observed that the equilibrium equations (6.2.43) will be identically satisfied, and the compatibility relation (6.2.46) becomes

$$\frac{\partial^4 \phi}{\partial x^4} + 2\frac{\partial^4 \phi}{\partial x^2 \partial y^2} + \frac{\partial^4 \phi}{\partial y^4} = \nabla^4 \phi = 0 \tag{6.2.48}$$

The form $\nabla^4 = \nabla^2 \nabla^2$ is called the *biharmonic operator*, and relation (6.2.48) is known as the *biharmonic equation*. Thus, the plane stress problem of linear elasticity has been reduced to a single equation in terms of the Airy stress function ϕ. This reduction to a single partial differential equation now offers many solutions to be found to a large variety of problems types.

One common solution method useful for problems in Cartesian geometries is a polynomial/power series representation of the Airy stress function of the form

$$\phi(x,y) = \sum_{m=0}^{\infty} \sum_{n=0}^{\infty} A_{mn} x^m y^n \tag{6.2.49}$$

where A_{mn} are constant coefficients to be determined from problem boundary conditions. It is noted that the three lowest order terms with $m+n \le 1$ do not contribute to the stresses and are thus are dropped. Terms with $m+n \le 3$ will automatically satisfy the biharmonic equation for any choice of constants A_{mn}; however, for higher-order terms, the constants A_{mn} will have to be related in order to have the polynomial satisfy the governing equation. It is observed that the second-order terms will produce a constant stress field, third-order terms will give a linear distribution of stress, and so on for higher-order polynomials. Since this method will produce only polynomial stress distributions, the scheme will not satisfy general boundary conditions.

Another more general method that is useful in polar coordinate problems comes from a general solution to the biharmonic equation originally credited to Michell (1899). A final form (commonly called the Michell solution) can be written as

$$\begin{aligned}\phi &= a_0 + a_1 \log r + a_2 r^2 + a_3 r^2 \log r \\ &+ (a_4 + a_5 \log r + a_6 r^2 + a_7 r^2 \log r)\theta \\ &+ (a_{11} r + a_{12} r \log r + \frac{a_{13}}{r} + a_{14} r^3 + a_{15} r\theta + a_{16} r\theta \log r)\cos\theta \\ &+ (b_{11} r + b_{12} r \log r + \frac{b_{13}}{r} + b_{14} r^3 + b_{15} r\theta + b_{16} r\theta \log r)\sin\theta \\ &+ \sum_{n=2}^{\infty} (a_{n1} r^n + a_{n2} r^{2+n} + a_{n3} r^{-n} + a_{n4} r^{2-n})\cos n\theta \\ &+ \sum_{n=2}^{\infty} (b_{n1} r^n + b_{n2} r^{2+n} + b_{n3} r^{-n} + b_{n4} r^{2-n})\sin n\theta\end{aligned} \tag{6.2.50}$$

where a_n, $a_{nm,}$ and b_{nm} are constants to be determined. Note that this general solution is restricted to the periodic case, which has the most practical applications since it allows the Fourier method to be applied to handle general boundary conditions.

We will now explore a few specific example solutions using these listed methods, and these will focus on a simple Cartesian geometry, and two polar coordinate problems involving stress concentration and stress singularity.

EXAMPLE 6.2.3 SOLUTION TO A RECTANGULAR PLATE UNDER UNIFORM BIAXIAL LOADING

Consider the rectangular plate under uniform biaxial loading N_x and N_y as shown in Fig. 6.11. Determine the plane stress solution for the stresses, strains, and displacements.

Solution: For such Cartesian geometries, we use the polynomial/power series representation (6.2.49). Since a uniform distribution of stress in the plate is expected, based on relations (6.2.47) we are motivated to try a stress function of the general form $\phi(x, y) = Ax^2 + By^2$, where A and B are constants to be determined. Using (6.2.47), the stresses take the general form

$$T_{xx} = \frac{\partial^2 \phi}{\partial y^2} = 2B, \quad T_{yy} = \frac{\partial^2 \phi}{\partial x^2} = 2A, \quad T_{xy} = -\frac{\partial^2 \phi}{\partial x \partial y} = 0 \tag{6.2.51}$$

The boundary conditions on this problem are all traction type and because the boundaries are coordinate surfaces, they will reduce to a stress specification as per our previous discussion (see Fig. 6.9). Thus, the boundary conditions are

$$\begin{aligned}T_{xx}(\pm a, y) &= N_x, \quad T_{yy}(x, \pm b) = N_y \\ T_{xy}(\pm a, y) &= T_{xy}(x, \pm b) = 0\end{aligned} \tag{6.2.52}$$

Applying these conditions to the general stress field (6.2.51) determines the constants $A = N_y / 2$ and $B = N_x / 2$, and thus the stress field is now determined

$$T_{xx} = N_x, \quad T_{yy} = N_y, \quad T_{xy} = 0 \tag{6.2.53}$$

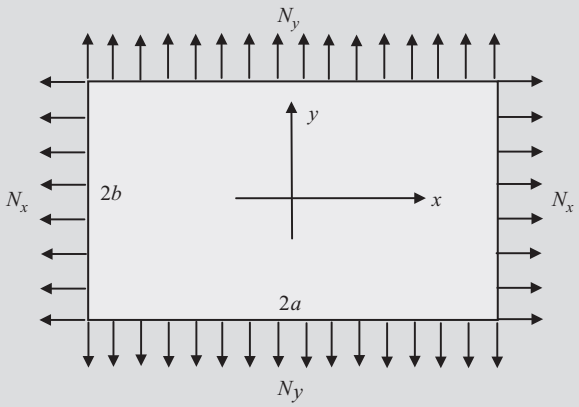

FIGURE 6.11

Rectangular plate under uniform biaxial loading.

The strains follow from Hooke's law $(6.2.31)_2$, for the plane stress case

$$\begin{aligned}
\varepsilon_x &= \frac{1}{E}(T_{xx} - \nu T_{yy}) = \frac{1}{E}(N_x - \nu N_y) \\
\varepsilon_y &= \frac{1}{E}(T_{yy} - \nu T_{xx}) = \frac{1}{E}(N_y - \nu N_x) \\
\varepsilon_{xy} &= \frac{1+\nu}{E} T_{xy} = 0
\end{aligned} \tag{6.2.54}$$

Finally, using the strain displacement relations (6.2.28)

$$\begin{aligned}
&\frac{\partial u}{\partial x} = \varepsilon_x = \frac{1}{E}(N_x - \nu N_y) \Rightarrow u = \frac{x}{E}(N_x - \nu N_y) + f(y) \\
&\frac{\partial v}{\partial y} = \varepsilon_y = \frac{1}{E}(N_y - \nu N_x) \Rightarrow v = \frac{y}{E}(N_y - \nu N_x) + g(x) \\
&\frac{\partial u}{\partial y} + \frac{\partial v}{\partial x} = 2\varepsilon_{xy} = 0 \Rightarrow f'(y) + g'(x) = 0
\end{aligned} \tag{6.2.55}$$

Following the arguments and steps in Example 3.11.2, we find that $g'(x) = -f'(y) = \text{constant}$, and these results can be easily integrated to get $f(y) = -\omega_o y + u_o$, and $g(x) = \omega_o x + v_o$. Thus, the displacement field becomes

$$\begin{aligned}
u &= \frac{x}{E}(N_x - \nu N_y) + u_o - \omega_o y \\
v &= \frac{y}{E}(N_y - \nu N_x) + v_o + \omega_o x
\end{aligned} \tag{6.2.56}$$

where ω_o, u_o, v_o are arbitrary constants of integration. The expressions $f(y)$ and $g(x)$ represent *rigid-body motion* terms where ω_o is the rotation about the

z-axis, and u_o and v_o are the translations in the x- and y-directions. Such terms will always result from the integration of the strain–displacement relations, and it is noted that they do not contribute to the strain or stress field. Thus *the displacements are determined from the strain field only up to an arbitrary rigid-body motion*. Additional boundary conditions on the displacements are needed to explicitly determine these terms. For example, if we agree that the center of the plate does not move, then $u_o = v_o = 0$; and if the x-axis does not rotate, then $\omega_o = 0$; and then all rigid-body terms will vanish and $f = g = 0$.

Notice for this very simple problem that the stress and strain field was uniform (no spatial variation) and the displacements varied linearly with position. The next two examples will explore elasticity solutions with significant variation in stress distribution including concentration and singularity behaviors.

EXAMPLE 6.2.4 SOLUTION TO A STRESS CONCENTRATION PROBLEM OF A STRESS-FREE HOLE IN AN INFINITE MEDIUM UNDER UNIAXIAL FAR-FIELD LOADING

Determine the elastic stress distribution in an infinite medium with a circular stress-free hole subjected to a uniform far-field tension T in a single direction as shown in Fig. 6.12. For ease of solution, we choose the loading direction to coincide with the x-axis and the hole radius is a.

Solution: For this geometry, it is best to formulate the problem in polar coordinates as shown. The boundary conditions on the problem are zero stresses on the hole and uniform axial stress at infinity:

$$\begin{aligned} T_{rr}(a,\theta) &= T_{r\theta}(a,\theta) = 0 \\ T_{rr}(\infty,\theta) &= \frac{T}{2}(1+\cos 2\theta) \\ T_{\theta\theta}(\infty,\theta) &= \frac{T}{2}(1-\cos 2\theta) \\ T_{r\theta}(\infty,\theta) &= -\frac{T}{2}\sin 2\theta \end{aligned} \tag{6.2.57}$$

Note that the far-field conditions have been determined using the transformation laws established in Exercise 4.4.

We first consider the state of stress in the medium if there was no hole. This stress field is simply $T_{xx} = T, \quad T_{yy} = T_{xy} = 0$ and can be derived from the Airy stress function

$$\phi = \frac{1}{2}Ty^2 = \frac{T}{2}r^2\sin^2\theta = \frac{T}{4}r^2(1-\cos 2\theta)$$

The presence of the hole acts to disturb this uniform field. We expect that this disturbance will be local in nature, and thus the disturbed field will disappear as we move far away from the hole. Based on this, we choose a trial

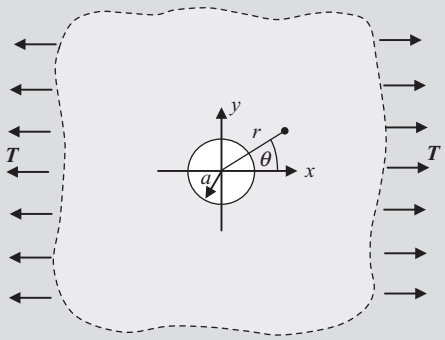

FIGURE 6.12

Stress-free hole in an infinite medium under uniform far-field loading.

solution that includes the axisymmetric and cos 2θ terms from the general Michell solution (6.2.50):

$$\begin{aligned}\phi &= a_0 + a_1 \log r + a_2 r^2 + a_3 r^2 \log r \\ &\quad + (a_{21} r^2 + a_{22} r^4 + a_{23} r^{-2} + a_{24}) \cos 2\theta\end{aligned} \tag{6.2.58}$$

Using the polar coordinate forms, the stresses corresponding to this Airy function are

$$\begin{aligned}T_{rr} &= \frac{1}{r}\frac{\partial \phi}{\partial r} + \frac{1}{r^2}\frac{\partial^2 \phi}{\partial \theta^2} = a_3(1 + 2\log r) + 2a_2 + \frac{a_1}{r^2} - (2a_{21} + \frac{6a_{23}}{r^4} + \frac{4a_{24}}{r^2})\cos 2\theta \\ T_{\theta\theta} &= \frac{\partial^2 \phi}{\partial r^2} = a_3(3 + 2\log r) + 2a_2 - \frac{a_1}{r^2} + (2a_{21} + 12a_{22} r^4 + \frac{6a_{23}}{r^4})\cos 2\theta \\ T_{r\theta} &= -\frac{\partial}{\partial r}\left(\frac{1}{r}\frac{\partial \phi}{\partial \theta}\right) = (2a_{21} + 6a_{22} r^2 - \frac{6a_{23}}{r^4} - \frac{2a_{24}}{r^2})\sin 2\theta\end{aligned} \tag{6.2.59}$$

For finite stresses at infinity, we must take $a_3 = a_{22} = 0$. Applying the five boundary conditions in (6.2.57) generates five simple algebraic equations to solve for the remaining five unknown constants giving

$$a_1 = -\frac{a^2 T}{2}, \quad a_2 = \frac{T}{4}, \quad a_{21} = -\frac{T}{4}, \quad a_{23} = -\frac{a^4 T}{4}, \quad a_{24} = \frac{a^2 T}{2}$$

Substituting these values back into (6.2.59) gives the stress field

$$\begin{aligned}T_{rr} &= \frac{T}{2}\left(1 - \frac{a^2}{r^2}\right) + \frac{T}{2}\left(1 + \frac{3a^4}{r^4} - \frac{4a^2}{r^2}\right)\cos 2\theta \\ T_{\theta\theta} &= \frac{T}{2}\left(1 + \frac{a^2}{r^2}\right) - \frac{T}{2}\left(1 + \frac{3a^4}{r^4}\right)\cos 2\theta \\ T_{r\theta} &= -\frac{T}{2}\left(1 - \frac{3a^4}{r^4} + \frac{2a^2}{r^2}\right)\sin 2\theta\end{aligned} \tag{6.2.60}$$

The strain and displacement fields could then be determined using the standard procedures used previously.

The hoop stress variation around the boundary of the hole is given by

$$T_{\theta\theta}(a,\theta) = T(1 - 2\cos 2\theta) \tag{6.2.61}$$

and this is shown in the polar plot in Fig. 6.13. This distribution indicates that the stress is negative T at $\theta = 0$, actually vanishes at $\theta = \pm 30°$ and leads to a maximum value at $\theta = \pm 90°$:

$$T_{\theta\theta\,\max} = T_{\theta\theta}(a, \pm\pi/2) = 3T \tag{6.2.62}$$

Therefore, there is a stress concentration factor of 3 for this problem. The effects of the hole in perturbing the uniform stress field can be shown by plotting the stress variation with radial distance. Considering the case of the hoop stress $T_{\theta\theta}$ at an angle $\pi/2$, Fig. 6.13 also illustrates the distribution of $T_{\theta\theta}(r, \pi/2)/T$ vs nondimensional radial distance r/a. It is seen that the stress concentration around the hole is highly localized and decays very rapidly, essentially disappearing when $r > 5a$. These results come from MATLAB Code C-4.

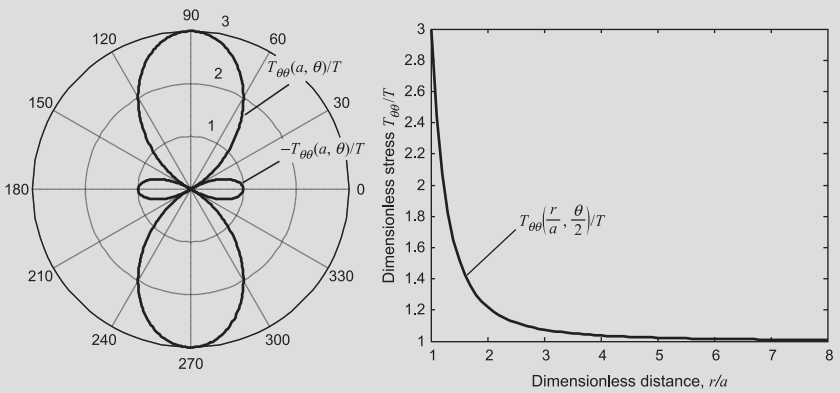

(Hoop stress around hole boundary)

(Hoop stress vs radial distance from hole)

FIGURE 6.13

$T_{\theta\theta}$ stress behavior for stress concentration around hole.

EXAMPLE 6.2.5 SOLUTION TO A HALF-SPACE UNDER A CONCENTRATED NORMAL FORCE

Determine the stress distribution in an elastic half-space that carries a concentrated normal force acting on the free surface as illustrated in Fig. 6.14. This problem is commonly known as the *Flamant problem*.

Solution: Specifying boundary conditions for such problems with concentrated loadings requires a little modification of our previous examples. For this case, the tractions on any semicircular arc C enclosing the origin must balance the applied concentrated loadings. Since the area of such an arc is proportional to the radius r, the stresses must be of the order $1/r$ to allow such an equilibrium statement to hold on any radius. The appropriate terms in the general Michell solution (6.2.50) that will give stresses of the order $1/r$ are specified by

$$\phi = (a_{12} r \log r + a_{15} r\theta)\cos\theta + (b_{12} r \log r + b_{15} r\theta)\sin\theta \tag{6.2.63}$$

The stresses resulting from this stress function are

$$\begin{aligned} T_{rr} &= \frac{1}{r}[(a_{12} + 2b_{15})\cos\theta + (b_{12} - 2a_{15})\sin\theta] \\ T_{\theta\theta} &= \frac{1}{r}[a_{12}\cos\theta + b_{12}\sin\theta] \\ T_{r\theta} &= \frac{1}{r}[a_{12}\sin\theta - b_{12}\cos\theta] \end{aligned} \tag{6.2.64}$$

With zero normal and shear stresses on $\theta = 0$ and π, $a_{12} = b_{12} = 0$ and thus $T_{\theta\theta} = T_{r\theta} = 0$ everywhere. Therefore, this state of stress is sometimes called

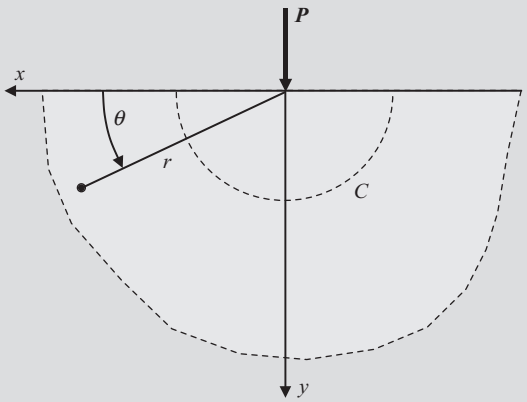

FIGURE 6.14

Half-space under concentrated normal force.

a *radial distribution*. To determine the remaining constants a_{15} and b_{15}, we apply the equilibrium statement that the summation of the tractions over the semicircular arc C of radius a must balance the applied loadings,

$$\begin{aligned} 0 &= -\int_0^{\pi} T_{rr}(a,\theta) a \cos\theta \, d\theta = -\pi b_{15} \\ P &= -\int_0^{\pi} T_{rr}(a,\theta) a \sin\theta \, d\theta = \pi a_{15} \end{aligned} \tag{6.2.65}$$

Thus, the constants are determined as $a_{15} = P/\pi$ and $b_{15} = 0$, and the stress field is now given by

$$\begin{aligned} T_{rr} &= -\frac{2P}{\pi r}\sin\theta \\ T_{\theta\theta} &= T_{r\theta} = 0 \end{aligned} \tag{6.2.66}$$

As expected, the stress field is singular at the origin directly under the point loading.

The Cartesian components corresponding to this stress field are determined using the transformation relations given in Exercise 4.5. The results are found to be

$$\begin{aligned} T_{xx} &= T_{rr}\cos^2\theta = -\frac{2Px^2y}{\pi(x^2+y^2)^2} \\ T_{yy} &= T_{rr}\sin^2\theta = -\frac{2Py^3}{\pi(x^2+y^2)^2} \\ T_{xy} &= T_{rr}\sin\theta\cos\theta = -\frac{2Pxy^2}{\pi(x^2+y^2)^2} \end{aligned} \tag{6.2.67}$$

The distribution of the normal and shearing stresses on a horizontal line located a distance a below the free surface of the half-space is shown in Fig. 6.15. The maximum normal stress directly under the load is given

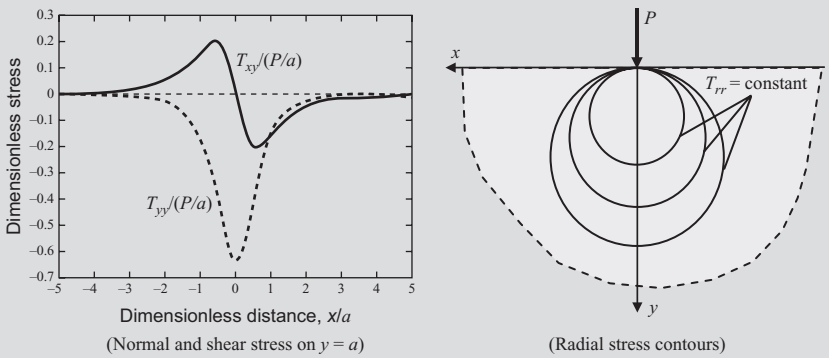

FIGURE 6.15

Stress distribution plots for Flamant problem.

by $|T_{yy}| = 2P/\pi a$. It is observed that the effects of the concentrated loading are highly localized, and the stresses are vanishingly small for distances where $x > 5a$. Stress contours of T_{rr} are also shown in Fig. 6.15. From solution (6.2.66), lines of constant radial stress are circles tangent to the half-space surface at the loading point. These results come from MATLAB Code C-5.

Many additional analytical elasticity solutions exist in the literature for a large variety of both two- and three-dimensional problem types. The interested reader is directed to the general references given at the beginning of this section. Dynamic problems in linear elasticity, sometimes referred to as *elastodynamics*, forms yet another field of study that contains hyperbolic partial differential field equations yielding wave propagation phenomena. This study will not be discussed here, but details can be found in Achenbach (1976) and Graff (1991).

6.3 IDEAL NONVISCOUS FLUIDS

We now begin our study of fluid mechanics and will first explore the simplest case of an ideal nonviscous fluid. Experiments indicate that some media cannot sustain a shear stress and be in static equilibrium. A deformation or *flow* will continue as long as any shear stress is applied. This type of behavior is normally associated with what we call a *fluid*. Fluids are commonly separated into liquids and gases. A liquid is generally difficult to compress, has an approximate fixed volume, and takes the shape the container that it is placed in. On the other hand, a gas can easily be compressed and will tend to expand unless it is confined in a container. Liquids will form a free surface (under normal gravity conditions), whereas a gas will not. Unlike elastic solids, the constitutive response for fluids indicates that the magnitude of applied shear stress is not a function of the strain, but rather is related to the *rate of strain*. However, in some cases, this functional relationship is very small, and so we can model this special type of material by concluding that the fluid is *frictionless* or *inviscid* and that no shearing stresses will be present during deformation. We will now briefly explore this type of fluid behavior and the viscous fluid case will be developed later in Section 6.4. Further, more detailed information on fluid mechanics can be found in Batchelor (2010), White (2016), Lamb (1993), Milne-Thomson (1974), and Schlichting (2017).

6.3.1 CONSTITUTIVE LAW

For the ideal nonviscous fluid, no shear stress will be present even under flow, and thus only a hydrostatic pressure p will exist in such a continuum. Therefore, the constitutive law reduces to the simple form

$$\boldsymbol{T} = -p\boldsymbol{I} \quad or \quad T_{ij} = -p\delta_{ij} \tag{6.3.1}$$

This type of material is commonly referred to as an *elastic fluid*. Often there exists an *equation of state* relating the pressure to the density

$$p = p(\rho) \tag{6.3.2}$$

and for such a case we say that the fluid is *barotropic*. Note that for a thermomechanical theory, the equation of state would include the temperature as well, that is, $p = p(\rho, \theta)$.

6.3.2 GENERAL FORMULATION

In order to provide a general formulation for inviscid flow problems, we start by using the constitutive form (6.3.1) in the equations of motion (5.36), and this gives the result

$$-\frac{1}{\rho}\nabla p + \boldsymbol{b} = \frac{\partial \boldsymbol{v}}{\partial t} + \boldsymbol{v}\cdot\nabla\boldsymbol{v} \tag{6.3.3}$$

which are called *Euler's equations of motion for inviscid fluids.* Notice that because of the convection term $\boldsymbol{v}\cdot\nabla\boldsymbol{v}$ in the acceleration, these equations will be nonlinear.

If we further restrict our study and consider only incompressible inviscid fluids, the equation of state reduces to

$$\rho = \text{constant} \tag{6.3.4}$$

and the conservation of mass or continuity equation as per relation (5.2.5) then becomes

$$\nabla\cdot\boldsymbol{v} = 0 \tag{6.3.5}$$

Consider next the case of *irrotational flows* where the vorticity or angular velocity vectors are zero. Using results (3.13.5),

$$\boldsymbol{w} = \frac{1}{2}\nabla\times\boldsymbol{v} = 0 \tag{6.3.6}$$

Next employing Stoke's Theorem (2.17.14), result (6.3.6) then implies that

$$\oint_C \boldsymbol{v}\cdot d\boldsymbol{s} = 0 \tag{6.3.7}$$

where $d\boldsymbol{s}$ is the tangential differential element along the closed contour C. In fluid mechanics, the integral appearing in relation (6.3.7) in commonly denoted as the *circulation* Γ around contour C. It can be shown (see Malvern, 1969 for details) that *for a barotropic fluid with conservative body forces, the circulation around any material contour will be zero*, a result known as *Kelvin's Theorem*. It can be shown that this theorem implies that if an inviscid fluid flow starts as irrotational it will remain that way, and this is one reason why this type of flow kinematics is assumed.

In light of relation (6.3.7), we conclude that the integrand $\boldsymbol{v}\cdot d\boldsymbol{s}$ must be an exact differential, and thus we can write

$$\boldsymbol{v} = \nabla\phi \tag{6.3.8}$$

where ϕ is a scalar *potential function*. Using this result in the continuity relation (6.3.5) gives

$$\nabla^2\phi = 0 \tag{6.3.9}$$

and thus the potential function satisfies the classical Laplace equation. This relation is then the governing equation for irrotational flows of incompressible inviscid fluids. This is often called *potential flow theory*.

For the potential flow problem, let us assume that the body force is derivable from a potential function such that $\boldsymbol{b} = -\nabla\Omega$. Under these conditions, Euler's equation (6.3.3) becomes

$$-\nabla\left(\frac{p}{\rho}+\Omega\right) = \frac{\partial \boldsymbol{v}}{\partial t} + \boldsymbol{v}\cdot\nabla\boldsymbol{v} \tag{6.3.10}$$

Using (6.3.8), this can be rewritten as

$$\nabla\left(\frac{\partial\phi}{\partial t}+\frac{v^2}{2}+\frac{p}{\rho}+\Omega\right) = 0 \tag{6.3.11}$$

where $v^2 = \boldsymbol{v}\cdot\boldsymbol{v}$. Relation (6.3.11) then implies that

$$\frac{\partial\phi}{\partial t}+\frac{v^2}{2}+\frac{p}{\rho}+\Omega = f(t) \tag{6.3.12}$$

where $f(t)$ is an arbitrary function of time. If the flow is *steady*, then (6.3.12) reduces to

$$\frac{v^2}{2}+\frac{p}{\rho}+\Omega = 0 \tag{6.3.13}$$

Relations (6.3.12) and (6.3.13) are known as *Bernoulli's equations*. This derivation also shows that irrotational flows are always dynamically possible under the stated conditions, since the equations of motion will always be integrable to yield (6.3.12) and (6.3.13).

We will focus our problem solution formulation for only two-dimensional flow problems in the x,y-plane, and thus the velocity vector will have two components v_x and v_y. The distributions of these velocities are the unknowns to be found. In addition to the potential formulation given by relations (6.3.8) and (6.3.9), another common solution approach is to introduce a stream function $\psi(x,y)$. Lines of ψ = constant are called *streamlines* and the fluid velocity vector is always *tangent* to streamlines. The potential function and the stream function are related through the following equations

$$\begin{aligned} v_x &= \frac{\partial\phi}{\partial x} = \frac{\partial\psi}{\partial y} \\ v_y &= \frac{\partial\phi}{\partial y} = -\frac{\partial\psi}{\partial x} \end{aligned} \tag{6.3.14}$$

Using relations (6.3.14), it can be shown that contours of the potential function and stream function are orthogonal to each other and that the stream function also satisfies Laplace's equation

$$\nabla^2\psi=\frac{\partial^2\psi}{\partial x^2}+\frac{\partial^2\psi}{\partial y^2}=0 \tag{6.3.15}$$

Notice that the governing equations in terms of the stream or potential function reduce to a single relation, thus making the flow solution easier to be found.

The boundary conditions for such inviscid flow problems are quite simple. For fluid contact with a fixed surface, the normal velocity component would vanish and the tangential component would not be specified. Actually the tangential component will be determined as part of the flow solution. Thus, based on our previous definitions of the potential and stream function, we can either specify the normal derivative $d\phi/dn = 0$ or the condition $\psi =$ constant on a fixed surface in contact with the inviscid fluid flow. As we shall see in Section 6.4, these boundary conditions will be different for viscous fluids.

6.3.3 PROBLEM SOLUTIONS

We now explore the solution to a few selected two-dimensional potential flow problems. This involves solving the governing Laplace equation (6.3.9) or (6.3.15) for the specific problem geometry. Once the potential or stream function is determined, relation (6.3.14) can then be used to find the velocity distribution. We will use MATLAB software to plot velocity vector distributions. As before, analytical solutions are most likely to be found for two-dimensional problems of limited geometric complexity.

EXAMPLE 6.3.1 TWO-DIMENSIONAL UNIFORM FLOW

Consider uniform two-dimensional flow with velocity V in the x-direction. Determine the potential and stream functions and plot their contours in the x,y-plane.

Solution: For this simple problem, the velocity distribution is already given as $v_x = V$ and $v_y = 0$. Using relations (6.3.14),

$$\begin{aligned} v_x &= \frac{\partial\phi}{\partial x}=\frac{\partial\psi}{\partial y}=V \\ v_y &= \frac{\partial\phi}{\partial y}=-\frac{\partial\psi}{\partial x}=0 \end{aligned} \quad\Rightarrow\quad \begin{aligned} \phi &= Vx+\text{constant} \\ \psi &= Vy+\text{constant} \end{aligned} \tag{6.3.16}$$

The velocity distribution and contours of the stream and potential functions are shown in Fig. 6.16 for the region $0 \le (x, y) \le 1$. The flow is uniform in the x-direction and the contours form an orthogonal vertical and horizontal mesh. Note these results come from MATLAB Code C-6.

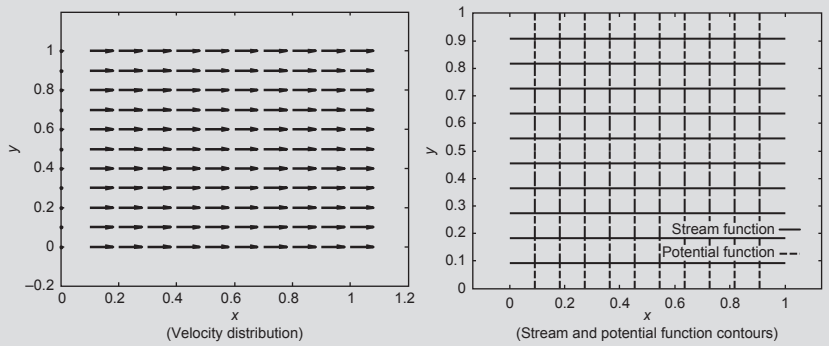

FIGURE 6.16

Velocity and stream and potential functions for uniform flow problem.

EXAMPLE 6.3.2 INVISCID FLOW IN A 90° CORNER

Determine the potential fluid flow in a 90° corner as shown in Fig. 6.17. Assume that the flow occurs down in the vertical and off to the right in the horizontal directions.

Solution: From our previous definitions, the boundaries $x = 0$ and $y = 0$ will be a streamline. Further, the origin $x = y = 0$ will be a stagnation point with zero fluid velocity. Since these boundary streamlines pass through the stagnation point, they must have a value of zero, and so $\psi(0, y) = \psi(x, 0) = 0$. Based on these boundary conditions, we look for the stream function solution to Laplace's equation (6.3.15) in the form

$$\psi(x, y) = Axy \tag{6.3.17}$$

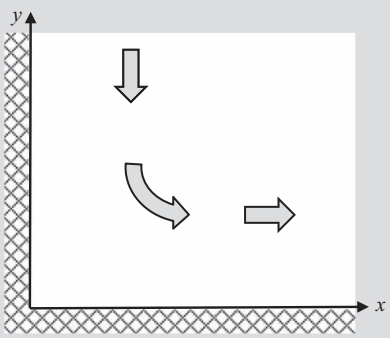

FIGURE 6.17

Flow in a corner.

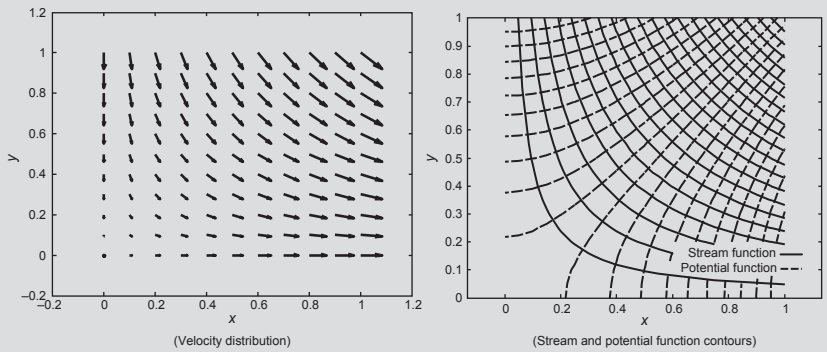

FIGURE 6.18

Velocity and stream and potential functions for corner flow problem.

where A is an arbitrary constant related to the far-field velocity. Using this form in (6.3.14), the velocity components are

$$v_x = \frac{\partial \psi}{\partial y} = Ax, \quad v_y = -\frac{\partial \psi}{\partial x} = -Ay \tag{6.3.18}$$

The potential function can then be obtained from integrating relations (6.3.14) to get

$$\phi(x, y) = \frac{1}{2} A(x^2 - y^2) \tag{6.3.19}$$

The velocity distribution and contours of the stream and potential functions are shown in Fig. 6.18 for the region $0 \le (x, y) \le 1$. As in the previous example, the contours form an orthogonal mesh. These plots come from MATLAB Code C-7.

EXAMPLE 6.3.3 INVISCID FLOW AROUND A CYLINDER

As a final example, consider the two-dimensional potential flow around a fixed cylinder of radius a as shown in Fig. 6.19. Far away from the cylinder, the flow is uniform with $v_x = U$ and $v_y = 0$. Determine the stream function solution and velocity distribution.

Solution: This problem is best formulated and solved in polar coordinates (r, θ) as shown the figure. For this case, the del operator becomes $\nabla = \boldsymbol{e}_r \dfrac{\partial}{\partial r} + \boldsymbol{e}_\theta \dfrac{1}{r} \dfrac{\partial}{\partial \theta}$ and the governing Laplace equation (6.3.15) can thus be written as

$$\nabla^2 \psi = \frac{\partial^2 \psi}{\partial r^2} + \frac{1}{r} \frac{\partial \psi}{\partial r} + \frac{1}{r^2} \frac{\partial^2 \psi}{\partial \theta^2} = 0 \tag{6.3.20}$$

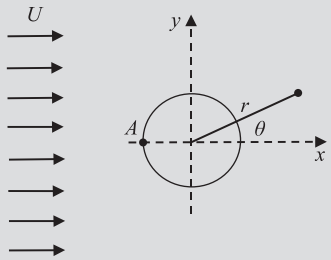

FIGURE 6.19

Two-dimensional flow around a fixed cylinder.

and the polar velocity components follow from the transformation relations in Example 2.18.1 giving the result

$$v_r = \frac{1}{r}\frac{\partial \psi}{\partial \theta}, \quad v_\theta = -\frac{\partial \psi}{\partial r} \tag{6.3.21}$$

Note that the relationship between the velocity components in Cartesian and polar coordinates can be expressed by (see Appendix B)

$$\begin{aligned} v_x &= v_r \cos\theta - v_\theta \sin\theta \\ v_y &= v_r \sin\theta + v_\theta \cos\theta \end{aligned} \tag{6.3.22}$$

Using the standard separation of variables approach, we choose $\psi = \psi(r,\theta) = R(r)T(\theta)$ and can further argue that the problem solution should be an odd function of θ. We thus try $T(\theta) = \sin\theta$, and substituting the form $\psi = R(r)\sin\theta$ into Eq. (6.3.20) gives

$$r^2 \frac{d^2R}{dr^2} + r\frac{dR}{dr} - R = 0 \tag{6.3.23}$$

which is a Euler–Cauchy differential equation. The solution follows from standard methods giving $R = C_1 r + C_2 / r$, where C_1 and C_2 are arbitrary constants to be determined from the boundary conditions. Thus, the solution for the stream function takes the form

$$\psi = \left(C_1 r + \frac{C_2}{r}\right)\sin\theta \tag{6.3.24}$$

The boundary conditions are argued in the following manner. First, we note that point A on the cylinder is a *stagnation point* in that no flow velocity can occur at this location. Since the streamline that passes through a stagnation point has a value of zero, the stream function on the entire surface of the cylinder of radius a should vanish, leading to the boundary condition $\psi(a) = 0$. Next, far away from the cylinder, the flow is supposed to be uniform and only in the x-direction so that as $r \to \infty$, $v_x = v_r \cos\theta - v_\theta \sin\theta = U$, and

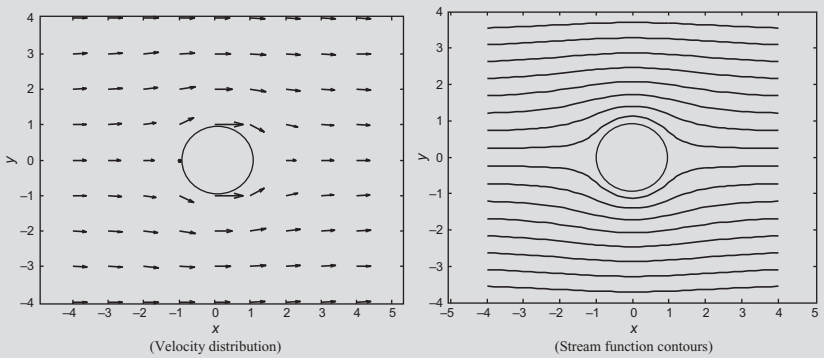

FIGURE 6.20

Velocity and stream function for flow around a cylinder.

$v_y = v_r \sin\theta + v_\theta \cos\theta = 0$. Note, however, that this second condition will be identically or automatically satisfied and thus will not yield a useful result.

Thus, the two useful boundary conditions become

$$\begin{gathered} \psi(a) = 0 \\ \lim_{r\to\infty}\left(\frac{1}{r}\frac{\partial\psi}{\partial\theta}\cos\theta + \frac{\partial\psi}{\partial r}\sin\theta\right) = U \end{gathered} \tag{6.3.25}$$

Using these two conditions gives the following values for the constants $C_1 = U$, $C_2 = -Ua^2$, and thus the solution to the problem becomes

$$\psi = Ur\left(1 - \frac{a^2}{r^2}\right)\sin\theta \tag{6.3.26}$$

Finally, the velocity solution follows from (6.3.21)

$$\begin{aligned} v_r &= \frac{1}{r}\frac{\partial\psi}{\partial\theta} = U\left(1 - \frac{a^2}{r^2}\right)\cos\theta \\ v_\theta &= -\frac{\partial\psi}{\partial r} = -U\left(1 + \frac{a^2}{r^2}\right)\sin\theta \end{aligned} \tag{6.3.27}$$

The velocity distribution and contours of the stream function are shown in Fig. 6.20. Notice the elevation of the fluid velocity near the cylinder. This behavior is analogous to the stress concentration problem shown in Example 6.2.4. These plots come from MATLAB Code C-8.

6.4 LINEAR VISCOUS FLUIDS

The previous section dealing with ideal inviscid fluids neglected the viscous effects between shear stress and rate of deformation. However, for many fluids and for many types of flows, viscous effects are significant and cannot be neglected. In light of this,

the ideal fluid constitutive law (6.3.1) must be modified to include shear stresses in the fluid continuum. Experiments have shown that these shear stresses are related to the rate of deformation of the material. Over the years, several fluid constitutive relationships have been established, and in this section we will restrict ourselves to only the *linear viscous* case. More complicated nonlinear constitutive relations for fluids will be discussed later in Chapter 8. There is a wealth of literature dealing with linear viscous flows including Serrin (1959), Batchelor (2010),White (2016), and Schlichting (2017).

6.4.1 CONSTITUTIVE LAW

We now wish to determine the linear constitutive law that describes the relationship between the stress and the rate of deformation in fluids. Numerous experiments using instruments called *viscometers* have collected data on shear stress vs shear strain rate for special flow geometries in laboratory settings. Generally, such studies involve creating a local shearing flow in a thin gap and then measure the shear stress and rate of shear strain. Fig. 6.21 illustrates a common flow geometry and shows typical qualitative results for several material types such as oils, paints, pastes, gels, polymeric fluids, cornstarch liquids, etc. It is seen that various materials have flow characteristics that are quite different. In this section, however, we will focus our studies for the case originally proposed by Newton where the functional relationship is linear, that is, $T_{12} = \mu\dot{\gamma}_{12}$, where μ is a material constant known as the *viscosity*. Furthermore, experiments indicate that a fluid at rest (i.e. zero rate of deformation) will be in a state of hydrostatic pressure. Hence, similar to the previous elastic case, we can write a general constitutive equation for a viscous fluid as

$$\begin{aligned} \boldsymbol{T} &= -p\boldsymbol{I} + \boldsymbol{f}(\boldsymbol{D}) \\ T_{ij} &= -p\delta_{ij} + f_{ij}(D_{kl}) \end{aligned} \tag{6.4.1}$$

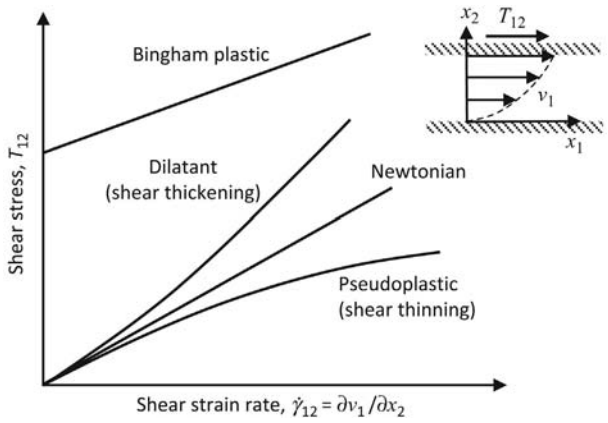

FIGURE 6.21

Typical shear stress vs shear strain rate behaviors.

where $\boldsymbol{D}$ is the rate of deformation tensor define by $(3.13.4)_1$ as $\boldsymbol{D} = \left((\nabla \boldsymbol{v}) + (\nabla \boldsymbol{v})^T\right)/2$. Such a constitutive relation commonly defines a *Stokesian fluid*. It is further assumed that $\boldsymbol{f}(\boldsymbol{0}) = \boldsymbol{0}$, so that under zero deformation rate, only hydrostatic pressure will be present.

Now the fluid constitutive form is to be linear and thus (6.4.1) must reduce to

$$T_{ij} = -p\delta_{ij} + M_{ijkl} D_{kl} \tag{6.4.2}$$

Normally, fluids are not nonhomogeneous or anisotropic, and therefore the fourth-order tensor M_{ijkl} is a constant tensor with the isotropic form

$$M_{ijkl} = \alpha\delta_{ij}\delta_{kl} + \beta\delta_{ik}\delta_{jl} + \gamma\delta_{il}\delta_{jk} \tag{6.4.3}$$

where α, β, and γ are arbitrary constants. Substituting (6.4.3) into (6.4.2) yields

$$T_{ij} = -p\delta_{ij} + \lambda D_{kk}\delta_{ij} + 2\mu D_{ij} \tag{6.4.4}$$

where we have let $\lambda = \alpha$ and $2\mu = \beta + \gamma$. Constitutive relation (6.4.4) represents the *Navier–Poisson law of linear viscous or Newtonian fluids*. Note the similarity with the isotropic linear elastic constitutive development given by relation (6.2.20). Here, the two material constants λ and μ are referred to as the *dilatational and shear viscosity coefficients*, respectively. For the case of an incompressible fluid, $D_{kk} = 0$, and (6.4.4) reduces to

$$T_{ij} = -p\delta_{ij} + 2\mu D_{ij} \tag{6.4.5}$$

It should be pointed out that the previous constitutive relations were all developed for what is called *laminar or streamline flow*. Such a flow is generally described as orderly motion in which fluid particles move smoothly in adjacent layers sliding over each other with no mixing between layers. Motions of this type are common at low fluid velocities. However, at high speeds, fluid motions often become more random resulting in significant motions normal to these laminae directions. This type of random intermingling fluid motion is referred to a *turbulent flow*. For many particular flow geometries, the transition from laminar to turbulent flow can be determined by the value or range of a particular dimensionless parameter called the *Reynold's number*. This number is the ratio of the fluid's inertial force to the shearing force, that is, how fast the fluid is moving relative to how large is its viscosity. Thus, it is directly proportional to the fluid velocity and inversely proportional to the viscosity. For turbulent flow, the shear stress must be modified by momentum transfer between flow layers due to turbulent eddies and mixing. Thus, the original Newtonian linear relation $T_{12} = \mu\dot{\gamma}_{12}$ would require some modification with an additional term to account for this behavior. Such turbulent flow theories are well established (see Batchelor, 2010; White, 2016; Schlichting, 2017); however, we will not pursue them here.

Fig. 6.22 illustrates a special flow geometry called a *shear flow* velocity field which is specified by

$$\boldsymbol{v} = \{v_1(x_2), 0, 0\} \tag{6.4.6}$$

For this flow, the rate of deformation tensor becomes

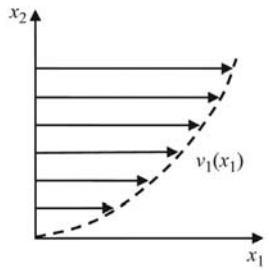

FIGURE 6.22

Shear flow geometry.

$$\boldsymbol{D} = \frac{1}{2}\begin{bmatrix} 0 & \dfrac{\partial v_1}{\partial x_2} & 0 \\ \dfrac{\partial v_1}{\partial x_2} & 0 & 0 \\ 0 & 0 & 0 \end{bmatrix} \tag{6.4.7}$$

Using the fluid constitutive law (6.4.4) then yields the simplified result for the shear stress

$$T_{12} = \mu \frac{\partial v_1}{\partial x_2} \Rightarrow \mu = \frac{T_{12}}{\partial v_1 / \partial x_2} \tag{6.4.8}$$

Thus, the viscosity coefficient μ is the slope of the T_{12} vs $\partial v_1 / \partial x_2$ curve as shown previously in Fig. 6.21.

Going back to the general flow case, the Newtonian fluid constitutive law (6.4.4) gives

$$\frac{1}{3}T_{kk} = -p + \left(\lambda + \frac{2}{3}\mu\right) D_{kk} \tag{6.4.9}$$

and thus

$$\begin{aligned} -\frac{1}{3}T_{kk} - p &= -\left(\lambda + \frac{2}{3}\mu\right) D_{kk} \\ &= -\left(\lambda + \frac{2}{3}\mu\right) v_{k,k} \\ &= \left(\lambda + \frac{2}{3}\mu\right) \frac{1}{\rho}\frac{D\rho}{Dt} \end{aligned} \tag{6.4.10}$$

where we have used the continuity equation (5.2.4). The quantity $(\lambda + 2/3\mu)$ is normally called the *bulk viscosity*. Stokes assumed that $p = -(1/3)T_{kk}$, and thus claimed that for general flows

$$\lambda + \frac{2}{3}\mu = 0 \tag{6.4.11}$$

which is the somewhat controversial *Stokes condition* used throughout classical fluid mechanics. Truesdell (1966) gives an extended discussion on the history and some experimental contradictions associated with this assumption. Nevertheless, most fluid dynamics studies incorporate Stokes condition $\lambda = -(2/3)\mu$, which eliminates the dilatational viscosity and thus constitutive relation (6.4.4) becomes

$$T_{ij} = -p\delta_{ij} - \frac{2}{3}\mu D_{kk}\delta_{ij} + 2\mu D_{ij} \tag{6.4.12}$$

6.4.2 GENERAL FORMULATION

We now wish to formulate the basic governing equations of linear viscous fluids. Problems in fluid mechanics are commonly formulated in terms of the velocity components rather than stresses. This is similar to the displacement formulation previously discussed in the linear elasticity section. Using the rate of deformation relation $(3.13.4)_1$ and constitutive relation (6.4.12) in the equations of motion (5.3.5) gives

$$\begin{aligned} -p_{,i} + \frac{\mu}{3}v_{k,ki} + \mu v_{i,kk} + \rho b_i &= \rho\left(\frac{\partial v_i}{\partial t} + v_j v_{i,j}\right) \\ -\nabla p + \frac{\mu}{3}\nabla(\nabla\cdot\boldsymbol{v}) + \mu\nabla^2\boldsymbol{v} + \rho\boldsymbol{b} &= \rho\left(\frac{\partial \boldsymbol{v}}{\partial t} + \boldsymbol{v}\cdot\nabla\boldsymbol{v}\right) \end{aligned} \tag{6.4.13}$$

These relations are called the *Navier–Stokes equations* of classical fluid mechanics. For the compressible case, Eqs. (6.4.13) must be coupled with the continuity relations and an equation of state

$$\begin{gathered} \frac{\partial\rho}{\partial t} + (\rho v_k)_{,k} = 0, \quad \frac{\partial\rho}{\partial t} + \nabla\cdot(\rho\boldsymbol{v}) = 0 \\ p = p(\rho) \end{gathered} \tag{6.4.14}$$

This will then yield an isothermal mechanical theory with five equations for the five unknowns p, ρ, v_i.

For the incompressible case, the Navier–Stokes equations reduce to

$$\begin{aligned} -p_{,i} + \mu v_{i,kk} + \rho b_i &= \rho\left(\frac{\partial v_i}{\partial t} + v_j v_{i,j}\right) \\ -\nabla p + \mu\nabla^2\boldsymbol{v} + \rho\boldsymbol{b} &= \rho\left(\frac{\partial \boldsymbol{v}}{\partial t} + \boldsymbol{v}\cdot\nabla\boldsymbol{v}\right) \end{aligned} \tag{6.4.15}$$

and these must be coupled with the incompressible form of the continuity relation

$$v_{k,k} = 0, \quad \nabla\cdot\boldsymbol{v} = 0 \tag{6.4.16}$$

This will then yield an isothermal mechanical theory with four equations for the four unknowns p, v_i. Note that because of the convective term in the acceleration, either previous form of the Navier–Stokes equations is *nonlinear*. Thus, even though we incorporated a linear constitutive law, the general problem in Newtonian fluid dynamics is nonlinear.

Boundary conditions for this fluid mechanics theory would normally be applied at a solid or free surface. On a solid surface, the fluid velocity is assumed to match the velocity of the surface. This is the so-called *no-slip condition* in which fluid particles in contact with an external boundary move with the boundary's motion. For the case of a free surface (not in contact with another body), the fluid traction would have to match those applied from the surroundings. For example, if the free surface is simply exposed to atmospheric conditions, then neglecting surface tension effects, the normal traction would be equal to the ambient pressure while the shear tractions would have to vanish. For time dependent nonsteady flows, particular initial conditions on the velocity components would be required.

6.4.3 PROBLEM SOLUTIONS

We now explore the solution to a few selected two-dimensional linear viscous flow problems. This involves solving the governing Navier–Stokes equations (6.4.13) or (6.4.15) and the associated continuity equations (6.4.14) and (6.4.16) for some specific geometries. We will use MATLAB software to plot velocity distributions. As before, analytical solutions are most likely to be found for two-dimensional problems of limited geometric complexity. We will focus on incompressible flows and will avoid the nonlinear acceleration terms by considering only steady fluid motions.

EXAMPLE 6.4.1 PLANE POISEUILLE FLOW

Consider the two-dimensional steady flow of an incompressible linearly viscous fluid between two stationary plane boundaries as shown in Fig. 6.23. We assume that the boundaries are parallel to each other and are of infinite extent. The flow occurs only in the x_1-direction and is solely a function of the x_2-coordinate. This type of flow is commonly called *plane Poiseuille flow*. Determine the velocity field for this case.

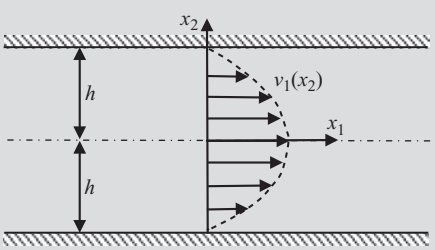

FIGURE 6.23

Plane Poiseuille flow geometry.

Solution: For this case, we assume no body forces, zero acceleration terms, and a velocity field of the form $v_1(x_2)$, $v_2 = v_3 = 0$. Under these conditions, the governing Navier–Stokes equations (6.4.13) reduce to

$$\frac{\partial p}{\partial x_1} = \mu \frac{\partial^2 v_1}{\partial x_2^2}$$
$$\frac{\partial p}{\partial x_2} = \frac{\partial p}{\partial x_3} = 0 \tag{6.4.17}$$

and the continuity equation (6.4.16) is identically satisfied.

From the second equation in (6.4.17), we conclude that the pressure will depend only on x_1, $p = p(x_1)$. Using this result in relation $(6.4.17)_1$ allows us to argue that its left-hand side depends only on x_1, whereas the right-hand side is a function only of x_2, and therefore both sides must equal and common constant. Thus, we can write

$$\frac{dp}{dx_1} = \mu \frac{d^2 v_1}{dx_2^2} = -k \tag{6.4.18}$$

where $-k$ is the constant pressure gradient in the x_1-direction, and we have chosen the constant to be negative, thus indicating that the pressure is decreasing in the flow direction. Using the second relation in (6.4.18),

$$\frac{d^2 v_1}{dx_2^2} = -\frac{k}{\mu} \Rightarrow v_1 = -\frac{k}{\mu} x_2^2 + C_1 x_2 + C_2 \tag{6.4.19}$$

where C_1 and C_2 are arbitrary constants of integration. The boundary conditions on the problem are that the velocity must vanish at the channel's top and bottom, and thus $v_1(\pm h) = 0$. This statement then gives two simple equations that allow the solution for the two unknowns C_1 and C_2. Putting these results together then gives the final form for the velocity distribution

$$v_1 = \frac{k}{2\mu}(h^2 - x_2^2) \tag{6.4.20}$$

Result (6.4.20) indicates that the velocity distribution is parabolic with a maximum value occurring at mid-channel ($x_2 = 0$) given by

$$v_{1\max} = \frac{kh^2}{2\mu} \tag{6.4.21}$$

Fig. 6.24 illustrates a MATLAB (Code C-9) plot of this velocity distribution normalized by $kh^2/2\mu$. This distribution is the same at all sections (x_1 locations) along the channel. Another quantity that is sometimes of interest is

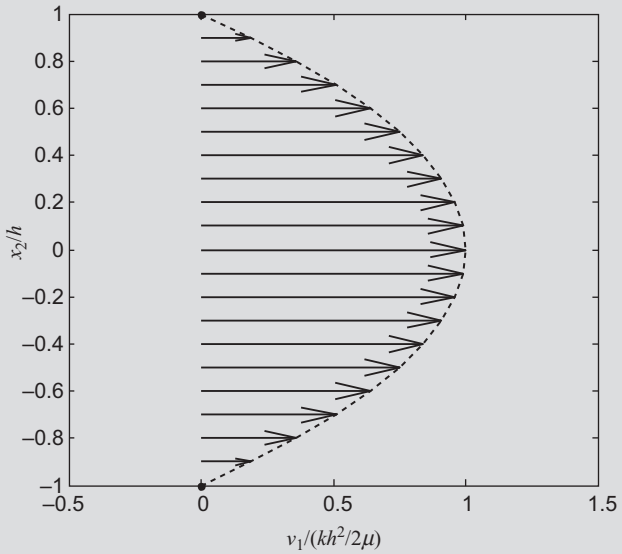

FIGURE 6.24

Plane Poiseuille flow field.

the *volume flow rate*, and for this problem the volume flow per unit time per unit x_3-width is given by integrating (6.4.18)

$$Q = \int_{-h}^{h} v_1 \, dx_2 = \frac{k}{\mu}\left(\frac{2h^3}{3}\right) \tag{6.4.22}$$

EXAMPLE 6.4.2 PLANE COUETTE FLOW

Consider the two-dimensional steady flow of an incompressible linearly viscous fluid between two plane boundaries. One boundary at $x_2 = 0$ is to remain fixed, whereas the other boundary at $x_2 = h$ moves with a constant speed V as shown in Fig. 6.25. We assume that the boundaries are parallel to each other and are of infinite extent. The flow occurs only in the x_1-direction and is solely a function of the x_2-coordinate. This type of flow is generally referred to as *plane Couette flow*. Determine the velocity field for this case.

Solution: Similar to the previous example, we assume no body forces, zero acceleration terms, and a velocity field of the form $v_1(x_2)$, $v_2 = v_3 = 0$.

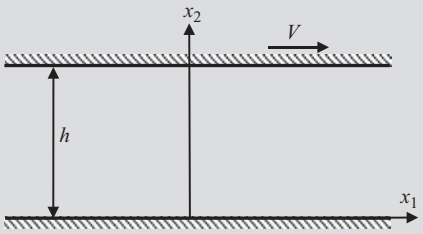

FIGURE 6.25

Plane Couette flow geometry.

Under these conditions, the continuity equation is identically satisfied and the Navier–Stokes equations again reduce to

$$\begin{aligned} \frac{\partial p}{\partial x_1} &= \mu \frac{\partial^2 v_1}{\partial x_2^2} \\ \frac{\partial p}{\partial x_2} &= \frac{\partial p}{\partial x_3} = 0 \end{aligned} \tag{6.4.23}$$

Applying the same arguments used in the previous example, we conclude that the pressure must be of the form $p = p(x_1)$, and again find

$$\frac{dp}{dx_1} = \mu \frac{d^2 v_1}{dx_2^2} = -k \tag{6.4.24}$$

where $-k$ is the constant pressure gradient in the x_1-direction. This again allows direct integration of relation (6.4.24) to determine the unknown velocity component

$$v_1 = -\frac{k}{\mu} x_2^2 + C_1 x_2 + C_2 \tag{6.4.25}$$

where C_1 and C_2 are arbitrary constants of integration. The boundary conditions on this problem are that the velocity must match with the speed of the top of the channel and vanish at the bottom. These two conditions then yield values for C_1 and C_2:

$$\begin{aligned} v_1(0) = 0 &\Rightarrow C_2 = 0 \\ v_1(h) = V &\Rightarrow C_1 = \frac{V}{h} + \frac{k}{\mu} h \end{aligned} \tag{6.4.26}$$

Putting these results together then gives the final form for the velocity distribution

$$v_1 = \frac{V}{h} x_2 + \frac{k}{\mu} (h - x_2) x_2 \tag{6.4.27}$$

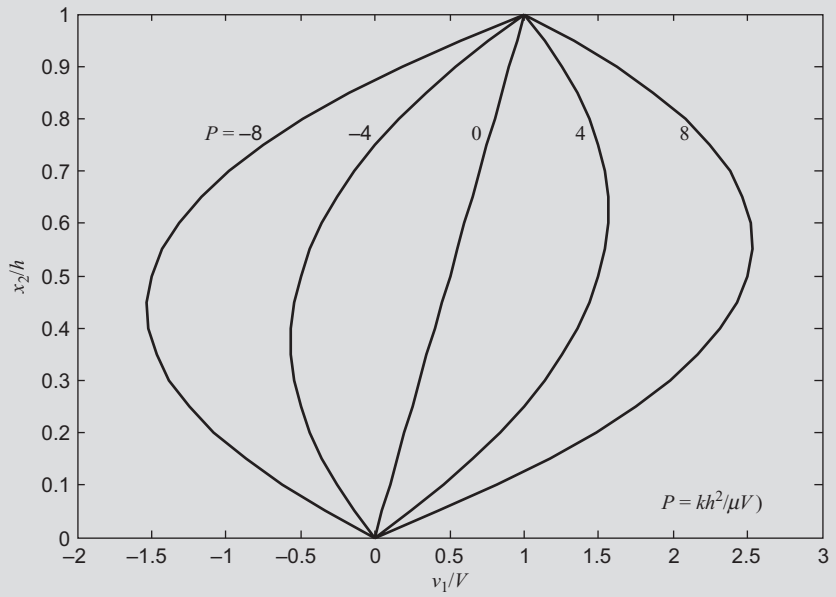

FIGURE 6.26

Velocity profiles for plane Couette flows.

For this example, the velocity distribution depends on V and will not in general be parabolic as found in Example 6.4.1 (unless $V = 0$). Fig. 6.26 shows several velocity profiles for different values of a dimensionless parameter $P = kh^2 / \mu V$. Plots are generated from MATLAB Code C-9. As $V \to 0$, $P \to \infty$ and the velocity profile becomes parabolic. Note that for the special case with no pressure gradient k, the velocity becomes simply $v_1 = \dfrac{V}{h} x_2$, which is just a linear distribution as shown in Fig. 6.26 for $P = 0$. It is also interesting to notice that for cases with $P < 0$, the flow exhibits reversal behavior with zones of both positive and negative flow directions.

EXAMPLE 6.4.3 HAGEN–POISUEILLE FLOW

We now explore the steady incompressible flow in a circular cylindrical tube and assume the velocity field has only one axisymmetric component along the tube's axis. Thus, we will use cylindrical coordinates to formulate and solve the problem which is shown in Fig. 6.27. For this flow case, the velocity field may be taken as $v_r = v_\theta = 0, \quad v_z = v_z(r)$. This type of flow is com-

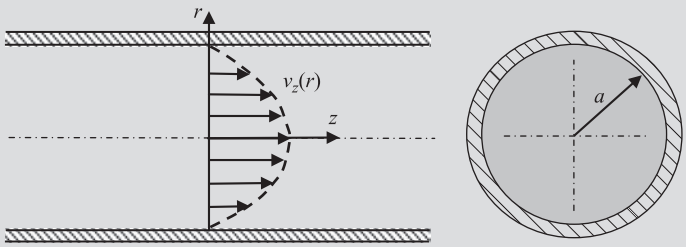

FIGURE 6.27

Hagen–Poiseuille flow geometry.

monly called *Hagen–Poiseuille flow*. We now wish to solve the viscous flow to determine the velocity $v_z = v_z(r)$.

Solution: We first explore the continuity equation (6.4.14) in cylindrical coordinates using some help from relation (2.18.20):

$$\nabla \cdot \boldsymbol{v} = \frac{1}{r}\frac{\partial}{\partial r}(rv_r) + \frac{1}{r}\frac{\partial v_\theta}{\partial \theta} + \frac{\partial v_z}{\partial z} = 0 \tag{6.4.28}$$

It is therefore observed that the given velocity field satisfies this relation identically. Next moving on to the Navier–Stokes equations in cylindrical coordinates, we find that the restricted velocity field reduces the system to

$$\begin{aligned} &\frac{\partial p}{\partial r} = \frac{\partial p}{\partial \theta} = 0 \\ &\frac{\partial p}{\partial z} = \mu\left[\frac{1}{r}\frac{d}{dr}\left(r\frac{\partial v_z}{\partial z}\right)\right] \end{aligned} \tag{6.4.29}$$

Thus, we can conclude that the pressure p depends only on z and can apply similar arguments as used in the previous examples to conclude that

$$\frac{dp}{dz} = \mu\left[\frac{1}{r}\frac{d}{dr}\left(r\frac{dv_z}{dz}\right)\right] = \text{constant} = -k \tag{6.4.30}$$

and so

$$\frac{1}{r}\frac{d}{dr}\left(r\frac{dv_z}{dz}\right) = \frac{-k}{\mu} \tag{6.4.31}$$

Relation (6.4.31) can be integrated to get

$$v_z = -\frac{k}{4\mu}r^2 + C_1 \ln r + C_2 \tag{6.4.32}$$

where C_1 and C_2 are arbitrary constants of integration. The boundary conditions on the problem are that the velocity must vanish at $r = a$, and the solution

must remain bounded for $0 \le r \le a$. The boundedness condition implies that C_1 must vanish, while the condition at $r = a$ gives $C_2 = ka^2 / 4\mu$. Putting these results together provides the final form for the velocity distribution

$$v_z = \frac{k}{4\mu}(a^2 - r^2) \tag{6.4.33}$$

and thus the axial velocity component is distributed as a paraboloid of revolution, which could be generated by a 2π rotation of the plane distribution shown in Fig. 6.24. This plot comes from MATALB Code C-9. The three-dimensional velocity vector distribution is shown in Fig. 6.28. The maximum velocity occurs at $r = 0$ and is given by

$$v_{z\max} = \frac{ka^2}{4\mu} \tag{6.4.34}$$

The volume flow rate is again found by integrating the velocity distribution (6.4.31):

$$Q = \int_0^a v_z 2\pi r \, dr = \frac{k\pi a^4}{8\mu} \tag{6.4.35}$$

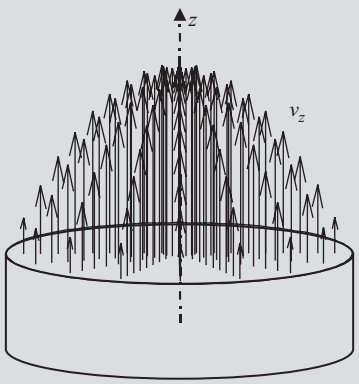

FIGURE 6.28

Hagen–Poiseuille velocity distribution.

Many additional analytical solutions to the Navier–Stokes equations exist in the literature for more general fluid conditions and more complicated flow geometries. The interested reader is directed to the general references given at the beginning of this section.

6.5 LINEAR VISCOELASTIC MATERIALS

Up to this point, we have explored the basics of linear elastic and linear viscous material models. We found that for the linear elastic case, the stress was proportional to strain and the theory was applicable to many solid materials under small deformations. On the other hand, for the linear viscous model, stress was proportional to the rate of strain and this theory had applications to materials that flow, that is, fluid mechanics. For many materials, both elastic and viscous behaviors are observed together, and such materials are generally called *viscoelastic*. For such media, the distinction between solid and fluid behavior can become somewhat difficult to make. Typical behaviors commonly include a time-dependent response with permanent deformation, and these phenomena manifest themselves as *creep*, *stress relaxation, hysteresis*, and *history-dependent response.* Such behaviors are common in high polymers (see amorphous material illustration in Fig. 6.1), many metals and plastics at elevated temperatures, bitumens, and some biological materials. In this section, we will limit discussion to linear viscoelasticity where the strains and strain rates are small and the constitutive relations will be linear. Chapter 8 will consider the more general case of nonlinear viscoelastic modeling. As with the previous linear continuum theories, our presentation here will be only introductory. Entire texts have been devoted to linear viscoelasticity, and the interested reader is directed to Christensen (2010), Flügge (1975), Bland (2016), Golden and Graham (1988), and Gutierrez-Lemini (2014).

6.5.1 CONSTITUTIVE LAWS

Often viscoelastic behaviors can be thought of as a range of response with elastic behavior, at one extreme, and viscous behavior, at the other end. In between these two ends, the material response is a combination of both elastic and viscous behaviors. As we will see, our developed constitutive models will often exhibit this same structure. To demonstrate this point, it is instructive to explore the behavior of an old toy from the 1950s called *Silly Putty.* This pliable material (silicone polymer) is a classic viscoelastic as it behaves as an elastic solid under rapid deformation, but completely changes to a flowing creeping liquid under slow loadings. The author has used this material as a classroom demonstration countless times. Fig. 6.29 illustrates two of these behaviors using a sample initially rolled into an approximate spherical ball shape. Fig. 6.29A shows a time sequence of the ball dropped onto a rigid horizontal surface. Under such dynamic impact loading, the sample bounces off of the surface with a high degree of elastic response. Fig. 6.29B illustrates the same ball sample gently placed on the rigid horizontal surface at time $t = 0$. Under just static self-weight loading, the ball slowly begins to change shape through a flowing creep deformation. After about 12 h (at room temperatures), the shape has significantly changed as shown. For larger static loadings and/or higher temperatures, this material would show even more flow behavior.

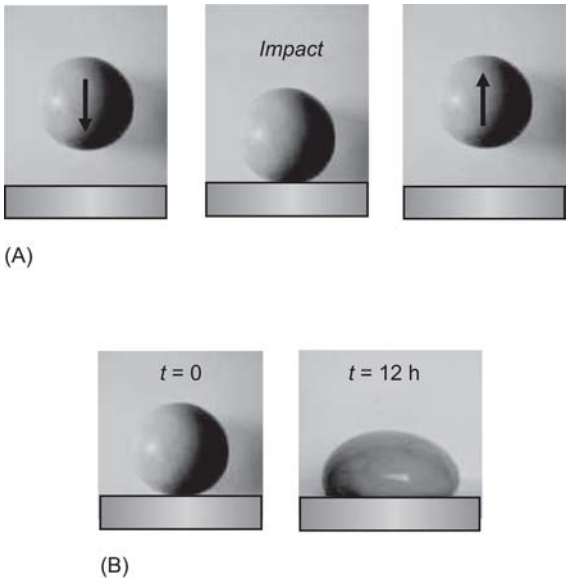

FIGURE 6.29

Viscoelastic behaviors of silly putty: (A) silly putty ball bounces off rigid horizontal surface behaving like elastic solid under rapid impact loading; (B) silly putty ball exhibiting flowing creep deformation under static loading of self-weight.

We again start our constitutive equation development with some comments on experimental observations. Extensive data on many materials indicate that if we subject a one-dimensional sample to a step change in strain

$$\varepsilon = \varepsilon_o H(t) \tag{6.5.1}$$

where $H(t)$ is the Heaviside step function defined by

$$H(t) = \begin{cases} 1, & t > 0 \\ 0, & t < 0 \end{cases} \tag{6.5.2}$$

then the stress response will be time dependent of the form

$$T = G(t)\varepsilon_o \tag{6.5.3}$$

This type of experiment is called the *stress relaxation test*, and the time function $G(t)$ is referred to as the *stress relaxation function*. Typical time plots of this behavior are shown in Fig. 6.30. It should be noted that for linear viscoelastic behavior, the relaxation function is independent of the applied strain ε_o. If $G(t) \to 0$ as $t \to \infty$, we say the material is *fluid-like*, whereas if $G(t) \to G_o > 0$ as $t \to \infty$, the material is *solid-like*. Each of these cases are illustrated in the figure.

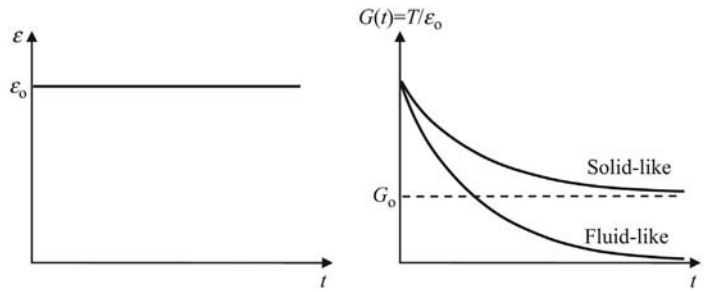

FIGURE 6.30

Stress relaxation behaviors for viscoelastic materials.

Next, consider another one-dimensional standard experiment where the sample is subjected to a step function in stress

$$T = T_o H(t) \tag{6.5.4}$$

Under this type of loading, many materials will exhibit the following time dependent strain response

$$\varepsilon = J(t) T_o \tag{6.5.5}$$

where $J(t)$ is called the *creep function* or *creep compliance*. Again note that for linear viscoelastic behavior, the creep function is independent of the applied stress T_o. If $J(t) \to \infty$ as $t \to \infty$, we say the material is *fluid-like*, whereas if $J(t) \to J_o > 0$ as $t \to \infty$, the material is *solid-like*. These cases are illustrated in Fig. 6.31.

6.5.1.1 Analog or mechanical viscoelastic constitutive models

Past studies of viscoelastic materials have often employed one-dimensional analog or mechanical models to develop simplified constitutive relations between stress, stress rates, strain, and strain rates. While this approach is simplistic and nontensorial, it does allow one to combine elastic and viscous behaviors in various ways. The

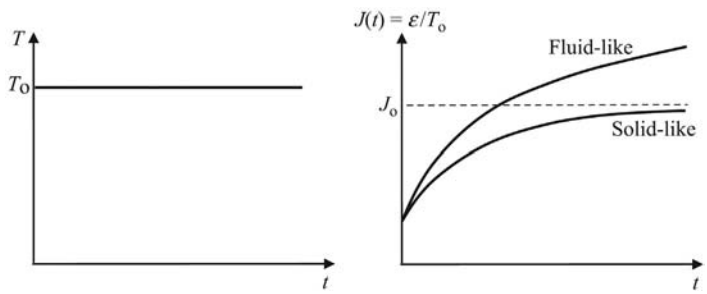

FIGURE 6.31

Creep compliance behaviors for viscoelastic materials.

scheme also brings out fundamental properties and definitions and provides a means to extend these fundamentals to multidimensional relations.

We start this method by defining the basic elastic and viscous elements. Within these models, axial force will represent the continuum stress, and axial deformation and velocity will represent the strain and strain rate. The particular stress or strain component to be modeled could be normal, shear, or volumetric; however, further discussion will be needed to extend things to multi-dimensional relations. The fundamental elastic element is a *spring* with a linear force–deformation stiffness E, as shown in Fig. 6.32. The element's constitutive law is then simply

$$T = E\varepsilon \tag{6.5.6}$$

(a) Elastic element, $T = E\varepsilon$ (b) Viscous element, $T = \eta\dot{\varepsilon}$

FIGURE 6.32

Basic elastic and viscous elements.

The relaxation and creep functions for just the spring element follow from the previous definitions

$$\begin{aligned} G(t) &= E \\ J(t) &= 1/E \end{aligned} \tag{6.5.7}$$

which are all constants.

The fundamental viscous element is a *dashpot* with a linear force–deformation rate viscosity η, as illustrated in Fig. 6.32, and thus the constitutive law is

$$T = \eta\dot{\varepsilon} \tag{6.5.8}$$

Note that superimposed dots used here simply indicate ordinary time derivatives. The relaxation and creep functions for the dashpot are

$$\begin{aligned} G(t) &= \eta\delta(t) \\ J(t) &= \frac{1}{\eta}t \end{aligned} \tag{6.5.9}$$

where $\delta(t)$ is the *Dirac delta function* defined by the following properties:

$$\delta(t) = \begin{cases} 0, & t < 0, \\ \infty, & t = 0, \\ 0, & t > 0, \end{cases} \qquad \int_{-\infty}^{\infty} \delta(t)\,dt = 1, \quad \delta(t) = \frac{dH(t)}{dt} \tag{6.5.10}$$

6.5.1.2 Maxwell model

Now the primary idea in this modeling approach is to connect spring and dashpot models in various ways to establish particular constitutive equations that may be useful to simulate real material behavior. We start with a very simple fundamental combination

FIGURE 6.33

Maxwell fluid model.

of connecting a spring and dashpot in a series arrangement as shown in Fig. 6.33, and this is referred to as a *Maxwell model* that has characteristics of a fluid-like material. For this configuration, the stress in each element is identical, while the sum of the strains in the spring and dashpot equals the total strain in the combined model. This information yields the following relations and produces the constitutive law:

$$\left.\begin{aligned} T_s = T_d = T \\ \varepsilon_s + \varepsilon_d = \varepsilon \end{aligned}\right\} \Rightarrow \dot{T} + \frac{E}{\eta} T = E\dot{\varepsilon} \tag{6.5.11}$$

We can see that even in this most simple viscoelastic model, the constitutive law contains rate-dependent terms. Thus, if the strain is specified, (6.5.11) is an ordinary differential equation with constant coefficients whose solution would give the stress response. Note that an often used parameter $\tau = \eta/E$ is commonly referred to as the *relaxation or retardation time constant.* Since this constitutive model only includes two material constants E and η, it will likely be limited in its ability to quantitatively predict real material behavior. Nevertheless, it does provide a simple starting point to understand viscoelastic modeling.

EXAMPLE 6.5.1 RELAXATION AND CREEP FUNCTIONS FOR MAXWELL MODEL

Determine the relaxation and creep functions for the Maxwell model and plot the results for different values of relaxation times.

Solution: For the stress relaxation behavior, the strain is specified by (6.5.1), $\varepsilon = \varepsilon_o H(t)$. Substituting this form into constitutive relation (6.5.11) gives

$$\dot{T} + \frac{E}{\eta} T = 0, \quad t > 0$$

The solution to this standard first-order ordinary differential equation is given by

$$T = Ke^{-(E/\eta)t}$$

where K is an arbitrary constant. We assume an initial condition on this case to be $T(0) = E\varepsilon_o$, and thus the constant is determined to be $K = E\varepsilon_o$. So, the stress response is

$$T = E\varepsilon_o e^{-(E/\eta)t}$$

and thus using (6.5.3) the relaxation function follows to be

$$G(t) = Ee^{-(E/\eta)t} = Ee^{-t/\tau} \tag{6.5.12}$$

For the creep function, the stress is specified by $T = T_o H(t)$, and using this in constitutive relation (6.5.11) gives

$$\dot{\varepsilon} = T_o / \eta, \quad t > 0$$

This differential equation can easily be integrated to get

$$\varepsilon = T_o t / \eta + C$$

where C is an arbitrary constant. Again applying the expected initial condition $\varepsilon(0) = T_o / E$ determines the constant C and gives the final form for the strain response

$$\varepsilon = T_o \left(\frac{t}{\eta} + \frac{1}{E} \right)$$

Using (6.5.5) the creep function follows is then given by

$$J(t) = \frac{t}{\eta} + \frac{1}{E} \tag{6.5.13}$$

Fig. 6.34 generated by MATLAB Code C-10 illustrates the relaxation and creep behaviors of the Maxwell model for different relaxation times τ. It can be seen that for a given value of time, as the relaxation time parameter increases, less model relaxation is predicted. Likewise, the amount of creep predicted will be less for larger values of τ. This is typical relaxation time behavior for viscoelastic models; however, the linear creep prediction with time is not likely to match with real material behavior.

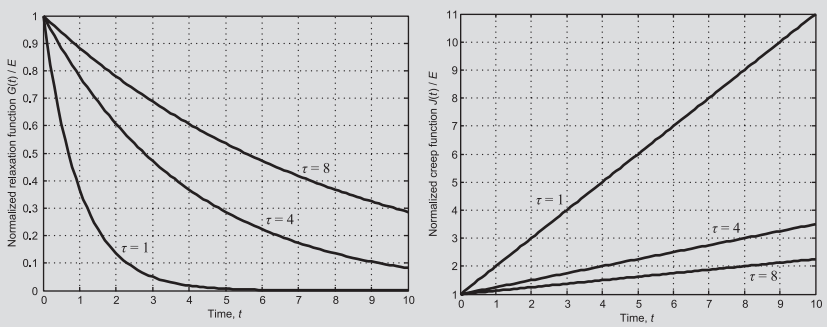

FIGURE 6.34

Relaxation and creep functions for Maxwell model.

6.5.1.3 Kelvin–voigt model

Next, consider the case of connecting a spring and dashpot in a parallel combination as shown in Fig. 6.35. This produces the *Kelvin–Voigt model* that has characteristics of a solid-like material. For this configuration, the strain in each element is identical, while the sum of the stresses in the spring and dashpot equals the total stress in the combined model. This information yields the following relations and produces the constitutive law:

$$\left.\begin{aligned} T_s + T_d &= T \\ \varepsilon_s &= \varepsilon_d = \varepsilon \end{aligned}\right\} \Rightarrow T = E\varepsilon + \eta\dot{\varepsilon} \tag{6.5.14}$$

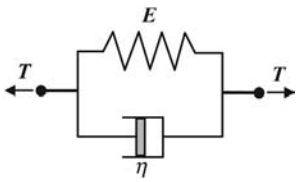

FIGURE 6.35

Kelvin–Voigt model.

As in the previous Maxwell model, we observe a constitutive law that contains rate-dependent terms. Thus, if the stress is specified, (6.5.14) is an ordinary differential equation whose solution would give the strain response. As before, since this constitutive model only includes two material constants E and η, it will likely be limited in its ability to predict real material behavior. However, like the Maxwell model, it does provide a simple starting point to understand viscoelastic modeling.

EXAMPLE 6.5.2 RELAXATION AND CREEP FUNCTIONS FOR KELVIN–VOIGT MODEL

Determine the relaxation and creep functions for the Kelvin–Voigt model and plot the results for different values of relaxation times.

Solution: For the stress relaxation behavior, the strain is specified by (6.5.1), $\varepsilon = \varepsilon_o H(t)$. Substituting this form into constitutive relation (6.5.14) gives

$$T = E\varepsilon_o, \quad t > 0$$

and using (6.5.3) the relaxation function follows to be

$$G(t) = E \tag{6.5.15}$$

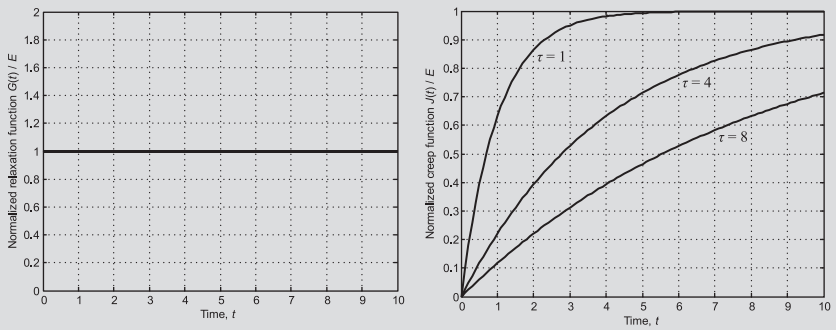

FIGURE 6.36

Relaxation and creep functions for Kelvin model.

For the creep function, the stress is specified by $T = T_o H(t)$, and using this in constitutive relation (6.5.14) gives

$$T_o = E\varepsilon + \eta\dot{\varepsilon}$$

The solution to this nonhomogeneous first-order differential equation follows from standard methods to be

$$\varepsilon = Ce^{-(E/\eta)t} + \frac{T_o}{E}$$

where C is an arbitrary constant. Again applying the expected initial condition $\varepsilon(0) = 0$ determines the constant C and gives the final form for the strain response

$$\varepsilon = \frac{T_o}{E}\left(1 - e^{-(E/\eta)t}\right)$$

Using (6.5.5), the creep function is then given by

$$J(t) = \frac{1}{E}\left(1 - e^{-(E/\eta)t}\right) \tag{6.5.16}$$

Fig. 6.36 generated by MATLAB Code C-11 illustrates the relaxation and creep behaviors of the Kelvin model for different relaxation times τ. It can be seen that the relaxation predictions are independent of the relaxation time parameter as shown in relation (6.5.15). This situation would indicate that the Kelvin model is not likely to be able to predict real material relaxation behavior. Similar to the Maxwell case, the amount of creep predicted for the Kelvin model will be less for larger values of τ.

EXAMPLE 6.5.3 STRAIN RECOVERY AFTER UNLOADING FOR MAXWELL AND KELVIN–VOIGT MODELS

Using the following loading history

$$T(t)=\begin{cases} T_o, & 0\le t\le t_1 \\ 0, & t>t_1 \end{cases}$$

determine the strain behavior or *recovery after unloading* for the Maxwell and Kelvin models and plot the strain responses.

Solution: Denote the strain responses in the Maxwell and Kelvin models by ε_M and ε_K. Over the time range $0\le t\le t_1$, this stress history simply creates the standard creep strain responses given previously in Examples 6.5.1 and 6.5.2:

$$\varepsilon_M = T_o\left(\frac{t}{\eta}+\frac{1}{E}\right), \quad \varepsilon_K=\frac{T_o}{E}\left(1-e^{-(E/\eta)t}\right), \quad 0\le t\le t_1 \tag{6.5.17}$$

For time $t>t_1$, the stress is now zero. For the Maxwell model, the instantaneous drop in stress T_o at $t=t_1$ would result in an immediate elastic recovery of T_o/E from just the spring. Since for $t>t_1$, both the stress and stress rate are zero, this implies that $\dot{\varepsilon}_M=0$. This results in a constant strain over this time interval

$$\varepsilon_M = T_o\left(\frac{t_1}{\eta}+\frac{1}{E}\right)-\frac{T_o}{E}=\frac{t_1}{\eta}T_o, \quad t>t_1 \tag{6.5.18}$$

For time $t>t_1$, the Kelvin model would predict an exponentially decreasing strain response of the form

$$\varepsilon = Ke^{-(E/\eta)(t-t_1)}$$

where K is a constant. For this model, there can be no strain discontinuity at $t=t_1$, and enforcing this condition gives an equation to determine the constant K:

$$K=\frac{T_o}{E}\left(1-e^{-(E/\eta)t_1}\right)$$

and so the Kelvin strain response for $t>t_1$ is then given by

$$\varepsilon_K=\frac{T_o}{E}\left(1-e^{-(E/\eta)t_1}\right)e^{-(E/\eta)(t-t_1)}, \quad t>t_1 \tag{6.5.19}$$

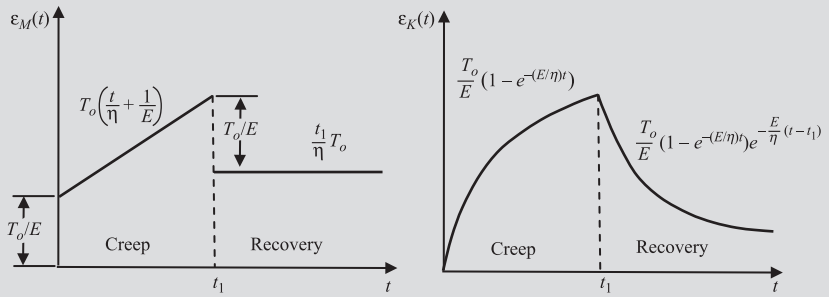

FIGURE 6.37

Recovery behavior for Maxwell and Kelvin models.

Thus, we have determined two different strain–time responses for each model and these are put together and shown in Fig. 6.37. The Kelvin predictions are qualitatively correct with a nonlinear increasing creep phase followed by a decreasing recovery response. However, as mentioned previously, these simple model predictions would likely not match with experimental data for real materials. For the Maxwell model, no inelastic recovery is found, but a permanent strain is present for large time.

EXAMPLE 6.5.4 CONSTANT LOADING RATE RESPONSE FOR KELVIN–VOIGT MODEL USING MATLAB TO SOLVE ODE CONSTITUTIVE LAW

Determine the stress-–time, strain–time, and stress–strain response of the Kelvin model for a loading rate specified by $T = Rt$, where R is the constant loading rate.

Solution: Although the Kelvin model under these conditions will yield an ordinary differential equation that has a known analytical solution, we will solve and plot the required results using the numerical tools in MATLAB. Code C-12 in Appendix C lists the fairly simple code using the built-in ODE45 solver that handles differential equations of first order. The results are shown in Fig. 6.38 as three separate plots of the stress–time, strain–time, and stress–strain behaviors for a set of three loading rates $R = 10$, 20, and 40. Using suitable units, the model parameters were chosen to be $E = 50$ and $\eta = 100$. The figure illustrates the loading rate effect on viscoelastic material behavior.

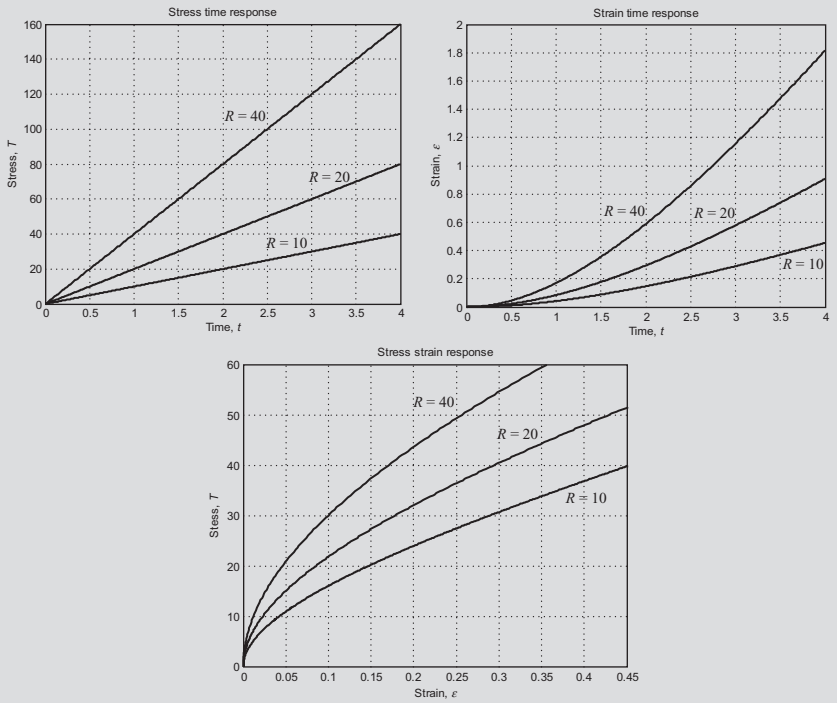

FIGURE 6.38

Stress–time, strain–time, and stress–strain response of Kelvin model under constant loading rate $T = Rt$. R = 10, 20, 40, and $E = 50$ and $\eta = 100$.

The stress–strain curves show the usual rate dependency with higher values of stress occurring at higher loading rates.

EXAMPLE 6.5.5 LOADING AND UNLOADING RESPONSE FOR KELVIN–VOIGT MODEL USING MATLAB TO SOLVE ODE CONSTITUTIVE LAW

Determine the stress–strain response of the Kelvin model for a loading history shown in Fig. 6.39. This history corresponds to a constant loading rate followed by a constant unloading rate.

Solution: Although the Kelvin model under these conditions will again yield an ordinary differential equation that has a known analytical solution, as in the previous example we will solve and plot the required results using the numerical tools in MATLAB. Code C-13 in Appendix C lists the code using the built-in ODE45 solver that handles differential equations of first order.

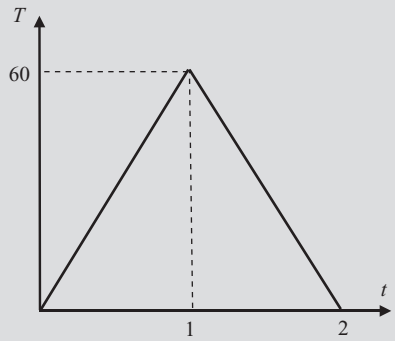

FIGURE 6.39

Loading history for Example 6.5.5.

The stress–strain results are shown in Fig. 6.40 for the case with model parameters $E = 200$ and $\eta = 100$. It is noted that the behavior is of course inelastic with no complete strain recovery even though the stress was completely removed. Permanent deformation is thus predicted, and an energy loss will result over this loading cycle.

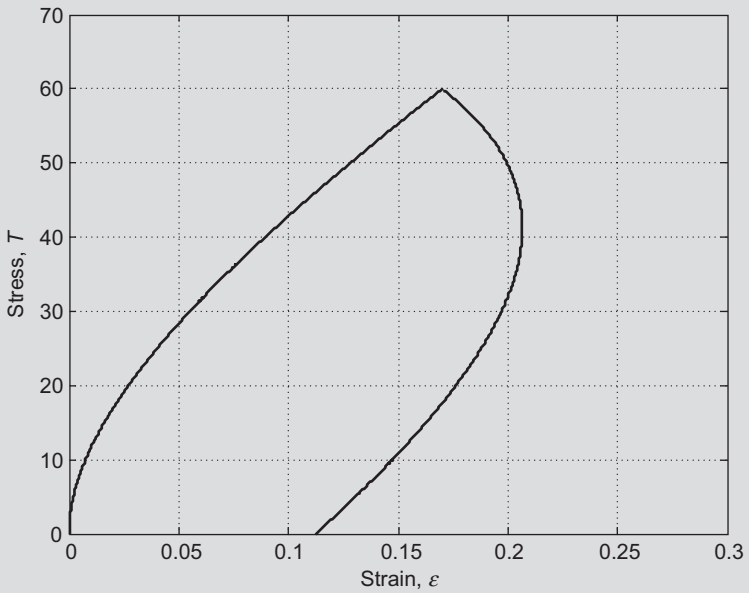

FIGURE 6.40

Stress–strain response for Kelvin model in Example 6.5.5 with parameters $E = 200$ and $\eta = 100$.

The previous five examples illustrate many of the unique behaviors associated with viscoelastic materials. Using simple Maxwell and Kelvin models, qualitative behaviors of stress relaxation, creep, strain recovery, and inelastic loading–unloading stress–strain responses were demonstrated. Next, we explore more sophisticated analog models that will have improved chances of quantitatively modeling real material behaviors.

6.5.1.4 More general analog models

As previously mentioned, while the simple Maxwell and Kelvin models provide many qualitatively correct viscoelastic behaviors, they will not in general simulate actual data of real materials. With this in mind, efforts to improve analog modeling have combined additional spring and dashpot elements in more complex arrangements. Some of these combined models are shown in Fig. 6.41. Note that models

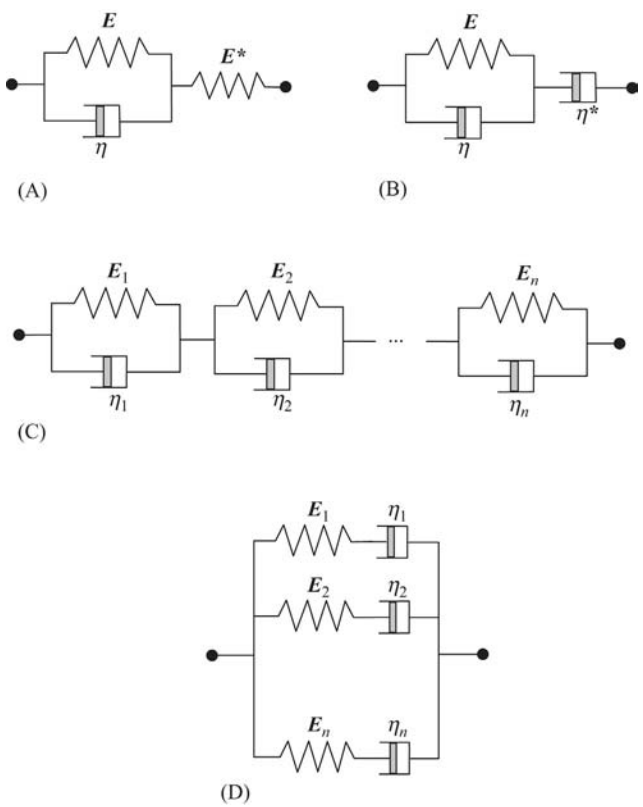

FIGURE 6.41

More general analog viscoelastic models: (A) Three-parameter solid; (B) three-parameter fluid; (C) generalized Kelvin chain; (D) generalized Maxwell chain.

with a free spring as shown in Fig. 6.41A will generally produce solid-like behaviors, whereas a free dashpot as shown in Fig. 6.41B will result in a fluid-like long-term response.

The three-parameter solid shown in Fig. 6.41A represents a Kelvin model in series with an elastic element. To arrive at the constitutive model for the entire combination, we note that the sum of the strains in Kelvin and elastic components add to give the total overall strain, and the stress in each of these components are the same and equal the overall stress

$$\left.\begin{array}{l} T_K = T_s = T \\ \varepsilon_K + \varepsilon_s = \varepsilon \end{array}\right\} \Rightarrow T + p_1 \dot{T} = q_o \varepsilon + q_1 \dot{\varepsilon} \tag{6.5.20}$$

where the coefficients are given by

$$p_1 = \frac{\eta}{E + E^*}, \quad q_o = \frac{EE^*}{E + E^*}, \quad q_1 = \frac{\eta E^*}{E + E^*} \tag{6.5.21}$$

The relaxation and creep functions for this model are found to be

$$\begin{aligned} G(t) &= \frac{q_1}{p_1} e^{-t/p_1} + q_o (1 - e^{-t/p_1}) \\ J(t) &= \frac{p_1}{q_1} e^{-q_o t/q_1} + \frac{1}{q_o} (1 - e^{-q_o t/q_1}) \end{aligned} \tag{6.5.22}$$

Note that this model carries the restriction $q_1 > p_1 q_o$ to guarantee that the relaxation/creep functions remain positive (see Flügge, 1975) for more details on this requirement.

Following a similar analysis, the constitutive relation for the three-parameter fluid shown in Fig. 6.41B can be developed as the form

$$T + p_1 \dot{T} = q_1 \dot{\varepsilon} + q_2 \ddot{\varepsilon} \tag{6.5.23}$$

where the coefficients are given by

$$p_1 = \frac{\eta + \eta^*}{E}, \quad q_1 = \eta^*, \quad q_2 = \frac{\eta \eta^*}{E} \tag{6.5.24}$$

The relaxation and creep functions for this model are given by

$$\begin{aligned} G(t) &= \frac{q_1^2}{p_1 q_1 - q_2} e^{-t/p_1} \\ J(t) &= \frac{t}{q_1} + \frac{p_1 q_1 - q_2}{q_1^2} (1 - e^{-q_1 t/q_2}) \end{aligned} \tag{6.5.25}$$

Similar to the three-parameter solid, this model also carries a restriction $p_1 q_1 > q_2$ to guarantee that relaxation/creep functions remain positive (see Flügge, 1975).

Clearly, these three-parameter models offer additional model constants to fit with real material relaxation and/or creep behavior. This concept can be extended to even

larger numbers of Maxwell or Kelvin chains as shown in Fig. 6.41C and D, thus producing a general differential constitutive relations of the form

$$p_o T + p_1 \dot{T} + p_2 \ddot{T} + \cdots = q_o \varepsilon + q_1 \dot{\varepsilon} + q_2 \ddot{\varepsilon} + \cdots$$
$$\sum_{k=0}^{m} p_k \frac{d^k T}{dt^k} = \sum_{k=0}^{m} q_k \frac{d^k \varepsilon}{dt^k} \tag{6.5.26}$$

or in operator form

$$\boldsymbol{P} T = \boldsymbol{Q} \varepsilon$$
$$\text{where} \quad \boldsymbol{P} = \sum_{k=0}^{m} p_k \frac{d^k}{dt^k}, \quad \text{and} \quad \boldsymbol{Q} = \sum_{k=0}^{m} q_k \frac{d^k}{dt^k} \tag{6.5.27}$$

Of course we notice that including more analog elements raises the order of the differential equation constitutive law. This complexity can be offset by using Laplace transforms to solve most of these higher-order ODEs. However, we will not pursue this approach to solve specific problems, but will employ Laplace transforms later in a more general way. The MATLAB ODE solver used in Examples 6.5.4 and 6.5.5 can also easily handle such higher-order equations (see Exercise 6.32). At this stage, we could rethink the analog constitutive concepts and eliminate the idea of spring–dashpot models and simply view (6.5.26) or (6.5.27) as just a general rate-dependent constitutive relation. In this regard, we could think of the general relaxation solution coming from a series form $T(t) = \varepsilon_o \sum_k G_k e^{-t/\tau_k}$, thus yielding a relaxation function $G(t) = \sum_k G_k e^{-t/\tau_k}$ with a discrete set of relaxation time τ_k.

Next, we wish to pursue the issue of how to apply these analog models to multi-dimensional continuum problems. Starting with either relation (6.5.26) or (6.5.27), it would be tempting to simply substitute the Cauchy stress tensor T_{ij} for the scalar stress T, and likewise substitute the small strain tensor ε_{ij} for the scalar variable ε. However, many experiments have shown that most isotropic engineering materials behave elastically in volumetric deformation, and this would imply that isotropic viscoelastic constitutive laws should only be applied to the deviatoric stress and strain tensors. With this in mind, let us review the decomposition of stress and strain into spherical and deviatoric components. Sections 3.10 and 4.5 provide the appropriate decomposition relations for the small strain and Cauchy stress tensors and are repeated here

$$\varepsilon_{ij} = \tilde{\varepsilon}_{ij} + \hat{\varepsilon}_{ij}$$
$$\tilde{\varepsilon}_{ij} = \frac{1}{3}\varepsilon_{kk}\delta_{ij}, \quad \hat{\varepsilon}_{ij} = \varepsilon_{ij} - \frac{1}{3}\varepsilon_{kk}\delta_{ij} \tag{6.5.28}$$

$$T_{ij} = \tilde{T}_{ij} + \hat{T}_{ij}$$
$$\tilde{T}_{ij} = \frac{1}{3}T_{kk}\delta_{ij}, \hat{T}_{ij} = T_{ij} - \frac{1}{3}T_{kk}\delta_{ij} \tag{6.5.29}$$

It can easily be shown that the isotropic form of Hooke's law (6.2.20) can be decomposed into spherical and deviatoric expressions (see Exercise 6.4):

$$\begin{aligned} \tilde{T}_{kk} &= 3k\tilde{\varepsilon}_{kk} \quad \text{or} \quad T_{kk} = 3k\varepsilon_{kk} \\ \hat{T}_{ij} &= 2\mu\hat{\varepsilon}_{ij} \end{aligned} \tag{6.5.30}$$

Likewise, a similar decomposition can be made for the linear viscous constitutive law (6.4.4):

$$T_{kk} = -3p + (3\lambda + 2\mu)D_{kk}, \quad \hat{T}_{ij} = 2\mu\hat{D}_{ij} \tag{6.5.31}$$

where for (6.5.31), μ would now correspond to the fluid viscosity. Noting that $D_{ij} \approx \dot{\varepsilon}_{ij} q$, the second relation in (6.5.31) would imply that the constitutive relation for the viscous element would $\hat{T}_{ij} = 2\mu\dot{\hat{\varepsilon}}_{ij}$. All of this then would allow elastic and viscous components to be put together in a tensor format in terms of deviatoric components. Thus, say, for a Kelvin model, the one-dimensional relation (6.5.14) could be written in tensor form as

$$\hat{T}_{ij} = 2\mu\hat{\varepsilon}_{ij} + 2\eta\dot{\hat{\varepsilon}}_{ij} \tag{6.5.32}$$

where μ is the elastic shear modulus and η is the viscosity. Likewise, the general form (6.5.27) could be expressed as

$$\boldsymbol{P}\hat{T}_{ij} = 2\boldsymbol{Q}\hat{\varepsilon}_{ij} \tag{6.5.33}$$

The spherical or volumetric deformation would then be governed by just the elastic constitutive relation.

6.5.1.5 Linear integral constitutive relations

Although the previous viscoelastic analog modeling provided an efficient way to combine elastic and viscous material response, the resulting general relation (6.5.27) becomes cumbersome if many terms are needed to accurately model real materials. To avoid this, a linear integral constitutive form can be constructed that will provide a more convenient means to model viscoelastic behavior. Using the *Boltzmann principle of superposition* for our linear theory, we can state that the total strain is equal to the sum of a sequence of strains caused by individual stresses. This concept is illustrated in Fig. 6.42 where the stresses are changing in incremental steps, and the resulting strains come from using the creep function definition over each step. The superposition concept can thus be written as

$$\begin{aligned} \varepsilon(t) &= J(t)T_o + J(t-t_1)\Delta T_1 + J(t-t_2)\Delta T_2 + \cdots \\ &= J(t)T_o + \sum_k J(t-t_k)\Delta T_k \end{aligned} \tag{6.5.34}$$

where J is the material's creep function. In the limit as the step size becomes infinitesimal and the number of steps goes to infinity, the summation in (6.5.34) becomes an integral

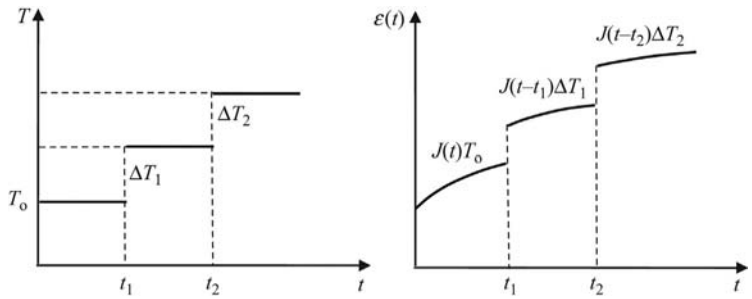

FIGURE 6.42

Stepwise stress loading and resulting strain response.

$$\begin{aligned}\varepsilon(t) &= J(t)T_o + \int_0^t J(t-t')\,dT(t') \\ &= J(t)T_o + \int_0^t \mathrm{J}(t-t')\frac{dT(t')}{dt'}\,dt' \\ &= \int_{-\infty}^t J(t-t')\frac{dT(t')}{dt'}\,dt'\end{aligned} \tag{6.5.35}$$

where the last line comes from the fact that $J(t) = 0$ for $t < 0$. Note that the integrand $J(t-t')$ could also be thought of as an *influence function*.

Relations (6.5.35) indicate that the strain at time t depends on the entire *stress history* $T(t')$, where $0 \le t' \le$ or $-\infty \le t' \le$. This fact is quite different than what occurs in elastic models where the strain at time t depends only on the stress at that particular time. The integrals in (6.5.35) are commonly referred to as *hereditary integrals*, and the particular form in $(6.5.35)_1$ is often called a *Stieltjes integral*. This history-dependent behavior brings up the interesting issue of how the influence or creep function $J(t-t')$ will vary over the integration range. We would normally expect that the recent past history would have a more significant effect on the behavior at time t than the effects that occurred in the distant history. Based on this, we would claim that the material's response has *fading memory*, and thus $J(t-t')$ would be a decreasing function of its argument. More significant use of the fading memory postulate is made in the nonlinear theories of material behavior.

Several alternative forms of relation (6.5.35) can be developed. Integration by parts will yield

$$\begin{aligned}\varepsilon(t) &= J(0)T(t) + \int_0^t \frac{dJ(t-t')}{d(t-t')}T(t')\,dt' \\ &= J(0)T(t) + \int_0^t \frac{dJ(t')}{d(t')}T(t-t')\,dt'\end{aligned} \tag{6.5.36}$$

It should be obvious that in the previous discussion leading to relations (6.5.35) and (6.5.36), the variables of strain and stress could be switched around by using the

relaxation function $G(t)$ instead of the creep function $J(t)$. Thus, we can express the stress $T(t)$ in terms of the *strain history* in any of the following hereditary integral forms:

$$\begin{aligned} T(t) &= G(t)\varepsilon_o + \int_0^t G(t-t')\,d\varepsilon(t') \\ &= G(t)\varepsilon_o + \int_0^t G(t-t')\frac{d\varepsilon(t')}{dt'}dt' \\ &= \int_{-\infty}^t G(t-t')\frac{d\varepsilon(t')}{dt'}dt' \\ &= G(0)\varepsilon(t) + \int_0^t \frac{dG(t-t')}{d(t-t')}\varepsilon(t')\,dt' \\ &= G(0)\varepsilon(t) + \int_0^t \frac{dG(t')}{d(t')}\varepsilon(t-t')\,dt' \end{aligned} \tag{6.5.37}$$

EXAMPLE 6.5.6 CORRESPONDENCE BETWEEN INTEGRAL AND ANALOG CONSTITUTIVE FORMS FOR MAXWELL MODEL CASE

Consider the hereditary integral form from $(6.5.37)_3$, with the following form for the relaxation function $G(t) = Ee^{-t/\tau}$, where E is the elastic stiffness and $\tau = \eta/E$ is the relaxation time. This form corresponds to a single relaxation time function and is actually the Maxwell model prediction for the relaxation function (see Eq. (6.5.12)). Show by differentiation of the integral form, the resulting expression will be the usual Maxwell constitutive law (6.5.11).

Solution: Using Leibnitz rule, we formally take the time derivative of the integral form with the given relaxation function

$$\begin{aligned} \dot{T} &= \frac{d}{dt}\int_{-\infty}^t Ee^{-(t-t')/\tau}\frac{d\varepsilon(t')}{dt'}dt' \\ &= E\dot{\varepsilon} + \int_{-\infty}^t E\frac{d}{dt}e^{-(t-t')/\tau}\frac{d\varepsilon(t')}{dt'}dt' \\ &= E\dot{\varepsilon} - \frac{1}{\tau}\int_{-\infty}^t Ee^{-(t-t')/\tau}\frac{d\varepsilon(t')}{dt'}dt' \\ &= E\dot{\varepsilon} - \frac{1}{\tau}T \\ &\Rightarrow \dot{T} + \frac{E}{\eta}T = E\dot{\varepsilon} \end{aligned}$$

Thus, we arrive at relation (6.5.11), the usual Maxwell differential constitutive law.

Next we move on to incorporating the integral constitutive form for general three-dimensional behaviors. This can be done by changing the scalar variables to tensors

of appropriate orders. If $\varepsilon_{ij}(t')$ represents the strain tensor history $(-\infty \le t' \le t)$, we can then express the stress response $T_{ij}(t)$ in any of the following forms:

$$\begin{aligned} T_{ij}(t) &= \int_{-\infty}^{t} G_{ijkl}(t-t')\frac{d\varepsilon_{kl}(t')}{dt'}\,dt' \\ &= G_{ijkl}(0)\varepsilon_{kl}(t) + \int_{0}^{t}\frac{dG_{ijkl}(t-t')}{d(t-t')}\varepsilon_{kl}(t')\,dt' \\ &= G_{ijkl}(0)\varepsilon_{kl}(t) + \int_{0}^{t}\frac{dG_{ijkl}(t')}{d(t')}\varepsilon_{kl}(t-t')\,dt' \end{aligned} \tag{6.5.38}$$

where G_{ijkl} is the fourth-order tensor relaxation function. As before, the roles of stress and strain can be interchanged leading to similar expressions

$$\begin{aligned} \varepsilon_{ij}(t) &= \int_{-\infty}^{t} J_{ijkl}(t-t')\frac{dT_{kl}(t')}{dt'}\,dt' \\ &= J_{ijkl}(0)T_{kl}(t) + \int_{0}^{t}\frac{dJ_{ijkl}(t-t')}{d(t-t')}T_{kl}(t')\,dt' \\ &= J_{ijkl}(0)T_{kl}(t) + \int_{0}^{t}\frac{dJ_{ijkl}(t')}{d(t')}T_{kl}(t-t')\,dt' \end{aligned} \tag{6.5.39}$$

where J_{ijkl} is the fourth-order tensor creep function. Based on similar arguments used in the elasticity theory, the tensors $\boldsymbol{G}$ and $\boldsymbol{J}$ must satisfy

$$\begin{aligned} G_{ijkl} &= G_{jikl} = G_{ijlk} \\ J_{ijkl} &= J_{jikl} = J_{ijlk} \end{aligned} \tag{6.5.40}$$

If the material is isotropic, then following our previous discussion for elastic materials, the fourth-order tensor $\boldsymbol{G}$ can be expressed as

$$G_{ijkl}(t) = \lambda(t)\delta_{ij}\delta_{kl} + \mu(t)(\delta_{ik}\delta_{jl} + \delta_{il}\delta_{jk}) \tag{6.5.41}$$

where $\lambda(t)$ and $\mu(t)$ are additional material relaxation functions. Using this in constitutive relation $(6.5.38)_1$ yields

$$T_{ij}(t) = \delta_{ij}\int_{-\infty}^{t}\lambda(t-t')\dot{\varepsilon}_{kk}(t')\,dt' + \int_{-\infty}^{t}2\mu(t-t')\dot{\varepsilon}_{ij}(t')\,dt' \tag{6.5.42}$$

As before we can separate (6.5.42) into spherical and deviatoric parts and write

$$\begin{aligned} \hat{T}_{ij}(t) &= \int_{-\infty}^{t}2\mu(t-t')\dot{\hat{\varepsilon}}_{ij}(t')\,dt' \\ T_{kk}(t) &= \int_{-\infty}^{t}3k(t-t')\dot{\varepsilon}_{kk}(t')\,dt' \end{aligned} \tag{6.5.43}$$

where $k(t) = [3\lambda(t) + 2\mu(t)]/3$. When viewed in this scheme, $\mu(t)$ would be referred to as the *shear relaxation function*, while $k(t)$ would be called the *bulk relaxation function*. Note that as mentioned previously, we could drop the viscoelastic spherical or volumetric response relation $(6.5.43)_2$ and assume this behavior is governed by the elastic relation $T_{kk} = 3k\varepsilon_{kk}$.

6.5.2 GENERAL FORMULATION

We now continue with the linear viscoelastic formulation by coupling the previous constitutive law(s) with other governing equations. Some further manipulations are necessary and we introduce the *correspondence principle* which is a very convenient strategy to find solutions to many problems. As with the previous elasticity case, we will limit our study to only quasi-static problems and will thus drop the acceleration term in the equations of motion. It should be noted that even with this assumption, viscoelastic deformation will produce time-dependent stresses, strains, and displacements. Since we are again setting up a mathematical boundary value problem, we must also establish appropriate boundary conditions applicable for the theory.

The general formulation of linear viscoelasticity is quite similar to that of linear elasticity previously presented in Section 6.2. The governing equations include

$$\text{Strain-Displacement Relations} \quad \varepsilon_{ij} = \frac{1}{2}(u_{i,j} + u_{j,i}) \tag{6.5.44}$$

$$\text{Compatibility Relations} \quad \varepsilon_{ij,kl} + \varepsilon_{kl,ij} - \varepsilon_{ik,jl} - \varepsilon_{jl,ik} = 0 \tag{6.5.45}$$

$$\text{Equilibrium Equations} \quad T_{ij,j} + \rho b_i = 0 \tag{6.5.46}$$

$$\text{Constitutive Law} \quad T_{ij}(t) = \delta_{ij}\int_{-\infty}^{t} \lambda(t-t')\,\dot{\varepsilon}_{kk}(t')\,dt' + \int_{-\infty}^{t} 2\mu(t-t')\,\dot{\varepsilon}_{ij}(t')\,dt' \tag{6.5.47}$$

With time-dependent deformations, the conservation of mass relation could also be included in this set to determine mass density changes.

As previously mentioned, the compatibility relations ensure that the displacements are continuous and single-valued and are necessary only when the strains are arbitrarily specified. If the displacements are included in the original problem formulation, the solution will normally generate single-valued displacements and strain compatibility will automatically be satisfied. Therefore, similar to the elasticity case, the compatibility relations are normally set aside, to be used only with the stress formulation. This system involves 15 unknowns including three displacements u_i, six strains ε_{ij}, and six stresses T_{ij}. For isotropic materials, the equation system also includes two viscoelastic material functions $\lambda(t)$ and $\mu(t)$ and a body force density b_i, and these are to be given *a priori* with the problem formulation. As with the elasticity case, this general system of equations is of such complexity that solutions via analytical methods are very difficult and further simplification is required to solve even simple problems.

The common types of boundary conditions for linear viscoelasticity are quite similar to those of elasticity and normally include specification of how the body is being *supported* or *loaded*. This concept is mathematically formulated by specifying either the *displacements* or *tractions* at boundary points, and for the viscoelastic case we could have time-dependent values for each of these quantities. Referring back to the elastic case in Fig. 6.8, this graphic illustrates the three common cases including

tractions, displacements, and a mixed case where tractions are specified on boundary S_t and displacements are given on the remaining portion S_u such that the total boundary is given by $S = S_t + S_u$.

6.5.2.1 Correspondence principle

It has been repeatedly mentioned in this section that there exists considerable similarity between the elastic and viscoelastic field equations. The correspondence principle establishes a direct connection between viscoelastic and elastic problem solutions. Since there is a large body of elasticity solutions that exist in the open literature, this scheme provides a very useful method to solve viscoelastic problems.

The technique uses *Laplace transforms*, and so we will briefly review this mathematical method. Laplace transformation is one of several linear integral transform methods that are useful for the solution to both ordinary and partial differential equations. The common useful property is that the transform changes particular governing differential and integral forms into algebraic relations, thus making the governing equation easier to solve. For a general function $f(t)$, $(t > 0)$, the Laplace transform is denoted by $\overline{f}(s)$ and defined by

$$\overline{f}(s) = \mathfrak{L}\{f(t)\} = \int_0^\infty f(t)e^{st}\,dt \tag{6.5.48}$$

where s is the transformed time variable. Thus functions of t are transformed into functions of s. Particular special properties of this transform useful in this context are

$$\begin{aligned}
&\mathfrak{L}\left\{\dot{f}(t)\right\} = s\overline{f}(s) - f(0)\\
&\mathfrak{L}\left\{\ddot{f}(t)\right\} = s^2\overline{f}(s) - sf(0) - \dot{f}(0)\\
&\mathfrak{L}\left\{\int_0^t f(t-\tau)g(\tau)\,d\tau\right\} = \overline{f}(s)\overline{g}(s)
\end{aligned} \tag{6.5.49}$$

The inverse Laplace transform may be written in operator form as $f(t) = \mathfrak{L}^{-1}\left\{\overline{f}(s)\right\}$. Taking the transform of various functions and doing the inverse transformation to get back to forms involving the real variable t is commonly done using Laplace transform tables found in many texts and on-line. Sometimes the inverse transform is done using contour integration in the complex plane.

So if we relist our viscoelastic field equations assuming the case of deformations starting at $t = 0$ and take the Laplace transform of the entire system, we get

$$\begin{aligned}
\mathfrak{L}&\left\{\begin{array}{c}
\varepsilon_{ij} = \dfrac{1}{2}(u_{i,j} + u_{j,i})\\
T_{ij,j} + \rho b_i = 0\\
T_{ij} = \delta_{ij}\displaystyle\int_0^t \lambda(t-t')\dot{\varepsilon}_{kk}(t')\,dt' + \int_0^t 2\mu(t-t')\dot{\varepsilon}_{ij}(t')\,dt'
\end{array}\right\}\\
&= \left\{\begin{array}{c}
\overline{\varepsilon}_{ij} = \dfrac{1}{2}(\overline{u}_{i,j} + \overline{u}_{j,i})\\
\overline{T}_{ij,j} + \rho\overline{b}_i = 0\\
\overline{T}_{ij} = s\overline{\lambda}(s)\overline{\varepsilon}_{kk}\delta_{ij} + 2s\overline{\mu}(s)\overline{\varepsilon}_{ij}
\end{array}\right\}
\end{aligned} \tag{6.5.50}$$

where we have assumed zero initial conditions on all transformed variables. The resulting transformed system (6.5.50) is identical to linear elasticity field equations in terms of the transformed variables $\{\overline{T}_{ij}, \overline{\varepsilon}_{ij}, \overline{u}_i, \overline{b}_i\}$ providing that $s\overline{\lambda}(s)$ and $s\overline{\mu}(s)$ correspond to the elastic moduli λ and μ. It is then noted that for problems of this type, the Laplace transform viscoelastic solution can be obtained directly from the corresponding elastic solution by replacing λ and μ with $s\overline{\lambda}(s)$ and $s\overline{\mu}(s)$, respectively. All time-dependent loadings must also be replaced by their corresponding Laplace transforms. The solution can then be completed by inverting the transformed solution back to the time t domain. This association between viscoelastic and elastic problems is called the *correspondence principle*. Note that many elasticity solutions contain parts (either the stresses or the displacements) that do not contain any elastic constants. For such a case, the viscoelastic solution then coincides with that portion of the elastic solution. We will see this case in subsequent examples.

Laplace transforms can also be used to demonstrate a correspondence between analog and hereditary integral models. Neglecting history effects before $t = 0$, the one-dimensional hereditary integral relation (6.5.37) can be written as

$$T(t) = G(0)\varepsilon(t) + \int_0^t \frac{dG(t-t')}{d(t-t')}\varepsilon(t')\,dt' \tag{6.5.51}$$

Taking the Laplace transform of this relation yields

$$\overline{T}(s) = G(0)\overline{\varepsilon}(s) + \overline{\dot{G}}(s)\overline{\varepsilon}(s) = s\overline{G}(s)\overline{\varepsilon}(s) \tag{6.5.52}$$

Now the most general analog model was given by relation (6.5.26), and taking the Laplace transform of this equation for the case of zero initial conditions gives

$$(p_o + p_1 s + p_2 s^2 + \cdots)\overline{T}(s) = (q_o + q_1 s + q_2 s^2 + \cdots)\overline{\varepsilon}(s) \tag{6.5.53}$$

and solving for the stress gives

$$\overline{T}(s) = \frac{(q_o + q_1 s + q_2 s^2 + \cdots)}{(p_o + p_1 s + p_2 s^2 + \cdots)}\overline{\varepsilon}(s) \tag{6.5.54}$$

Comparing Eqs. (6.5.52) and (6.5.54), we find that the continuous relaxation function from the hereditary integral form is related to a combination of discrete analog models through the expression

$$\overline{G}(s) = \frac{(q_o + q_1 s + q_2 s^2 + \cdots)}{s(p_o + p_1 s + p_2 s^2 + \cdots)} \tag{6.5.55}$$

6.5.3 PROBLEM SOLUTIONS

We now wish to use the previous constitutive relations and formulation equations to explore a few analytical solutions to some viscoelastic problems. These specific examples will further demonstrate important features of the linear viscoelastic model.

EXAMPLE 6.5.7 HARMONIC RESPONSE OF LINEAR VISCOELASTIC MODELS—COMPLEX MODULUS AND COMPLIANCE

Consider the response of our linear viscoelastic constitutive models under harmonic loading or deformation. If we were to subject a viscoelastic sample to a harmonic input strain, we would expect a harmonic output stress response of the same frequency. Likewise, we would also expect the same cause and effect if the stress was the input and the strain was the output. In this example, we wish to explore this type of behavior for one-dimensional Maxwell, Kelvin, and integral models.

Solution: We first start with a harmonic input strain using the more convenient complex exponential form $\varepsilon(t)=\varepsilon_o e^{i\omega t}$, where ω is the frequency and ε_o is the amplitude. The expected harmonic output stress would then be $T(t)=T_o e^{i\omega t}$. Substituting these forms into the Maxwell and Kelvin models and cancelling the common $e^{i\omega t}$ term yields

$$\text{Maxwell model: } \dot{T}+\frac{1}{\tau}T=E\dot{\varepsilon}\Rightarrow T_o i\omega+\frac{1}{\tau}T_o=E\varepsilon_o i\omega\Rightarrow T_o=\frac{Ei\omega}{i\omega+(1/\tau)}\varepsilon_o\Rightarrow$$
$$T_o=(G_1+iG_2)\varepsilon_o,\quad G_1=\frac{E\tau^2\omega^2}{1+\tau^2\omega^2},\quad G_2=\frac{E\tau\omega}{1+\tau^2\omega^2} \tag{6.5.56}$$
$$\varepsilon_o=(J_1+iJ_2)T_o,\quad J_1=-\frac{1}{E},\quad J_2=\frac{1}{\eta\omega}$$

$$\text{Kelvin model: } T=E\varepsilon+\eta\dot{\varepsilon}\Rightarrow T_o=E\varepsilon_o+\eta i\omega\varepsilon_o\Rightarrow T_o=(E+i\eta\omega)\varepsilon_o\Rightarrow$$
$$T_o=(G_1+iG_2)\varepsilon_o,\quad G_1=E,\quad G_2=\eta\omega$$
$$\varepsilon_o=(J_1+iJ_2)T_o,\quad J_1=\frac{E}{E^2+\eta^2\omega^2},\quad J_2=\frac{-\eta\omega}{E^2+\eta^2\omega^2} \tag{6.5.57}$$

G_1 and G_2 are called the *real and imaginary parts of the complex modulus* and J_1 and J_2 are called the *real and imaginary parts of the complex compliance.* It can be shown that G_1 is related to the energy stored in a cycle and thus is often referred to as the *storage modulus*, while G_2 can be related to the energy dissipated over a cycle and is appropriately called the *loss modulus*.

For the general differential constitutive form

$$\sum_{k=0}^{m}p_k\frac{d^kT}{dt^k}=\sum_{k=0}^{m}q_k\frac{d^k\varepsilon}{dt^k}\Rightarrow T_o\sum_{k=0}^{m}p_k(i\omega)^k=\varepsilon_o\sum_{k=0}^{m}q_k(i\omega)^k\Rightarrow T_o=\frac{\sum_{k=0}^{m}q_k(i\omega)^k}{\sum_{k=0}^{m}p_k(i\omega)^k}\varepsilon_o\Rightarrow$$
$$G_1=Re\left\{\frac{\sum_{k=0}^{m}q_k(i\omega)^k}{\sum_{k=0}^{m}p_k(i\omega)^k}\right\}\quad\text{and}\quad G_2=Im\left\{\frac{\sum_{k=0}^{m}q_k(i\omega)^k}{\sum_{k=0}^{m}p_k(i\omega)^k}\right\} \tag{6.5.58}$$

Finally exploring the one-dimensional integral constitutive form

$$T(t)=\int_0^t G(t-t')\frac{d\varepsilon(t')}{dt'}dt'\Rightarrow T_o=i\omega\,\varepsilon_o\int_0^t G(t-t')e^{-i\omega(t-t')}dt'\Rightarrow$$
$$G_1=Re\left\{i\omega\int_0^t G(t-t')e^{-i\omega(t-t')}dt'\right\}\text{ and }\ G_2=Im\left\{i\omega\int_0^t G(t-t')e^{-i\omega(t-t')}dt'\right\} \tag{6.5.59}$$

EXAMPLE 6.5.8 ONE-DIMENSIONAL RELAXATION FUNCTIONS FROM THREE-DIMENSIONAL VISCOELASTIC CONSTITUTIVE RELATIONS

Determine the tensile relaxation function and Poisson's ratio function from the three-dimensional integral constitutive relations (6.5.47). Also explore the constitutive case where volumetric and deviatoric responses are separated as in (6.5.43) and the volumetric behavior is taken to be elastic.

Solution: For a uniaxial relaxation deformation, we consider the stress and strain matrices as

$$T_{ij}(t)=\begin{bmatrix} T_o(t) & 0 & 0 \\ 0 & 0 & 0 \\ 0 & 0 & 0 \end{bmatrix}, \quad \varepsilon_{ij}(t)=\begin{bmatrix} \varepsilon_o(t) & 0 & 0 \\ 0 & \varepsilon_{22}(t) & 0 \\ 0 & 0 & \varepsilon_{33}(t) \end{bmatrix} H(t) \tag{6.5.60}$$

with $\varepsilon_{22}(t)=\varepsilon_{33}(t)=\varepsilon_t(t)$. The Laplace transformed relation (6.5.50) gives

$$\begin{aligned} &\bar{T}_{ij}=s\bar{\lambda}(s)\bar{\varepsilon}_{kk}\delta_{ij}+2s\bar{\mu}(s)\bar{\varepsilon}_{ij} \Rightarrow \\ &\bar{T}_{\mathrm{o}}=s\bar{\lambda}(s)(\bar{\varepsilon}_{\mathrm{o}}+2\bar{\varepsilon}_t)+2s\bar{\mu}(s)\bar{\varepsilon}_{\mathrm{o}} \\ &\bar{T}_{22}=\bar{T}_{33}=0=s\bar{\lambda}(s)(\bar{\varepsilon}_{\mathrm{o}}+2\bar{\varepsilon}_t)+2s\bar{\mu}(s)\bar{\varepsilon}_t \end{aligned} \tag{6.5.61}$$

Solving $(6.5.61)_3$ for the transverse strain gives $\bar{\varepsilon}_t=\dfrac{-\bar{\lambda}(s)}{2[\bar{\lambda}(s)+\bar{\mu}(s)]}\bar{\varepsilon}_o$. Then using this in $(6.5.61)_2$ gives

$$\bar{T}_o=\frac{s\bar{\mu}(s)[3\bar{\lambda}(s)+2\bar{\mu}(s)]}{\bar{\lambda}(s)+\bar{\mu}(s)}\bar{\varepsilon}_o=s\bar{E}(s)\bar{\varepsilon}_o \tag{6.5.62}$$

and thus taking the inverse Laplace transform

$$T_o(t)=\int_0^t E(t-t')\frac{d\varepsilon_o(t')}{dt'}dt', \quad \text{where } E(t)=\mathcal{L}^{-1}\left\{\frac{\bar{\mu}(s)[3\bar{\lambda}(s)+2\bar{\mu}(s)]}{\bar{\lambda}(s)+\bar{\mu}(s)}\right\} \tag{6.5.63}$$

$E(t)$ is called the *tensile relaxation modulus*.

Reusing the previous relations between transverse and axial strains gives the ratio:

$$\frac{\bar{\varepsilon}_t}{\bar{\varepsilon}_o}=\frac{-\bar{\lambda}(s)}{2[\bar{\lambda}(s)+\bar{\mu}(s)]}$$

and the inverse Laplace transform gives the *Poisson's ratio modulus* ν:

$$\nu(t)=\left|\frac{\bar{\varepsilon}_t}{\bar{\varepsilon}_o}\right|=\mathcal{L}^{-1}\left\{\frac{\bar{\lambda}(s)}{2[\bar{\lambda}(s)+\bar{\mu}(s)]}\right\} \tag{6.5.64}$$

For the case where we use the separation of volumetric and deviatoric behaviors based on relation (6.5.43) with the volumetric response governed by the elastic relation, we have

$$T_{kk} = 3k\varepsilon_{kk},\ \hat{T}_{ij}(t) = \int_0^t 2\mu(t-t')\,\dot{\hat{\varepsilon}}_{ij}(t')\,dt' \tag{6.5.65}$$

Taking the Laplace transform of these relations gives

$$\begin{aligned} &\bar{T}_{kk} = 3k\bar{\varepsilon}_{kk},\quad \bar{\hat{T}}_{ij} = 2s\bar{\mu}(s)\,\bar{\hat{\varepsilon}}_{ij} \Rightarrow \\ &\bar{T}_{ij} - \frac{1}{3}\bar{T}_{kk}\delta_{ij} = 2s\bar{\mu}(s)\left(\bar{\varepsilon}_{ij} - \frac{1}{3}\bar{\varepsilon}_{kk}\delta_{ij}\right) \Rightarrow \\ &\bar{T}_{ij} - \frac{1}{3}\bar{T}_{kk}\delta_{ij} = 2s\bar{\mu}(s)\,\bar{\varepsilon}_{ij} - \frac{2}{9k}s\bar{\mu}(s)\bar{T}_{kk}\delta_{ij} \end{aligned} \tag{6.5.66}$$

For our one-dimensional loading case

$$\begin{aligned} &\bar{T}_{11} - \frac{1}{3}\bar{T}_{11} = 2s\bar{\mu}(s)\bar{\varepsilon}_o - \frac{2}{9k}s\bar{\mu}(s)\bar{T}_{11} \Rightarrow \\ &\bar{T}_{11} = \frac{9ks\bar{\mu}(s)}{3k + s\bar{\mu}(s)}\bar{\varepsilon}_o = s\bar{E}(s)\bar{\varepsilon}_o \end{aligned} \tag{6.5.67}$$

So for this case

$$T_o(t) = \int_0^t E(t-t')\frac{d\varepsilon_o(t')}{dt'}dt',\quad \text{where}\quad E(t) = \mathcal{L}^{-1}\left\{\frac{9k\bar{\mu}(s)}{3k + s\bar{\mu}(s)}\right\} \tag{6.5.68}$$

and the Poisson's ratio function becomes

$$\nu(t) = \mathcal{L}^{-1}\left|\frac{\bar{\varepsilon}_t}{\bar{\varepsilon}_o}\right| = \mathcal{L}^{-1}\left\{\frac{3k - 2\bar{\mu}(s)}{6k + 2\bar{\mu}(s)}\right\} \tag{6.5.69}$$

Some of these results will be useful in problem solutions to come.

EXAMPLE 6.5.9 VISCOELASTIC STRESSES AND DISPLACEMENTS IN A THICK-WALLED TUBE UNDER INTERNAL PRESSURE

Determine the viscoelastic stress and displacement solution for a thick-walled cylindrical tube under internal pressure $p(t) = pH(t)$ as shown in Fig. 6.43.

Solution: We wish to use the correspondence principle, so we first seek the elasticity solution to this problem. This solution is normally developed under plane strain conditions in polar coordinates. Sadd (2014) provides the necessary solution

$$\begin{aligned} &T_{rr} = \frac{r_1^2 p}{r_2^2 - r_1^2}\left(1 - \frac{r_2^2}{r^2}\right),\quad T_{\theta\theta} = \frac{r_1^2 p}{r_2^2 - r_1^2}\left(1 + \frac{r_2^2}{r^2}\right) \\ &u_r = \frac{1}{2\mu}\frac{r_1^2 p}{r_2^2 - r_1^2}\left(\frac{r_2^2}{r} + \frac{\mu}{\lambda + \mu}r\right) \end{aligned} \tag{6.5.70}$$

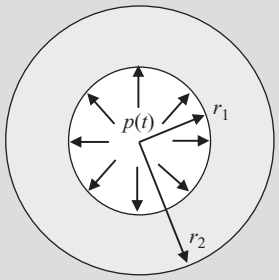

FIGURE 6.43

Pressurized thick-walled cylindrical tube.

Thus, according to the correspondence principle, the Laplace transformed viscoelastic solution will be

$$\begin{aligned}\overline{T}_{rr} &= \frac{r_1^2\overline{p}}{r_2^2-r_1^2}\left(1-\frac{r_2^2}{r^2}\right), \quad \overline{T}_{\theta\theta} = \frac{r_1^2\overline{p}}{r_2^2-r_1^2}\left(1+\frac{r_2^2}{r^2}\right)\\ \overline{u}_r &= \frac{1}{2s\overline{\mu}(s)}\frac{r_1^2\overline{p}}{r_2^2-r_1^2}\left(\frac{r_2^2}{r}+\frac{s\overline{\mu}(s)}{s\overline{\lambda}(s)+s\overline{\mu}(s)}r\right)\end{aligned} \tag{6.5.71}$$

Using the fact that $\overline{p} = p/s$, and taking the inverse Laplace transform of this set gives the viscoelastic solution

$$\begin{aligned}T_{rr} &= \frac{r_1^2 p}{r_2^2-r_1^2}\left(1-\frac{r_2^2}{r^2}\right), \quad T_{\theta\theta} = \frac{r_1^2 p}{r_2^2-r_1^2}\left(1+\frac{r_2^2}{r^2}\right)\\ u_r &= \frac{r_1^2 r_2^2 p}{2(r_2^2-r_1^2)r}\mathfrak{L}^{-1}\left(\frac{1}{s^2\overline{\mu}(s)}\right)+\frac{r_1^2 rp}{2(r_2^2-r_1^2)}\mathfrak{L}^{-1}\left(\frac{1}{s^2[\overline{\lambda}(s)+\overline{\mu}(s)]}\right)\end{aligned} \tag{6.5.72}$$

To complete the solution, we need to decide on the forms of the relaxation functions $\lambda(t)$ and $\mu(t)$. For convenience, choose the simple forms

$$\lambda(t) = \lambda_o e^{-t/\tau}, \quad \mu(t) = \mu_o e^{-t/\tau} \tag{6.5.73}$$

With this choice $\overline{\lambda}(s) = \dfrac{\lambda_o}{s+(1/\tau)}$, $\overline{\mu}(s) = \dfrac{\mu_o}{s+(1/\tau)}$, and thus

$$\frac{1}{s^2\overline{\mu}(s)} = \frac{s+(1/\tau)}{s^2\mu_o}, \quad \frac{1}{s^2[\overline{\lambda}(s)+\overline{\mu}(s)]} = \frac{s+(1/\tau)}{(\lambda_o+\mu_o)s^2} \tag{6.5.74}$$

Taking the inverse Laplace transforms from standard tables gives

$$\begin{aligned}\mathfrak{L}^{-1}\left(\frac{1}{s^2\overline{\mu}(s)}\right) &= \frac{1}{\mu_o}\mathfrak{L}^{-1}\left(\frac{1}{s}+\frac{1}{\tau s^2}\right) = \frac{1}{\mu_o}(H(t)+t)\\ \mathfrak{L}^{-1}\left(\frac{1}{s^2[\overline{\lambda}(s)+\overline{\mu}(s)]}\right) &= \frac{1}{(\lambda_o+\mu_o)}\mathfrak{L}^{-1}\left(\frac{1}{s}+\frac{1}{\tau s^2}\right) = \frac{1}{(\lambda_o+\mu_o)}(H(t)+t)\end{aligned} \tag{6.5.75}$$

Putting all these results together gives the final form for the viscoelastic solution

$$T_{rr} = \frac{r_1^2 p}{r_2^2 - r_1^2}\left(1 - \frac{r_2^2}{r^2}\right),\ T_{\theta\theta} = \frac{r_1^2 p}{r_2^2 - r_1^2}\left(1 + \frac{r_2^2}{r^2}\right)$$
$$u_r = \frac{r_1^2 p(1+t)}{2(r_2^2 - r_1^2)}\left(\frac{1}{\mu_o}\frac{r_2^2}{r} + \frac{r}{(\lambda_o + \mu_o)}\right) \tag{6.5.76}$$

Notice that for this problem the viscoelastic stresses are the same as those from elasticity since these fields did not contain any elastic constants. Furthermore, our simple relaxation models specified in (6.5.73) coincide with a Maxwell type model, and thus they predict fluid-like behavior in the radial displacement growing linearly with time t. This would of course produce unbounded displacements and eventually negate our small deformation assumption. For the case $t = 0$, the radial displacement will match with the elasticity solution with elastic moduli λ_o and μ_o. Different relaxation functions for $\lambda(t)$ and $\mu(t)$ would produce more reasonable temporal radial displacement predictions for solid-like behavior.

EXAMPLE 6.5.10 VISCOELASTIC STRESSES IN A HALF-SPACE UNDER CONCENTRATED NORMAL LOAD—BOUSSINESQ'S PROBLEM

Determine the viscoelastic stresses in a half-space under a concentrated load $P(t) = PH(t)$ acting normal to the free surface as shown in Fig. 6.44. This is a classic axisymmetric problem in elasticity theory and is called the *Boussinesq problem*.

Solution: We again wish to use the correspondence principle, so we first seek the elasticity solution to this problem. This axisymmetric solution is normally developed using cylindrical coordinates, and the complete stress field solution is given by Sadd (2014):

$$T_{rr} = \frac{P}{2\pi R^2}\left[-\frac{3r^2 z}{R^3} + \frac{(1-2\nu)R}{R+z}\right]$$
$$T_{\theta\theta} = \frac{(1-2\nu)P}{2\pi R^2}\left[\frac{z}{R} - \frac{R}{R+z}\right] \tag{6.5.77}$$
$$T_{zz} = -\frac{3Pz^3}{2\pi R^5},\ T_{rz} = -\frac{3Prz^2}{2\pi R^5},\ T_{r\theta} = T_{z\theta} = 0$$

where $r = \sqrt{x^2 + y^2}$ and $R = \sqrt{r^2 + z^2}$. Note that the stresses T_{zz} and T_{rz} do not contain any elastic moduli and so they would also be the solution to the corresponding viscoelastic problem. Stress components T_{rr} and $T_{\theta\theta}$ contain the common moduli term $(1-2\nu)$, and so we will only work on the T_{rr} component in detail.

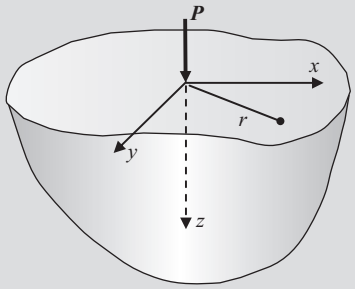

FIGURE 6.44

Boussinesq problem: normal force on the surface of a half-space.

Thus, according to the correspondence principle, the Laplace transformed viscoelastic solution will be

$$\bar{T}_{rr} = \frac{P}{2\pi R^2 s}\left[-\frac{3r^2 z}{R^3} + (1-2\bar{\nu}(s))\frac{R}{R+z}\right] \tag{6.5.78}$$

Taking the inverse Laplace transform gives the viscoelastic solution

$$T_{rr} = \frac{P}{2\pi R^2}\left[-\frac{3r^2 z}{R^3} + \mathcal{L}^{-1}\left(\frac{1-2\bar{\nu}(s)}{s}\right)\frac{R}{R+z}\right] \tag{6.5.79}$$

To complete the solution, we need to decide on the forms of the material Poisson ratio function $\nu(t)$. For this example, we will choose the constitutive scheme based on the separation of volumetric and deviatoric behaviors with the volumetric response governed by the elastic relation. Using the results from Example 6.5.8, the Poisson's ratio was given by

$$\bar{\nu}(s) = \frac{3k-2\bar{\mu}(s)}{6k+2\bar{\mu}(s)} \Rightarrow \frac{1-2\bar{\nu}(s)}{s} = \frac{3\bar{\mu}(s)}{s[3k+\bar{\mu}(s)]} \tag{6.5.80}$$

Next choosing a Kelvin-type shear relaxation function

$$\bar{\mu}(s) = \mu_o + \eta s \tag{6.5.81}$$

$$\begin{aligned}
\mathcal{L}^{-1}\left(\frac{1-2\bar{\nu}(s)}{s}\right) &= \mathcal{L}^{-1}\left(\frac{3\bar{\mu}(s)}{s[3k+\bar{\mu}(s)]}\right) = \mathcal{L}^{-1}\left(\frac{3(\mu_o+\eta s)}{s[3k+\mu_o+\eta s\ ]}\right) \\
&= \mathcal{L}^{-1}\left(\frac{3\mu_o}{s[3k+\mu_o+\eta s\ ]}\right) + \mathcal{L}^{-1}\left(\frac{3\eta}{[3k+\mu_o+\eta s\ ]}\right) \\
&= \frac{3\mu_o}{3k+\mu_o}\left(1-e^{-\frac{3k+\mu_o}{\eta}t}\right) + 3e^{-\frac{3k+\mu_o}{\eta}t} \\
&= \frac{3\mu_o}{3k+\mu_o} + \frac{9k}{3k+\mu_o}e^{-\frac{3k+\mu_o}{\eta}t}
\end{aligned}$$

Putting these inverse transform results back into (6.5.79) gives the viscoelastic solution for the T_{rr} stress component

$$T_{rr}(r,z,t)=\frac{P}{2\pi R^2}\left[-\frac{3r^2z}{R^3}+\left(\frac{3\mu_o}{3k+\mu_o}+\frac{9k}{3k+\mu_o}e^{-\frac{3k+\mu_o}{\eta}t}\right)\frac{R}{R+z}\right] \tag{6.5.82}$$

The other component $T_{\theta\theta}$ would follow by similar analysis. It is interesting to note that as $t\to\infty$,

$$T_{rr}(r,z,t)=\frac{P}{2\pi R^2}\left[-\frac{3r^2z}{R^3}+\frac{3\mu_o}{3k+\mu_o}\frac{R}{R+z}\right] \tag{6.5.83}$$

which coincides with the original elastic solution since $1-2\nu=\dfrac{3\mu}{3k+\mu}$.

6.6 CLASSICAL PLASTIC MATERIALS

We now extend our study to explore another type of inelastic behavior of solids called *plasticity*. This behavior has some fundamental differences from our previous discussion on viscoelasticity. As we have seen, many solids have linear elastic behavior followed by a change in the stress–strain response to a more flow-type behavior that will result in permanent material deformation when the loadings are removed. Plasticity theory can be a very complex study since it can include large deformations, rate-dependent effects, and various yield and strain hardening principles. Here we will only present a brief look at the classical small deformation, rate-independent models. More detailed presentations on plasticity are given in Hill (1950), Chakrabarty (1987), Lubliner (1990), Wu (2005), and Bower (2010). Applications of plasticity theory provide many important behavior models used in metal forming and machining, crash resistant structures, and inelastic structural analysis and design.

6.6.1 YIELD CRITERIA AND CONSTITUTIVE LAW

Consider again in more detail typical uniaxial tensile behavior of a ductile material as shown in Fig. 6.45A. We will describe the behavior in general approximate terms realizing that particular materials may deviate somewhat from our simplified descriptions. As loading begins, the material initially behaves linearly elastic under small deformations. In this region, the loading and unloading paths are the same and remain on line OA. As mentioned in Section 6.2.1, as loading continues a point will be reached where the material response will fundamentally change. At this location, linear elastic behavior will end, and a new and different constitutive response will begin. Again as per our previous discussion, several different descriptors could be used

to describe these changes including the *proportional limit*, *elastic limit*, and the *yield point*. It is common that the distinction between these different events and locations on the stress–strain curve are normally dropped, and we simply mark a single location labeled A, and refer to it as the *yield point*. The primary descriptor of this point is normally the stress value called the *yield stress,* designated by *Y*. Loading beyond point A invokes a new inelastic constitutive behavior with flow characteristics in the plastic region. Note that for many materials the stress will still exhibit an increasing function with strain during plastic flow, and this is called *work* or *strain hardening*. If the loading continues to point B, and then unloading is done, the downward unloading path will be approximately parallel to line OA. Thus, unloading is normally done elastically. If unloading is taken to zero stress, there will be permanent irreversible deformation, ε_p. Thus, at any generic point B, we can separate the total strain through the additive relation $\varepsilon = \varepsilon_e + \varepsilon_p$. If the unloading continues into the compression zone, a new compressive yield point will be reached. It is generally found that this compressive yield point (in absolute value) is smaller than the initial value in tension, and this phenomenon is called the *Bauschinger effect*. Finally, if the material is reloaded, the new loading path will not exactly coincide with path CB. This lack of coincidence of loading and unloading paths implies that the stress is a *history-dependent function of the strain* for plastic deformations.

Fig. 6.45B illustrates typical stress–strain behavior for different loading or strain rates. The elastic modulus and yield point normally increase with loading/strain rate. Thus, the yield behavior is commonly *rate dependent*, and this is normally referred to as *viscoplastic* behavior. We will not explore this type of response as our discussion will be limited to classical rate-independent plasticity theories. Furthermore, we assume isotropic behavior, incompressible plastic deformation, and will generally drop any Bauschinger effects.

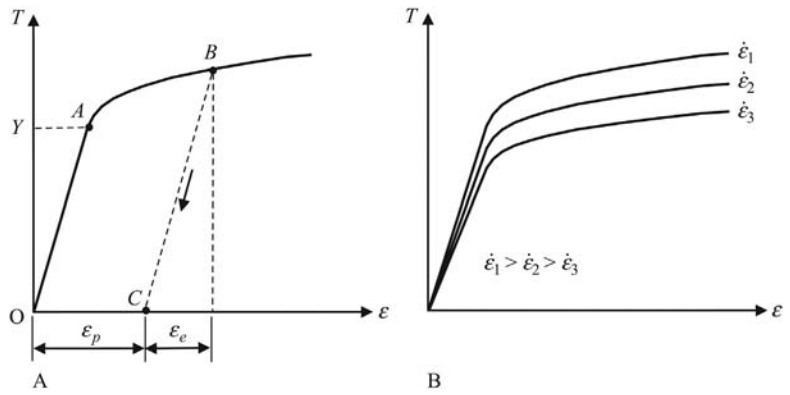

FIGURE 6.45

Typical uniaxial stress–strain behavior for ductile materials: (A) inelastic behavior; (B) rate-dependent behavior.

Summarizing our previous comments, experiments indicate that for many materials such as ductile metals, plastics, polymers, soils, rock, etc., the stress–strain constitutive behavior contains three features:

1. *initial elastic behavior*, followed by,
2. a combined stress or strain condition producing a change in the stress–strain behavior, that is, a *yield condition*,
3. a *plastic or flow response* governed by a different constitutive law.

We generally call this material behavior plasticity, and the essential characteristics are the yield condition and the plastic constitutive relation which is sometimes referred to as the *flow law*.

Before going into three-dimensional constitutive details, we first consider some simple one-dimensional models of idealized uniaxial plastic behaviors that have been developed in the literature. Fig. 6.46 illustrates four such models including *rigid perfectly plastic*, *elastic perfectly plastic*, *rigid linear strain hardening*, and *elastic linear strain hardening*. These models are somewhat similar to our previous analog spring–dashpot

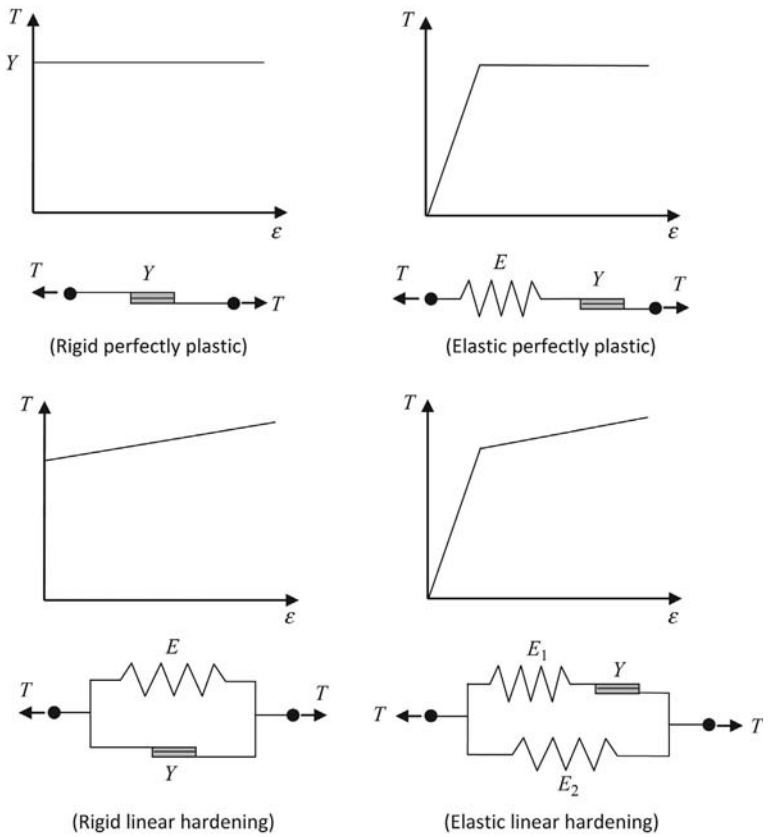

FIGURE 6.46

Idealized uniaxial plasticity models.

models used in linear viscoelasticity. The rigid perfectly plastic case can be generated by a simple *frictional element* with yield value *Y*. This element gives no deformation until the stress level reaches *Y*, and then unrestrained deformation occurs thereafter. The other cases shown are created through various combinations of frictional and elastic elements. Stress–stain curves for each of these models are illustrated, and these can be compared with more realistic behaviors shown in Fig. 6.45. These cases can be further generalized into viscoplastic models by including viscous dashpots previously presented.

6.6.1.1 Yield function

Development of yield functions goes back a century or more, and early work was related to various failure theories of solids. Such theories were often described by maximum principal stresses, or maximum shear stresses or maximum distortion energy. When particular points in the solid reached such a maximum strength value, it was assumed that material failure had initiated. Initially, we will explore a more general approach and then will focus attention on two particular theories.

Classical plasticity uses small deformation theory, and thus the total strain ε_{ij} can be decomposed into two parts, elastic strains ε_{ij}^{e}, and plastic strains ε_{ij}^{p} in the simple additive form

$$\varepsilon_{ij} = \varepsilon_{ij}^{e} + \varepsilon_{ij}^{p} \tag{6.6.1}$$

For the general three-dimensional case, the basic assumption of classical plasticity theory is that there exists a scalar *yield function* (or *loading function*), which depends on the *stress, plastic strain,* and the *history of loading*, in such a way as to characterize the material's yield behavior. This idea may be written as

$$f(T_{ij}, \varepsilon_{ij}^{p}, \kappa) = 0 \tag{6.6.2}$$

where κ is known as the *work-hardening parameter*. No change in plastic deformation occurs when $f < 0$. When $f = 0$, changes in plastic deformation occur, and no meaning is associated with $f > 0$. The work-hardening parameter κ is normally assumed to depend on the plastic deformation history of the material.

To clarify what is meant by loading and unloading, consider the time rate of change of f:

$$\dot{f} = \frac{\partial f}{\partial T_{ij}} \dot{T}_{ij} + \frac{\partial f}{\partial \varepsilon_{ij}^{p}} \dot{\varepsilon}_{ij}^{p} + \frac{\partial f}{\partial \kappa} \dot{\kappa} \tag{6.6.3}$$

The condition $f = 0$ and $\dot{f} < 0$ would imply that $f < 0$ at the next instant of time. This gives *unloading*. However, we also require that during the unloading, no plastic strain occurs, so $\varepsilon_{ij}^{p} = 0$, and that the rate of change of the strain hardening parameter κ must also vanish. Hence for *unloading and loading we may write*

$$\begin{aligned} f = 0, \quad & \frac{\partial f}{\partial T_{ij}} \dot{T}_{ij} < 0, \quad \textit{unloading} \\ f = 0, \quad & \frac{\partial f}{\partial T_{ij}} \dot{T}_{ij} > 0, \quad \textit{loading} \end{aligned} \tag{6.6.4}$$

Because of these definitions, f is sometimes referred to as the loading function.

Classical theories of plasticity often consider simplified yield functions which only depend on the stress and neglect the effects of the plastic strain and work hardening parameters. These are referred to as perfect plasticity, and a couple of simple examples were shown in the one-dimensional models in Fig. 6.46. Considering now only this case, we can express the yield function as

$$f = f(T_{ij}) \tag{6.6.5}$$

If the material is *isotropic*, then f must be invariant with respect to coordinate rotations, and hence must be only a function of the stress invariants. This is equivalent to employing the scalar-valued representation theorem (2.14.1). Thus, we can write

$$f = f(I_T, II_T, III_T) \tag{6.6.6}$$

or equivalently in terms of the principal stresses

$$f = f(T_1, T_2, T_3) \tag{6.6.7}$$

Relation (6.6.7) may be conveniently visualized as surface in a three-dimensional principal stress space as shown in Fig. 6.47. Stress states lying inside of the $f = 0$ surface will be elastic, while points on the $f = 0$ will have reached yield. In visualizing this concept for a loading situation, we start with zero stress at the origin. As loading increases, a loading path will be generated in the stress space. This path will depend on the multidimensional stress system that is being applied. As long as the loading path remains inside of the $f = 0$ surface, the material response will be elastic. Once any portion of the loading path reaches the yield surface, plastic deformation is initiated. What happens after this point will depend on the hardening characteristics and will be briefly discussed later.

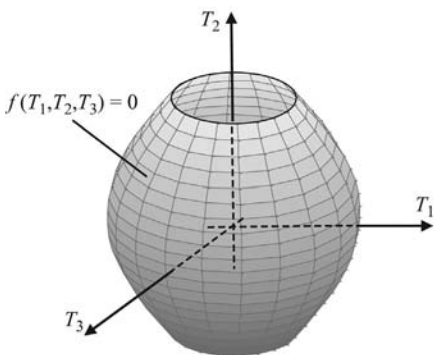

FIGURE 6.47

Yield surface in principal stress space.

Although not true for all materials, considerable experimental evidence for most metals indicates that the plastic yielding is independent of the hydrostatic pressure. Using this fact, relation (6.6.6) reduces to

$$f = f(II_T, III_T) \tag{6.6.8}$$

We can conclude that if the yield function is independent of $I_T = T_{kk}$, it is also independent of the spherical part of the stress tensor and must then depend only on the deviatoric stress $\hat{T}_{ij}$. Thus, the yield function further reduces to

$$f = f(II_{\hat{T}}, III_{\hat{T}}) \quad \text{or} \quad f = f(J_2, J_3) \tag{6.6.9}$$

It is common to denote the second and third invariants of the deviatoric stress tensor as J_2 and J_3, in the following fashion:

$$II_{\hat{T}} = -J_2 = -\frac{1}{2}\hat{T}_{ij}\hat{T}_{ij}\ ,\ III_{\hat{T}} = J_3 = \det(\hat{T}_{ij}) \tag{6.6.10}$$

We now explore in detail two classical yield functions of this type called *Mises* and *Tresca* yield criteria.

6.6.1.2 Mises yield condition

The *Mises yield condition* is defined from elastic strain energy concepts. From previous relation (6.2.41), the total strain energy was expressed in terms of the stress for isotropic materials. We can decompose this energy into two parts, one associated with *volumetric* change U_v and the other due to *distortional* (change in shape) deformation U_d:

$$U = U_v + U_d \tag{6.6.11}$$

where

$$\begin{aligned} U_v &= \frac{1-2\nu}{6E} I_T^2 = \frac{1-2\nu}{6E}\left(T_1 + T_2 + T_3\right)^2 \\ U_d &= -\frac{1}{6\mu}\left(I_T^2 + 3II_T\right) \\ &= \frac{1}{12\mu}\left[\left(T_1 - T_2\right)^2 + \left(T_2 - T_3\right)^2 + \left(T_3 - T_1\right)^2\right] = \frac{1}{4\mu}\hat{T}_{ij}\hat{T}_{ij} = \frac{1}{2\mu}J_2 \end{aligned} \tag{6.6.12}$$

It has been previously argued that the yield function will not depend on the hydrostatic pressure and thus cannot depend on the first invariant of stress. Thus, from (6.6.12) only U_d can be included in such an energy condition, and this distortional strain energy is linearly related to J_2. Therefore, the Mises yield condition related to maximum distortional strain energy is defined by

$$\begin{aligned} &f(T_{ij}) = J_2 - k^2 \Rightarrow \\ &\left(T_1 - T_2\right)^2 + \left(T_2 - T_3\right)^2 + \left(T_3 - T_1\right)^2 = 6k^2 \\ &T_1^2 + T_2^2 + T_3^2 - T_1T_2 - T_2T_3 - T_3T_1 = 3k^2 \end{aligned} \tag{6.6.13}$$

where k is a constant normally independent of the strain history. Relation (6.6.13) is sometimes called J_2 *flow theory*. Hence we have $J_2 \le k^2$, with plastic flow for the equality case. For a work hardening material k can be allowed to change with strain history.

Considering the simple shear state of stress $\boldsymbol{T} = T_{12}\boldsymbol{e}_1\boldsymbol{e}_2 + T_{12}\boldsymbol{e}_2\boldsymbol{e}_1$, for this case $J_2 = \hat{T}_{ij}\hat{T}_{ij}/2 = T_{12}^2$ and thus $f = 0 \Rightarrow k = (T_{12})_y$. Hence k corresponds to the yield stress in pure simple shear. Furthermore, if we consider the uniaxial tension state of stress $\boldsymbol{T} = T_{11}\boldsymbol{e}_1\boldsymbol{e}_1$, we find that $J_2 = \hat{T}_{ij}\hat{T}_{ij}/2 = T_{11}^2/3$, and for $f = 0 \Rightarrow k = (T_{11})_y/\sqrt{3} = Y/\sqrt{3}$. So k can also be related to the yield tensile stress.

6.6.1.3 Tresca yield condition

The *Tresca yield condition* proposes that the primary factor for yielding is the maximum shear stress in the material. The criterion then stipulates that the maximum shear stress must be equal to a constant material value of k during plastic flow.

To express this idea analytically, it is easier to use the principal stresses T_1, T_2, T_3. From our theory in Section 4.4 and Fig. 4.7, we can write the Tresca yield condition as

$$\begin{aligned}
&f = T_1 - T_3 - 2k, && T_1 \ge T_2 \ge T_3\\
&f = T_3 - T_1 - 2k, && T_3 \ge T_2 \ge T_1\\
&f = T_2 - T_1 - 2k, && T_2 \ge T_3 \ge T_1\\
&f = T_1 - T_2 - 2k, && T_1 \ge T_3 \ge T_2\\
&f = T_3 - T_2 - 2k, && T_3 \ge T_1 \ge T_2\\
&f = T_2 - T_3 - 2k, && T_2 \ge T_1 \ge T_3
\end{aligned} \tag{6.6.14}$$

We can collect all these separate conditions together by writing a product form

$$f = [(T_1 - T_2)^2 - 4k^2][(T_2 - T_3)^2 - 4k^2][(T_3 - T_1)^2 - 4k^2] \tag{6.6.15}$$

Finally, condition (6.6.15) can be written in an invariant form by

$$f = 4J_2^3 - 27J_3^2 - 36k^2J_2^2 + 96k^4J_2 - 64k^6 \tag{6.6.16}$$

For the case of uniaxial tension, $\boldsymbol{T} = T_{11}\boldsymbol{e}_1\boldsymbol{e}_1$, the Tresca condition $f = 0 \Rightarrow k = (T_{11})_y/2 = Y/2$.

These two yield functions may be plotted in principal stress space as shown in Fig. 6.48. Note that both Mises and Tresca conditions fall into the general form given by relation (6.6.9), and because they are independent of the hydrostatic stress both will be an open cylindrical shape with axis along the line OH defined by $T_1 = T_2 = T_3$ which makes equal angles with the T_1, T_2, T_3 axes. Thus, in principle no matter how large the stress, a loading path along line OH will never reach yield. The Mises function is a circular cylinder, whereas the Tresca condition is a hexagonal cylinder, both having the same axis along OH. The plane normal to line OH is referred to as the *deviatoric plane*. Stress states lying on this plane will be deviatoric, while states normal to the plane will be hydrostatic. Based on these observations, it is understandable why these two yield surfaces will be an open cylinder oriented with axes along OH.

The projection of the Mises and Tresca yield surface on the deviatoric plane is shown in Fig. 6.49. The Mises locus is a circle and the Tresca shape is a regular hexagon. Each

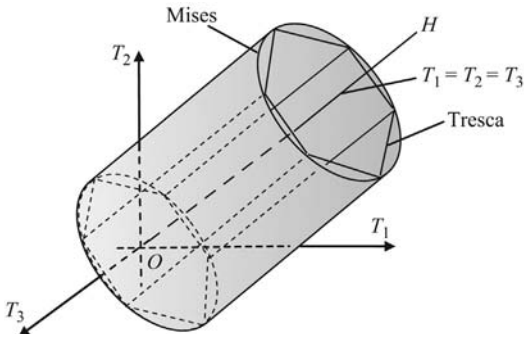

FIGURE 6.48

Mises and Tresca yield surfaces in principal stress space.

side of the Tresca hexagon represents one of the six equations listed in relation (6.6.14). We now make a few general comments about these deviatoric yield loci. For our isotropic case, the order of the principal stresses is immaterial, and this implies that the yield locus is symmetric about the projection of each principal axis. Furthermore, if we neglect any difference between tension and compression yield (no Bauschinger effect), then we have additional symmetry about directions orthogonal to each project principal axes. Collecting these ideas together provides the conclusion that a general yield locus must repeat over twelve 30° angular sections as verified in Fig. 6.49.

Since many experiments are often two-dimensional, it is more convenient to consider a plane stress case where one of the principal stresses is dropped. Thus, if we choose $T_3 = 0$, the Mises and Tresca yield conditions reduce to

$$\begin{aligned} &T_1^2 - T_1 T_2 + T_2^2 = Y \ldots \text{Mises} \\ &T_1 = \pm Y, T_2 = \pm Y, T_1 - T_2 = \pm Y \ldots \text{Tresca} \end{aligned} \tag{6.6.17}$$

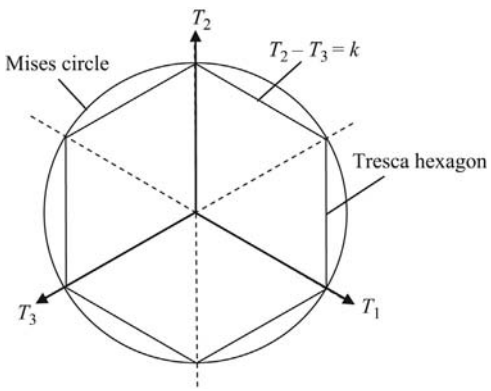

FIGURE 6.49

Mises and Tresca yield loci in deviatoric plane.

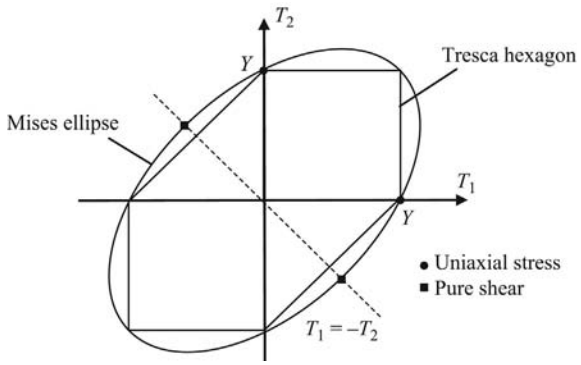

FIGURE 6.50

Mises and Tresca yield loci in T_1, T_2-plane.

Fig. 6.50 illustrates these yield loci in a T_1,T_2-system. For this case, the Mises locus is an ellipse oriented at a 45° angle as shown, whereas the Tresca criterion takes a skewed hexagonal shape within the Mises ellipse. Particular states of stress on the Mises ellipse can be identified, and the cases of uniaxial stress and pure shear are shown. Experimental data on several ductile metals commonly match better with the Mises yield model (Chakrabarty, 1987). However, differences between these two yield functions are generally small.

Several other more specialized yield criteria have been proposed. For many geomaterials such as sand and clay soils, rocks, and concretes, the inelastic deformation results from internal frictional sliding. This type of behavior then points out that normal stresses (including the hydrostatic stress) will have an effect on yielding. This reasoning has led to the development of *Mohr–Coulomb and Ducker–Prager yield criteria*; Asaro and Lubarda (2006) provide some specific details on these and a few other specialized yield functions.

Although we will not pursue strain hardening in detail, at this point we briefly present some fundamental qualitative aspects on how this would relate to the yield function. The basic idea is that once yield is reached, hardening will cause the yield surface to move in stress space. Fig. 6.51 shows two of the common model examples in T_1,T_2 stress space for the Mises criterion. Fig. 6.51A illustrates *isotropic hardening* where the yield surface undergoes uniform expansion. For this case, the material becomes stronger in all directions, thus implying no Bauschinger effect. The fundamental modification in the yield function could be expressed by $f = J_2 - \kappa^2$, where κ is no longer a constant but rather is a scalar variable dependent on the deformation history. For the Mises yield function in this stress space $T_1^2 - T_1T_2 + T_2^2 = Y$, we could simply add an addition term and write $T_1^2 - T_1T_2 + T_2^2 = Y + T_H$, where T_H would be a hardening stress increment that would result in uniform expansion of the Mises ellipse in all directions as shown. Another common model shown in Fig. 6.51B is *kinematic hardening* that takes into account the Bauschinger effect whereby yield in tension produces reduction in the yield value in compression. This can be accomplished if we

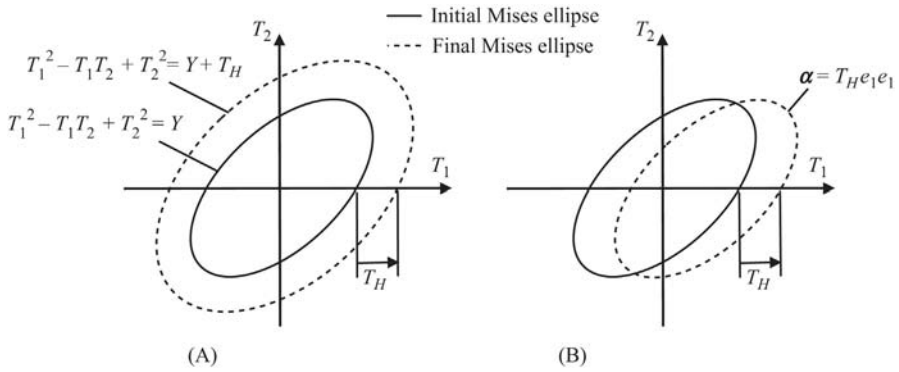

FIGURE 6.51

Isotropic and kinematic hardening in T_1, T_2-plane for Mises criterion: (A) isotropic hardening ($f = J_2 - \kappa^2$); (B) kinematic hardening ($f = f(T_{ij} - \alpha_{ij})$).

allow the yield locus to translate in the direction of the loading path. The fundamental modification in the yield function for this case could be expressed by $f = f(T_{ij} - \alpha_{ij})$, where α_{ij} is related to the translation of the yield surface center and is sometimes called the *back stress*. The situation shown in Fig. 6.51B would be for the case where $\alpha = T_H \boldsymbol{e}_1 \boldsymbol{e}_1$. This situation produces *stress-induced anisotropy* since the loading has modified the yield criterion in different directions in stress space. For some applications, it has been found necessary to use mixed hardening whereby both isotropic and kinematic hardening are included in particular combinations.

6.6.1.4 Plastic stress–strain relations

We now wish to explore plastic stress–strain constitutive laws. These are often referred to as *flow laws* since such deformations have flow-like time-dependent features. Generally the plastic strains depend on load history, and normally such constitutive relations will include strain and/or stress rates or use incremental forms of these variables. Commonly, the basic idea is that once the material has reached yield, we wish to determine the small change in the plastic strain $d\varepsilon_{ij}^p$ (or sometimes the total strain $d\varepsilon_{ij}$) due to a small change in applied stress dT_{ij}. Often numerical schemes like finite-element method codes are used to integrate such incremental relations. This study can be extensive and considerably complex; however, we will limit the presentation to only some of the more basic aspects of small deformation plasticity.

We start by neglecting elastic deformation and strain hardening and will thus focus on the rigid perfectly plastic response as shown in Fig. 6.46. We might expect such a constitutive equation for plastic deformation to be somewhat similar to that of a Newtonian fluid where the deviatoric stress would depend linearly on the rate of deformation. However, experimental observations do not support that type of relation. Over a century ago, Levy and later von Mises proposed that under plastic deformation, the principal axes of strain increment coincides with the principal axes of deviatoric stress and thus they suggested the equality of the following ratios:

$$\frac{d\varepsilon_{11}}{\hat{T}_{11}} = \frac{d\varepsilon_{22}}{\hat{T}_{22}} = \frac{d\varepsilon_{33}}{\hat{T}_{33}} = \frac{d\varepsilon_{12}}{\hat{T}_{12}} = \frac{d\varepsilon_{23}}{\hat{T}_{23}} = \frac{d\varepsilon_{31}}{\hat{T}_{31}} \tag{6.6.18}$$

or more compactly

$$d\varepsilon_{ij} = \hat{T}_{ij} d\lambda \tag{6.6.19}$$

where $d\lambda$ is a scalar proportionality factor. Within the context of small deformations, $\dot{\varepsilon}_{ij} \approx D_{ij}$, and thus relation (6.6.19) can be recast into the following flow law between the deviatoric stress and the rate of deformation:

$$\hat{T}_{ij} = \frac{k}{\sqrt{|II_D|}} D_{ij} \tag{6.6.20}$$

where $II_D = D_{ij} D_{ij} / 2$ is the second invariant of the rate of deformation tensor, and k is a constant. Forms (6.6.18)–(6.6.20) are referred to as the *Levy–Mises plastic constitutive relations.*

Constitutive form (6.6.20) directly gives the result $D_{kk} = 0$, thus implying plastic incompressibility. This constitutive form also actually implies the Mises yield condition since

$$\frac{1}{2} \hat{T}_{ij} \hat{T}_{ij} = \frac{k^2}{2|II_D|} D_{ij} D_{ij} = k^2$$

Note that it was previously shown that $k = (T_{11})_y / \sqrt{3} = (T_{12})_y$ and that there will be no strain hardening for this case. Within the Levy–Mises law, there is no elastic strain and thus $d\varepsilon_{ij} = d\varepsilon_{ij}^p$.

Next consider a generalization of the Levy–Mises constitutive model that includes the elastic strains. This case would then represent the elastic perfectly plastic model shown in Fig. 6.46. Using the additive strain decomposition (6.6.1), we can write

$$\begin{aligned} d\varepsilon_{ij} &= d\varepsilon_{ij}^e + d\varepsilon_{ij}^p \\ d\varepsilon_{ij}^e &= \frac{1+\nu}{E} dT_{ij} - \frac{\nu}{E} \delta_{ij} T_{kk} \\ &= \frac{1+\nu}{E} d\hat{T}_{ij} + \frac{1-2\nu}{E} \delta_{ij} T_{kk} \\ d\varepsilon_{ij}^p &= \hat{T}_{ij} d\lambda \\ d\varepsilon_{kk}^p &= 0 \end{aligned} \tag{6.6.21}$$

and using the Mises yield criteria gives

$$d\lambda = \frac{1}{k} \sqrt{|II_{d\varepsilon^p}|} = \frac{1}{k} \sqrt{d\varepsilon_{ij}^p d\varepsilon_{ij}^p / 2} = \frac{1}{Y} \sqrt{\frac{3}{2} d\varepsilon_{ij}^p d\varepsilon_{ij}^p} \tag{6.6.22}$$

Relations (6.6.21) and (6.6.22) are referred to as the *Prandtl–Reuss plastic constitutive laws.*

Another general flow rule concept is to represent the plastic strain increment as the derivative of a *potential function*

$$d\varepsilon_{ij}^{p} = \lambda \frac{\partial g}{\partial T_{ij}} \tag{6.6.23}$$

where g is a general plastic potential function that would be determined from experiments. If we set $g = f$, that is, make the potential function the same as the yield function, and choose the Mises yield criterion then

$$d\varepsilon_{ij}^{p} = \lambda \frac{\partial f}{\partial T_{ij}} = \lambda \hat{T}_{ij} \tag{6.6.24}$$

which is the same flow rule as (6.6.19). Furthermore, (6.6.24) indicates that the plastic strain increment is proportional to the gradient of the yield surface and is therefore *normal* to the surface. This fact is called the *normality condition*, and a flow rule that obeys this condition is called an *associated flow rule*. For the case where $g \neq f$, the plastic strain increment will not necessarily be normal to the yield surface and the flow rule is referred to as a *nonassociated flow rule*. Nonassociated flow rules are often used in geomechanics applications where the yield criterion depends on the hydrostatic pressure.

Much more could be said about additional features related to yield criteria and plastic flow rules, but because of space limitations we will end this discussion and move on to a few plasticity problem solutions.

6.6.2 PROBLEM SOLUTIONS

We now wish to use the previous yield criteria and constitutive relations to explore a few analytical solutions to some simple plasticity problems. The examples explore continuum elastic–plastic boundary-value problems starting with the elasticity solution, and then moving on to the case where yielding becomes present to develop plastic zones. These specific examples demonstrate some features on how the plasticity model is incorporated into problem solution.

EXAMPLE 6.6.1 ELASTOPLASTIC STRESSES IN A THICK-WALLED TUBE UNDER INTERNAL PRESSURE

Determine the elastic–plastic deformation behavior of a thick-walled cylindrical tube under internal pressure p that was previously shown in Fig. 6.43.

Solution: The elasticity solution is normally developed under plane strain conditions in polar coordinates ($\varepsilon_{zz} = 0$) and was previously provided in Example 6.5.9:

$$\begin{aligned} &T_{rr} = \frac{r_1^2 p}{r_2^2 - r_1^2}\left(1 - \frac{r_2^2}{r^2}\right), T_{\theta\theta} = \frac{r_1^2 p}{r_2^2 - r_1^2}\left(1 + \frac{r_2^2}{r^2}\right) \\ &T_{zz} = \nu(T_{rr} + T_{\theta\theta}), T_{r\theta} = T_{\theta z} = T_{rz} = 0 \\ &u_r = \frac{1}{2\mu}\frac{r_1^2 p}{r_2^2 - r_1^2}\left(\frac{r_2^2}{r} + \frac{\mu}{\lambda + \mu} r\right) \end{aligned} \tag{6.6.25}$$

Since all shear stresses vanish, T_{rr}, $T_{\theta\theta}$, T_{zz} are the principal stresses, and we can verify that $T_{\theta\theta} > T_{zz} > T_{rr}$.

If we use the Tresca yield criteria, the onset of yielding is given by

$$T_{\theta\theta} - T_{rr} = 2k \Rightarrow T_{\theta\theta} - T_{rr} = \frac{2r_1^2 p}{r_2^2 - r_1^2}\left(\frac{r_2^2}{r^2}\right) \tag{6.6.26}$$

This expression takes on a maximum value at $r = r_1$, and thus yielding begins at the inner radius when the applied pressure becomes

$$p_o = k\left(1 - \frac{r_1^2}{r_2^2}\right) \tag{6.6.27}$$

where k is equal to one-half the yield stress in tension.

For the case where we use the Mises yield criteria, we can use relation (6.6.13) to write

$$(T_{rr} - T_{\theta\theta})^2 + (T_{\theta\theta} - T_{zz})^2 + (T_{zz} - T_{rr})^2 = 6k^2 \tag{6.6.28}$$

Using the given elastic solution (6.6.25), the yield relation reduces to

$$\left[\frac{1}{3}(1-2\nu)^2 + \frac{r_2^4}{r^4}\right] K^2 p^2 = k^2 \tag{6.6.29}$$

where $K = r_1^2 / (r_2^2 - r_1^2)$. Similar to the Tresca case, it can be shown that Mises yielding will also begin at $r = r_1$, and relation (6.6.29) can then be solved for the initial yield pressure

$$p_o = \frac{k\left(1 - r_1^2 / r_2^2\right)}{\sqrt{1 + \frac{1}{3}(1-2\nu)^2 r_1^4 / r_2^4}} \tag{6.6.30}$$

where for the Mises case, $k = Y / \sqrt{3}$.

When the internal pressure increases beyond p_o, a *plastic zone* will spread from the inner boundary r_1 to some larger radius that we will denote by r_p as shown in Fig. 6.52. In the remaining elastic region $r_p < r < r_2$, the stresses will be given by relations similar to (6.6.25) but satisfying boundary conditions $T_{rr}(r_2) = 0$ and $T_{rr}(r_p) = -p_p$, where p_p is the pressure on the elastic–plastic boundary such that the yield criterion is satisfied.

$$\begin{aligned} T_{rr} &= \frac{r_p^2 p_p}{r_2^2 - r_p^2}\left(1 - \frac{r_2^2}{r^2}\right), \quad T_{\theta\theta} = \frac{r_p^2 p_p}{r_2^2 - r_p^2}\left(1 + \frac{r_2^2}{r^2}\right) \\ T_{zz} &= \nu\left(T_{rr} + T_{\theta\theta}\right) = \frac{2\nu r_p^2 p_p}{r_2^2 - r_p^2}, \quad T_{r\theta} = T_{\theta z} = T_{rz} = 0 \end{aligned} \tag{6.6.31}$$

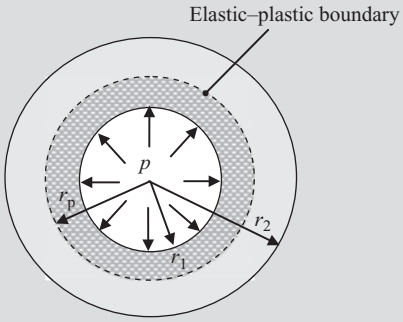

FIGURE 6.52

Elastic–plastic response of pressurized thick-walled cylindrical tube.

Using the Tresca yield function with $T_{\theta\theta} > T_{zz} > T_{rr}$, at $r = r_p$:

$$T_{\theta\theta} - T_{rr} = 2k \Rightarrow T_{\theta\theta} - T_{rr} = \frac{2r_2^2 p_p}{r_2^2 - r_p^2} = 2k \Rightarrow p_p = k\left(1 - \frac{r_p^2}{r_2^2}\right) \tag{6.6.32}$$

Within the plastic zone $r_1 < r < r_p$, the Tresca condition $T_{\theta\theta} - T_{rr} = 2k$ must be maintained. The stresses within this region can be found by going back to the basic equilibrium equation for this problem in polar coordinates (see Appendix A)

$$\frac{dT_{rr}}{dr} + \frac{T_{rr} - T_{\theta\theta}}{r} = 0 \Rightarrow \frac{dT_{rr}}{dr} = \frac{2k}{r} \Rightarrow T_{rr} = 2k \log r + C$$

Applying boundary condition $T_{rr}(r_1) = -p$, determines the value of the constant C and the form of the radial stress:

$$T_{rr} = -p + k \log\left(\frac{r^2}{r_1^2}\right) \tag{6.6.33}$$

Next, using the continuity relation across the elastic–plastic boundary $T_{rr}(r_p) = -p_p$ gives the internal pressure result

$$p = k\left[1 - \frac{r_p^2}{r_2^2} + \log\left(\frac{r_p^2}{r_1^2}\right)\right] \tag{6.6.34}$$

Collecting these results then determines the final results for the stresses in the plastic zone $r_1 < r < r_p$:

$$
\begin{aligned}
T_{rr} &= -k\left[1-\frac{r_p^2}{r_2^2}+\log\left(\frac{r_p^2}{r^2}\right)\right] \\
T_{\theta\theta} &= k\left[1+\frac{r_p^2}{r_2^2}-\log\left(\frac{r_p^2}{r^2}\right)\right] \\
T_{zz} &= 2\nu k\left[\frac{r_p^2}{r_2^2}-\log\left(\frac{r_p^2}{r^2}\right)\right]
\end{aligned}
\tag{6.6.35}
$$

and in the elastic zone $r_p < r < r_2$:

$$
\begin{aligned}
T_{rr} &= -k\left(\frac{r_p^2}{r^2}-\frac{r_p^2}{r_2^2}\right) \\
T_{\theta\theta} &= k\left(\frac{r_p^2}{r^2}+\frac{r_p^2}{r_2^2}\right) \\
T_{zz} &= 2k\nu\frac{r_p^2}{r_2^2}
\end{aligned}
\tag{6.6.36}
$$

The distribution of the in-plane stresses T_{rr} and $T_{\theta\theta}$ are shown in Fig. 6.53 for the case $r_1 / r_2 = 0.5$ with several different r_p / r_2 ratios. MATLAB Code C-15 was used for the calculations and plotting. The case $r_p / r_2 = 0.5$

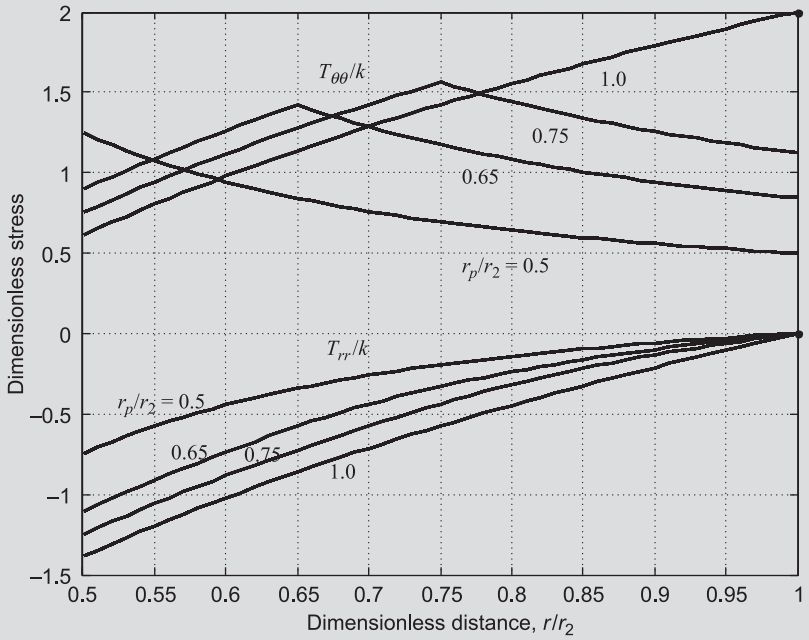

FIGURE 6.53

Elastic–plastic radial and hoop stresses in thick-walled tube problem.

corresponds to the elastic solution with no plastic zone, whereas the case $r_p / r_2 = 1.0$ represents the fully plastic situation with no elastic zone. The radial stresses T_{rr} are all negative, continuous, and approach zero at the outer boundary $r = r_2$. The hoop stresses $T_{\theta\theta}$ are all positive and continuous but the cases with $0.5 < r_p / r_2 < 1.0$ show a discontinuity in slope at elastic–plastic boundary $r = r_p$. It should be noted that there exists significant differences in hoop stress behavior between the fully elastic and fully plastic distributions.

The previous solution based on the Tresca yield condition was carried out without reference to the deformation field. Use was only made of the static equilibrium equation and the stresses were determined in terms of the elastic–plastic radius r_p. Attempting this same solution using the Mises yield function will result in a much more complicated analysis requiring the use of the Prandtl–Reuss relations (6.6.21). We will not pursue this analysis, and the interested reader is referred to Hill (1950), Chakrabarty (1987), or Lubliner (1990) for further details. Note that elastic–plastic expansion of a pressurized thick-walled spherical shell can also be handled in much the same way. Details on this can be found in the previous three references.

EXAMPLE 6.6.2 ELASTOPLASTIC STRESSES IN A CYLINDRICAL BAR UNDER TORSIONAL LOADING

Determine the elastic–plastic stress distribution in a cylindrical bar under pure torsional loading as shown in Fig. 6.54. The problem geometry is initially described in Cartesian coordinates (x,y,z) and involves the torsional loading of a prismatic cylinder with axis along the z-direction. The general cross-section is denoted by R but for simplicity, we will eventually only consider in detail the case of a circular cross-section.

Solution: As with the previous example, we start with the elasticity formulation and solution. The torsion problem is a classical one in elasticity and the complete formulation may be found in Sadd (2014). We outline here only a few of the necessary basic relations. Following the classical Saint Venant semi-inverse formulation, it is assumed that the character of the elastic stress field in most locations within the bar would depend only in a secondary way on the exact distribution of tractions on the ends. Thus, only the end resultant loading T is used as a condition on the problem. Following the semi-inverse scheme, the cross-section displacements are assumed to be rigid-body rotation about the z-axis, whereas the out-of-plane deformation is taken to be an unknown function of x and y. The section angle of twist is taken to vary linearly with the axial coordinate z. Under these assumptions, the displacements become

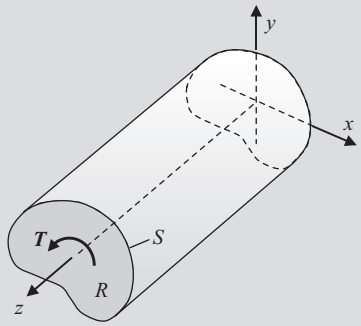

FIGURE 6.54

Torsion of a cylindrical bar.

$$u_x = -\alpha yz, u_y = \alpha xz, u_z = u_z(x, y) \tag{6.6.37}$$

where α is the *angle of twist per unit length*. This set of displacements produces a stress field with only two nonzero components of the form

$$T_{xx} = T_{yy} = T_{zz} = T_{xy} = 0$$
$$T_{xz} = T_{xz}(x, y),\ T_{yz} = T_{yz}(x, y)$$

The elasticity formulation commonly uses the *Prandtl stress function* $\phi = \phi(x, y)$ such that the two nonzero stresses can be expressed by

$$T_{xz} = \frac{\partial \phi}{\partial y}, T_{yz} = -\frac{\partial \phi}{\partial x} \tag{6.6.38}$$

Using this representation, the equilibrium equations will be identically satisfied and the compatibility condition gives a single relation

$$\nabla^2 \phi = \frac{\partial^2 \phi}{\partial x^2} + \frac{\partial^2 \phi}{\partial y^2} = -2\mu\alpha \tag{6.6.39}$$

which becomes the governing equation for the problem. Zero tractions on the lateral sides of the cylinder result in a boundary condition specifying that the stress function is a constant on section boundary *S*. For a simply connected cross-section, this constant may be chosen to be zero

$$\phi = 0 \quad \text{on } S \tag{6.6.40}$$

Finally, we can relate the applied torque *T* to the stress function by using

$$T = \iint_R (xT_{yz} - yT_{xz})\, dx\, dy = -\iint_R \left(x\frac{\partial \varphi}{\partial x} + y\frac{\partial \varphi}{\partial y}\right) dx\, dy = 2\iint_R \varphi\, dx\, dy \tag{6.6.41}$$

Relations (6.6.39)–(6.6.41) provide the basic governing stress formulation for the elasticity solution to the torsion problem.

We will now explore a specific cross-sectional shape and choose a solid circular section of radius a as shown in Fig. 6.55. Because of the symmetric section shape, the elastic–plastic solution will be straightforward with limited complexity. We begin by exploiting the problem symmetry and argue that all variables will be functions of only the radial coordinate r, and thus choose polar coordinates to formulate and solve the problem. For this case, governing equation (6.6.39) becomes

$$\nabla^2\phi = \frac{1}{r}\frac{d}{dr}\left(r\frac{d\phi}{dr}\right) = -2\mu\alpha \tag{6.6.42}$$

This ordinary differential equation can be easily integrated and applying the boundary condition (6.6.40) gives the result

$$\phi = \frac{\mu\alpha}{2}(a^2 - r^2) \tag{6.6.43}$$

In polar coordinates, the only nonzero stress component is given by

$$T_{\theta z} = \tau = -\frac{d\phi}{dr} = \mu\alpha r \tag{6.6.44}$$

The torque T can then be found using Eq. (6.6.41) giving the result

$$T = 2\iint_R \varphi\, dx\, dy = \frac{1}{2}\pi\mu\alpha a^4 \tag{6.6.45}$$

Combining the previous two equations determines the stress in terms of the torque loading

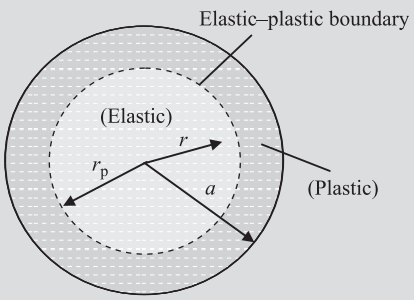

FIGURE 6.55

Elastic–plastic response for the torsion of bar with circular section.

$$\tau = \frac{2Tr}{\pi a^4} \tag{6.6.46}$$

These relations then provide the elastic stress distribution and load carrying capacity.

It is noted that the maximum stress occurs on the outer boundary $r = a$, and this is where yielding will begin as the applied torque or the angle of twist is increased. It can be shown that for any general cross-sectional shape, the maximum stress will always occur at the boundary. Both Tresca and Mises criteria predict yielding when the resultant shear stress $\tau = T_{\theta z} = \sqrt{T_{xz}^2 + T_{yz}^2} = k$, where for the Tresca case $k = Y / 2$ and for the Mises criteria $k = Y / \sqrt{3}$. Therefore, the torque and angle of twist at yield initiation follows from (6.6.45) and (6.6.46):

$$T_p = \frac{\pi k a^3}{2} \quad \text{and} \quad \alpha_p = \frac{k}{\mu a} \tag{6.6.47}$$

As the torque or angle of twist increases beyond these initiation values, an annular plastic zone will expand uniformly from the outer boundary. The elastic region remains in the inner core of the bar, and the elastic–plastic boundary is defined by radius r_p as illustrated in Fig. 6.55. The stress distribution in the elastic zone is linear with the radial coordinate as per (6.6.46). Neglecting any hardening effects, the stress in the entire plastic region will be constant, equaling the yield value k. Invoking the continuity of the stress at r_p, (6.6.44) determines this location

$$r_p = \frac{k}{\mu \alpha} \tag{6.6.48}$$

Thus, the stress distribution in each zone is given by

$$\begin{aligned} &\tau = k\frac{r}{r_p}, \quad 0 \le r \le r_p \\ &\tau = k, \quad r_p \le r \le a \end{aligned} \tag{6.6.49}$$

Note again that we have been able to determine the stresses without knowing the deformation, and thus this problem is statically determined. For the elastic–plastic case, the torque can be computed as

$$\begin{aligned} T &= 2\pi \int_0^a \tau r^2 \, dr = 2\pi \left[\int_0^{r_p} \frac{k r^3}{r_p} dr + \int_{r_p}^a k r^2 \, dr \right] \\ &= \frac{2}{3}\pi k \left[a^3 - \frac{r_p^3}{4} \right] = \frac{1}{3} T_p \left[4 - \left(\frac{\alpha_p}{\alpha} \right)^3 \right] = T_U \left[1 - \frac{1}{4} \left(\frac{\alpha_p}{\alpha} \right)^3 \right] \end{aligned} \tag{6.6.50}$$

The fully plastic torque T_U occurs as $r_p \to 0$, and this gives $T_U = \frac{2}{3}\pi k a^3$. A dimensionless plot of the torque vs angle of twist is shown in Fig. 6.56. MATLAB Code C-16 was used for the calculations and plotting. It is observed that the torque rapidly approaches the fully plastic ultimate value.

While elastic torsion solutions for other cross-sectional shapes can be determined, finding such plastic solutions is difficult. As previously mentioned, for any general cross-sectional shape, the maximum stress will always occur on the boundary. However, finding the subsequent development of the elastic–plastic zones is a challenging task, and most such problems are handled numerically.

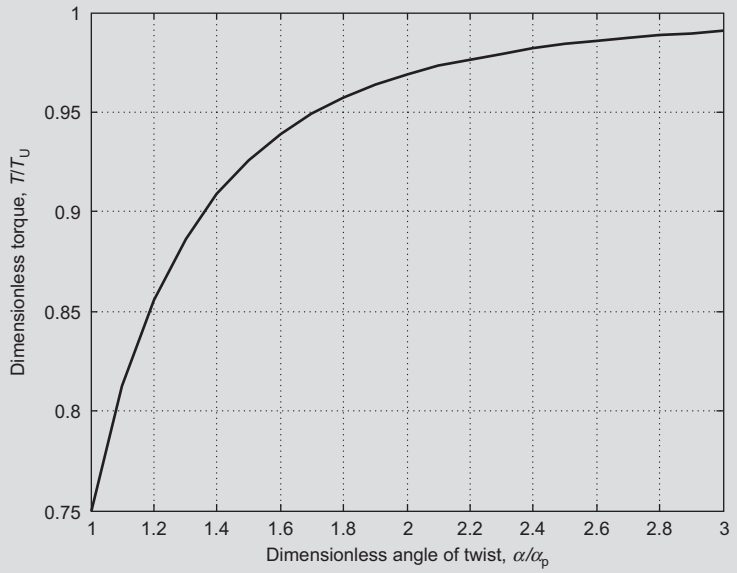

FIGURE 6.56

Torque vs angle of twist for circular section under elastic–plastic torsion.

REFERENCES

Achenbach, J.D., 1976. Wave Propagation in Elastic Solids. North Holland, Amsterdam.

Asaro, R.J., Lubarda, V.A., 2006. Mechanics of Solids and Materials. Cambridge University Press, Cambridge.

Barber, J.R., 2010. Elasticity. Springer, Dordrecht, the Netherlands.

Batchelor, G.K., 2010. An Introduction to Fluid Dynamics. Cambridge University Press, Cambridge.

Bland, D.R., 2016. The Linear Theory of Viscoelasticity. Dover, Mineola, NY.
Bower, A.F., 2010. Applied Mechanics of Solids. CRC Press, Boca Raton, FL.
Chakrabarty, J., 1987. Theory of Plasticity. McGraw Hill, New York.
Christensen, R.M., 2010. Theory of Viscoelasticity. Dover, New York.
Cowin, S.C., Mehrabadi, M.M., 1995. Anisotropic Symmetries of Linear Elasticity, Applied Mechanics Reviews. ASME 48, 247–285.
Flügge, W., 1975. Viscoelasticity. Springer, Berlin.
Golden, J.M., Graham, G.A.C., 1988. Boundary Value Problems in Linear Viscoelasticity. Springer, Berlin.
Graff, K.F., 1991. Wave Motion in Elastic Solids. Dover, New York.
Gutierrez-Lemini, D., 2014. Engineering Viscoelasticity. Springer, New York.
Hill, R., 1950. The Mathematical Theory of Plasticity. Oxford Press, Oxford.
Kachanov, M., Shafino, B., Tsukrov, I., 2003. Handbook of Elasticity Solutions. Kluwer Academic Press, Dordrecht, the Netherlands.
Lamb, S.H., 1993. Hydrodynamics. Cambridge University Press, Cambridge.
Lubliner, J., 1990. Plasticity Theory. Macmillan, New York.
Malvern, L.E., 1969. Introduction to the Mechanics of a Continuous Medium. Prentice-Hall, Englewood Cliffs, NJ.
Michell, J.H., 1899. On the direct determination of stress in an elastic solid with application of the theory of plates. Proc. London Math. Soc. 31, 100–124.
Milne-Thomson, L.M., 1974. Theoretical Hydrodynamics. Dover, New York.
Sadd, M.H., 2014. Elasticity: Theory, Applications and Numerics, Third ed. Elsevier, Waltham, MA.
Schlichting, H., 2017. Boundary-Layer Theory, Ninth ed. Springer, Berlin.
Sendeckyj, G.P., 1975. Some topics of anisotropic elasticity, composite materials. Chamis, C.C. (Ed.), Structural Design and Analysis Part I, 7, Academic Press, New York.
Serrin, J., 1959. Mathematical principles of classical fluid mechanics. Flugge, S. (Ed.), Handbuch der Physik, VIII/1, Springer, Berlin.
Timoshenko, S.P., Goodier, J.N., 1970. Theory of Elasticity. McGraw-Hill, New York.
Ting, T.C.T., 1996. Anisotropic Elasticity. Theory and Applications. Oxford University Press, New York.
Truesdell, C.A., 1966. Continuum Mechanics. I. The Mechanical Foundations of Elasticity and Fluid Dynamics. Gordon & Breach, New York.
White, F.M., 2016. Fluid Mechanics. McGraw-Hill, New York.
Wu, H.C., 2005. Continuum Mechanics and Plasticity. Boca Raton, FL, Chapman & Hall, CRC.
Zheng, Q.S., Spencer, A.J.M., 1993. Tensors which characterize anisotropies. Int. J. Eng. Sci. 31, 679–693.

EXERCISES

6.1 Using relations (6.2.2) and (6.2.7), explicitly show that $C_{ijkl} = C_{klij}$.

6.2 Starting with the general form (6.2.17), show that the isotropic fourth-order elasticity tensor can be expressed in the following forms:

$$C_{ijkl} = \lambda\delta_{ij}\delta_{kl} + \mu(\delta_{il}\delta_{jk} + \delta_{ik}\delta_{jl})$$
$$C_{ijkl} = \mu(\delta_{il}\delta_{jk} + \delta_{ik}\delta_{jl}) + (k - \frac{2}{3}\mu)\delta_{ij}\delta_{kl}$$
$$C_{ijkl} = \frac{E\nu}{(1+\nu)(1-2\nu)}\delta_{ij}\delta_{kl} + \frac{E}{2(1+\nu)}(\delta_{il}\delta_{jk} + \delta_{ik}\delta_{jl})$$

6.3 If the elastic constants E, k, and μ are required to be positive, show that Poisson's ratio must satisfy the inequality $-1 < \nu < \frac{1}{2}$. For most real materials, it has been found that $0 < \nu < \frac{1}{2}$. Show that this more restrictive inequality in this problem implies that $\lambda > 0$.

6.4 Show that Hooke's law for an isotropic material may be expressed in terms of spherical and deviatoric tensors by the two relations

$$\tilde{T}_{ij} = 3k\tilde{\varepsilon}_{ij}, \hat{T}_{ij} = 2\mu\hat{\varepsilon}_{ij}$$

6.5 For incompressible elastic materials, there will be a constraint on all deformations such that the change in volume must be zero, thus implying that $\varepsilon_{kk} = 0$. First show that under this constraint, Poisson's ratio will become 1/2 and the bulk modulus and Lamé's constant will become unbounded. Next show that the usual form of Hooke's law $T_{ij} = \lambda\varepsilon_{kk}\delta_{ij} + 2\mu\varepsilon_{ij}$ will now contain an indeterminate term. For such cases, Hooke's law is commonly rewritten in the form $T_{ij} = -p\delta_{ij} + 2\mu\varepsilon_{ij}$, where p is referred to as the *hydrostatic pressure* which cannot be determined directly from the strain field but is normally found by solving the boundary-value problem. Finally, justify that $p = T_{kk}/3$.

6.6 Go through the details and explicitly develop the Beltrami–Michell compatibility equations (6.2.35).

6.7 For the elasticity displacement formulation, use relations (6.2.36) in the equilibrium equations and develop the Navier equations (6.2.37).

6.8 Starting with the general strain energy expression (6.2.39), develop the strain and stress forms (6.2.40) and (6.2.41).

6.9 Since the elastic strain energy has physical meaning that is independent of the choice of coordinate axes, it must be invariant to all coordinate transformations. Because U is a *quadratic form* in the strains or stresses, it cannot depend on the third invariants III_ε or III_T, and so it must depend only on the first two invariants of the strain or stress tensors. Show that the strain energy can be written in the following two forms:

$$U = \left(\frac{1}{2}\lambda + \mu\right)I_\varepsilon^2 - 2\mu II_\varepsilon$$
$$= \frac{1}{2E}\left(I_T^2 - 2(1+\nu)II_T\right)$$

6.10 Using the stress–Airy stress function relations (6.2.47), show that this form does automatically satisfy the two-dimensional equilibrium equations with no body forces and that the compatibility relation will then lead to the biharmonic equation (6.2.48).

6.11 Verify that the Airy stress function

$$\phi = \frac{s}{4}\left(xy + \frac{ly^2}{c} + \frac{ly^3}{c^2} - \frac{xy^2}{c} + \frac{xy^3}{c^2} \right)$$

solves the problem of a cantilever beam loaded by uniform shear along its bottom edge as shown. Use pointwise boundary conditions on $y = \pm c$ and only resultant effects at ends $x = 0$ and l. Note, however, you should be able to show that T_{xx} vanishes at $x = l$.

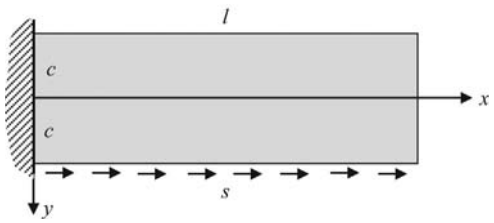

6.12 Consider the axisymmetric problem of an annular disk with a fixed inner radius and loaded with uniform shear stress τ over the outer radius. Using the Airy stress function term $a_4\theta$, show that stress solution for this problem is given by $T_{rr} = T_{\theta\theta} = 0, \quad T_{r\theta} = \tau r_2^2 / r^2$. Use the polar form of the stress–Airy stress function relations given in (6.2.59).

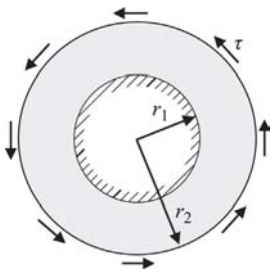

6.13 The starting point for the elastic torsion problem shown in Fig. 6.54 had displacements of the form $u_x = -\alpha yz, u_y = \alpha xz, u_z = u_z(x, y)$, where α is the constant angle of twist per unit length. Verify that this set of displacements produces a stress field with only two nonzero components of the form

$$T_{xx} = T_{yy} = T_{zz} = T_{xy} = 0$$
$$T_{xz} = T_{xz}(x, y), \; T_{yz} = T_{yz}(x, y)$$

6.14 Recall that for fluid flows, the velocity vector is always tangent to a streamline, and thus $\boldsymbol{v} \times d\boldsymbol{x} = 0$, where $d\boldsymbol{x}$ is the differential tangent vector to the streamline. Considering only a two-dimensional flow situation, show that this cross-product will yield a relation that confirms that the stream function ψ will be a constant along a streamline.

6.15 Prove that the streamlines are orthogonal to the potential lines. Hint: start with the relation $\phi = \text{constant} \Rightarrow d\phi = \dfrac{\partial \phi}{\partial x} dx + \dfrac{\partial \phi}{\partial y} dy = 0$ and a similar expression for the stream function. Then use relations (6.3.14).

6.16 Consider the following two-dimensional flow field $v_x = Ax$, $v_y = By$. Determine the relationship between the constants A and B for the flow to be incompressible (isochoric). Next show that the flow is irrotational. Finally determine the potential function ϕ defined by (6.3.8).

6.17 Using polar coordinates, explore the nature of a two-dimensional inviscid flow field for the case with stream function $\psi = K\theta$, where K is a constant. Make use of the polar coordinate relations in (6.3.21). Determine the velocity components and describe the nature of the flow field. Finally sketch the streamlines and potential lines.

6.18 Repeat Exercise 6.17 for the case where $\psi = K \log r$.

6.19 For the case with nonzero bulk viscosity, show that the Navier–Stokes equations become

$$-p_{,i} + (\lambda + \mu) v_{k,ki} + \mu v_{i,kk} + \rho b_i = \rho \left(\frac{\partial v_i}{\partial t} + v_j v_{i,j} \right)$$

$$-\nabla p + (\lambda + \mu) \nabla (\nabla \cdot v) + \mu \nabla^2 v + \rho b = \rho \left(\frac{\partial v}{\partial t} + v \cdot \nabla v \right)$$

6.20 Develop the differential form of the energy equation (5.6.12) using the linear viscous fluid constitutive law (6.4.12).

6.21 For very slow flows of an incompressible linearly viscous fluid, show that the Navier–Stokes equation with no body forces reduce to $\nabla p = \mu \nabla^2 \boldsymbol{v}$. Next show that the pressure field must be harmonic, that is, $\nabla^2 p = 0$. For the two-dimensional case, show that if the velocity is given by $\boldsymbol{v} = \nabla \times \boldsymbol{\psi}$, where $\boldsymbol{\psi} = (0, 0, \psi)$ is the stream function, then all equations are satisfied if the stream function is biharmonic, $\nabla^4 \psi = 0$.

6.22 The Navier–Stokes equation for an incompressible fluid without body forces can be written as

$$\frac{\partial v}{\partial t} + v \cdot \nabla v = -\frac{1}{\rho} \nabla p + \nu \nabla^2 v$$

where $\nu = \mu/\rho$ is called the ***kinematic viscosity***. If we define the vorticity vector by $\boldsymbol{\omega} = \nabla \times \boldsymbol{v}$, show that by taking the curl of the Navier–Stokes relation we can transform it into the ***vorticity equation***

$$\frac{D\boldsymbol{\omega}}{Dt} = \frac{\partial \boldsymbol{\omega}}{\partial t} + \boldsymbol{v} \cdot \nabla \boldsymbol{\omega} = (\boldsymbol{\omega} \cdot \nabla)v + \nu \nabla^2 \boldsymbol{\omega}$$

6.23 Consider a Couette flow between two concentric cylinders with inner radius r_i and outer radius r_o. We will assume that the inner cylinder is fixed, whereas the outer cylinder is rotating with a constant angular velocity Ω. This will establish the following cylindrical shearing flow field:

$$v_r = 0, v_\theta = v_\theta(r), v_z = 0$$

Show that in cylindrical coordinates, the Navier–Stokes equations reduce to the single relation

$$\frac{d^2 v_\theta}{dr^2} + \frac{1}{r}\frac{dv_\theta}{dr} - \frac{v_\theta}{r^2} = 0$$

Subject to the boundary conditions $v_\theta(r_i) = 0, v_\theta(r_o) = \Omega r_o$, show that the solution to this equation is

$$v_\theta = \frac{\Omega r_i^2 r_o^2}{r_o^2 - r_i^2}\left(\frac{r}{r_i^2} - \frac{1}{r}\right)$$

6.24 For Exercise 6.23, show that the shearing stress on the outer cylindrical surface is given by

$$T_{r\theta}(r_o) = 2\mu D_{r\theta}(r_o) = \mu r_o \frac{d}{dr}\left(\frac{v_\theta}{r}\right)\bigg|_{r=r_o} = \frac{2\Omega\mu r_i^2}{r_o^2 - r_i^2}$$

Using this result show that the torque per unit length of cylinder necessary to maintain the angular velocity Ω is given by $T = \dfrac{4\pi\Omega\mu r_i^2 r_o^2}{r_o^2 - r_i^2}$. Note that this relation could be used to determine the fluid viscosity if we know the torque, angular velocity, and the cylinder radii.

6.25 Recall from the energy equation (5.6.12), the rate of working of the stresses or stress power was contained in the term $T_{ij}D_{ij}$. For the general linearly viscous fluid (6.4.4) show that this term is given by $\Phi = T_{ij}D_{ij} = -pD_{kk} + \lambda(D_{kk})^2 + 2\mu D_{ij}D_{ij}$. Reduce this form for the incompressible case. These expressions are commonly called the *dissipation functions*.

6.26 Consider the response of a *viscoelastic fluid-like material* subjected to *simple shearing deformation* $\varepsilon_{12} = H(t)\kappa_o t$. Using a *Maxwell constitutive model*, determine the shear stress history $T_{12}(t)$ and make a temporal plot of this

response. Also develop and plot the corresponding linearly viscous fluid case. Assume an initial condition $T_{12}(0) = 0$.

6.27 For the viscoelastic three-parameter solid model shown in Fig. 6.41A, the sum of the strains in Kelvin and elastic components add to give the total overall strain, and the stress in each of these components are the same and equal the overall stress. Using these facts, develop the governing constitutive law (6.5.20) and relations (6.5.21).

6.28 For the viscoelastic three-parameter fluid model shown in Fig. 6.41B, following similar steps as suggested in Exercise 6.27, develop the governing constitutive law (6.5.23) and relations (6.5.24).

6.29 For the viscoelastic three-parameter solid model shown in Fig. 6.41A, verify the forms of the stress relaxation and creep functions given by relations (6.5.22).

6.30 For the viscoelastic three-parameter fluid model shown in Fig. 6.41B, verify the forms of the stress relaxation and creep functions given by relations (6.5.25).

6.31 Use the given MATLAB Code C-14 to make plots of the given relaxation and creep functions for the three-parameter solid (6.5.22) (with $p_1 = 5$, $q_o = 0.5$, $q_1 = 10$) and liquid (6.5.25) (with $p_1 = 5$, $q_1 = 10$, $q_2 = 10$). Next we wish to modify the three-parameter solid model parameters such that $E^* \to \infty \Rightarrow p_1 \to 0$, and for the three-parameter fluid $\eta \to 0 \Rightarrow q_2 \to 0$. Investigate this case numerically using the code with the parameter sets: three-parameter solid ($p_1 = 0.01$, $q_o = 0.5$, $q_1 = 10$) and liquid ($p_1 = 5$, $q_1 = 10$, $q_2 = 0.1$). Compare these modified numerical predictions with those from the previous Maxwell and Kelvin models.

6.32 Similar to Example 6.5.5, explore the loading and unloading behavior of the three-parameter solid model using the MATLAB ODE solver. Use parameters $p_1 = 0.3$, $q_o = 200$, $q_1 = 300$.

6.33 Using numerical methods, make plots of the Maxwell and Kelvin storage and loss moduli(given in Example 6.5.7) vs the frequency ω. For convenience, plot G_1/E and G_2/η for the case with $\tau = 1$.

6.34 Show that the storage and loss modulus for the three-parameter solid are given by

$$G_1 = \frac{q_o + p_1 q_1 \omega^2}{1 + p_1^2 \omega^2}, G_2 = \frac{(q_1 - q_o p_1)\omega}{1 + p_1^2 \omega^2}$$

6.35 Consider the one-dimensional integral relaxation and creep relations for a viscoelastic material with loading and deformation starting at $t = 0$:

$$T(t) = \int_0^t G(t - t') \frac{d\varepsilon(t')}{dt'} dt' \,, \; \varepsilon(t) = \int_0^t J(t - t') \frac{dT(t')}{dt'} dt'$$

Taking the Laplace transform of each of these relations, show that $\bar{G}(s)\bar{J}(s) = \dfrac{1}{s^2}$, and thus

$$\int_0^t G(t')J(t-t')\,dt' = t$$

Make use of property (6.5.49)$_3$ and the fact that $\mathcal{L}^{-1}\{1/s^2\} = t$.

6.36 Determine the solution to the thick-walled tube Example 6.5.9 for the case where the viscoelastic response is governed by Kelvin-like properties such that $\bar{\mu}(s) = \mu_o + \eta s$ and $\bar{\lambda}(s) = \lambda_o + \eta s$.

6.37 Determine the solution to the Boussinesq's Problem in Example 6.5.10 for the case where the viscoelastic response is governed by a Maxwell type law such that $\mu(t) = \mu_o e^{-t/\tau}$.

6.38 The one-dimensional nonlinear stress–strain behavior of materials that do not exhibit a well-defined yield has often been modeled by the *Ramberg–Osgood relation* $\varepsilon = \dfrac{T}{E}\left(1 + \alpha\left(\dfrac{T}{T_o}\right)^{m-1}\right) = \dfrac{T}{E} + \alpha\dfrac{T_o}{E}\left(\dfrac{T}{T_o}\right)^m$ where α and m are constants and T_o is a reference yield-like stress. Using a numerical routine (MATLAB) make a series of dimensionless stress–strain plots of T/T_o vs $E\varepsilon/T_o$ for values of $\alpha = 1$ and $m = 2, 3, 5, 10, 50$. Discuss the case $m \to \infty$. From your plots, what is the role of the α-parameter?

6.39 Using the fact that the volumetric strain energy may be determined by

$$U_v = \frac{1}{2}\tilde{T}_{ij}\tilde{\varepsilon}_{ij} = \frac{1}{6}T_{jj}\varepsilon_{kk} = \frac{1-2\nu}{6E}T_{jj}T_{kk}$$

explicitly justify relations (6.6.12).

6.40 Starting with relation (6.6.15) develop the invariant form of the Tresca yield condition (6.6.16).

6.41 As shown in Fig. 6.48, along line OH, $T_1 = T_2 = T_3$. Justify that along this line that according to both Mises and Tresca criteria, no yielding can occur.

6.42 Relation (6.6.13) expressed the Mises yield function in terms of the principal stresses. However, it is often more convenient to express this relation in terms of just the stresses. Show that this can be done with the expression $\sigma_e^2 = 3k^2$, where σ_e is the effective or von Mises stress defined previously in (4.5.6) as

$$\begin{aligned}\sigma_e = \sigma_{\text{von Mises}} &= \sqrt{\frac{3}{2}\hat{T}_{ij}\hat{T}_{ij}} \\ &= \frac{1}{\sqrt{2}}\left[\left(T_{11}-T_{22}\right)^2 + \left(T_{22}-T_{33}\right)^2 + \left(T_{33}-T_{11}\right)^2 + 6\left(T_{12}^2 + T_{23}^2 + T_{31}^2\right)\right]^{1/2}\end{aligned}$$

6.43 Consider the Levy–Mises plasticity model, for a *plane strain deformation* in the x_1,x_2-plane. For such a case, the deformation in the x_3-direction will vanish, and the only nonzero stress components are $T_{11},T_{22},T_{33},T_{12}$. First show that for the case of material incompressibility, $T_{33}=(T_{11}+T_{22})/2$. Next demonstrate that both the Mises and Tresca yield conditions give the identical result $(T_{11}-T_{22})^2+4T_{12}=4k^2$.

6.44 For the thick-walled tube problem in Example 6.6.1, using the elastic relations (6.6.25) justify that $T_{\theta\theta}>T_{zz}>T_{rr}$. Next verify the Tresca and Mises yield relations (6.6.26) and (6.6.29).

6.45 For the thick-walled tube problem in Example 6.6.1, use a numerical routine (MATLAB) to make a plot of the internal pressure versus plastic radius given by relation (6.6.34). Keep things dimensionless by plotting p/k vs r_p/r_2, and consider the cases of $r_1/r_2=0.1,0.2,0.3,0.4,0.5$. Comment on the significant differences in the pressure over the range of r_1/r_2.

6.46 For the torsion problem in Example 6.6.2, first verify the elastic solution details given by relations (6.6.43)–(6.6.46). Next show that the both Tresca and Mises criteria give the same result $\tau=T_{\theta z}=\sqrt{T_{xz}^2+T_{yz}^2}=k$, where for the Tresca case $k=Y/2$ and for the Mises criteria $k=Y/\sqrt{3}$.

6.47 Consider the torsion of the elliptical shape. It can be shown (Sadd, 2014) that the elasticity solution to this problem results in the stress distribution

$$T_{xz}=-\frac{2a^2\mu\alpha}{a^2+b^2}y=-\frac{2Ty}{\pi ab^3},\quad T_{yz}=\frac{2b^2\mu\alpha}{a^2+b^2}x=\frac{2Tx}{\pi ba^3}$$

This yields the resultant shear stress in the cross-section $\tau=\dfrac{2T}{\pi ab}\sqrt{\dfrac{x^2}{a^4}+\dfrac{y^2}{b^4}}$. For the case $a>b$, the maximum value of τ occurs at $x=0$ and $y=\pm b$. Determine the torque and angle of twist that will initiate yielding.